

# **Tectonics®**

#### RESEARCH ARTICLE

10.1029/2020TC006677

#### **Key Points:**

- The Maclaren and Kluane schists were a single metamorphic belt that was offset by the Denali fault
- Prograde metamorphism of the Maclaren-Kluane schist took place along E-dipping structures in the late Cretaceous
- Offset of the Maclaren-Kluane schist and associated plutons record ~480 km of dextral displacement on the Denali fault since ca. 52 Ma

#### **Supporting Information:**

Supporting Information may be found in the online version of this article.

#### Correspondence to:

T. S. Waldien, tswaldien@ucdavis.edu

#### Citation:

Waldien, T. S., Roeske, S. M., & Benowitz, J. A. (2021). Tectonic underplating and dismemberment of the Maclaren-Kluane schist records late Cretaceous terrane accretion polarity and ~480 km of post-52 Ma dextral displacement on the Denali fault. *Tectonics*, 40, e2020TC006677. https://doi.org/10.1029/2020TC006677

Received 21 DEC 2020 Accepted 6 SEP 2021

© Wiley Periodicals LLC. The Authors. This is an open access article under the terms of the Creative Commons Attribution License, which permits use, distribution and reproduction in any medium, provided the original work is properly cited.

## Tectonic Underplating and Dismemberment of the Maclaren-Kluane Schist Records Late Cretaceous Terrane Accretion Polarity and ~480 km of Post-52 Ma Dextral Displacement on the Denali Fault

T. S. Waldien<sup>1</sup>, S. M. Roeske<sup>1</sup>, and J. A. Benowitz<sup>2</sup>

<sup>1</sup>Department of Earth and Planetary Sciences, University of California, Davis, Davis, CA, USA, <sup>2</sup>Geophysical Institute, University of Alaska, Fairbanks, AK, USA

**Abstract** Terrane accretion introduces irregular geometry and allochthonous material to obliquely convergent margins, which create opportunities to quantify strike-slip displacement along otherwise margin-parallel fault systems. We present new bedrock geologic mapping and U-Pb and 40Ar/39Ar geochronology from the Alaska Range suture zone in the eastern Alaska Range, which confirm a longhypothesized correlation between the Maclaren Glacier metamorphic belt (Alaska, USA) and the Kluane metamorphic assemblage (Yukon Territory, Canada) across the right-lateral Denali fault. The new data inform a palinspastic reconstruction showing that the dissected metamorphic belts and associated plutons record ~480 km of dextral displacement along the Denali fault since ca. 52 Ma. Before strike-slip separation, the Maclaren-Kluane schist formed by west-vergent forearc underplating in the waning stage of the ca. 100-90 Ma arc built upon the Yukon-Tanana terrane. The prograde structural and metamorphic evolution of the Maclaren-Kluane schist records the final collision of the Wrangellia composite terrane at ca. 75-65 Ma along a set of east-dipping thrust shear zones, which we infer to record the polarity of the late Cretaceous plate boundary between the composite terrane and North America. Paleogene extension partially exhumed the schists to the upper crust and may be a consequence of regionally distributed strike-slip faulting at that time. Localization of the modern Denali fault after ca. 52 Ma dismembered the schists and four neighboring belts of plutonic, metasedimentary, and volcanic rocks. The transition to Yakutat oblique flat slab subduction at ca. 30-25 Ma marks the onset of transpressional deformation in the Denali fault system, which reactivated Late Cretaceous collisional structures bounding the Maclaren schist. Neogene reactivation of the Totschunda fault reduced strike-slip motion on the Denali fault east of the Denali-Totschunda intersection and continues to transfer residual plate boundary slip onto the Denali fault west of the intersection. Key outcomes of our synthesis include: (a) Much of the ~480 km of displacement on the Denali fault accumulated after strike-slip on the neighboring Tintina and Border Ranges fault systems had largely shut down; (b) The modern Denali fault system should not be grouped with strike-slip faults credited with large-scale margin-parallel transport of Cordilleran terranes in the Cretaceous. Instead, a poorly understood proto-Denali fault system may be a candidate for large-scale Cretaceous translation; and (c) the longevity (≥33 Myr) of the highly localized Denali fault master strand (≤1 km wide) implies that it occupies a major mechanical boundary that penetrates the lithosphere.

Plain Language Summary Many of the rocks that make up present-day western Canada and southern Alaska did not form as part of North America. Instead, most formed as coherent island chains (called terranes), collided with North America, and then slid northward along fault systems to their present location. The timing of collision and northward sliding of the terranes that make up western North America has been disputed for decades. To better bracket the timing of terrane collision and northward transport, we mapped and dated metamorphic and igneous rocks in southern Alaska that were sandwiched between western North America and the colliding terranes, then slid northward to Alaska via motion on the Denali fault. With the new maps and ages, we show that the terranes in southern Alaska collided with North America from about 90–65 million years ago, and then they moved northward along the Denali fault about 480 km (298 mi.) relative to correlative rocks in the Yukon Territory. Moreover, the youngest rocks that correlate across the Denali fault are about 52 million years old, which allows us to bracket the timing of the ~480 km of motion on the Denali fault to have happened since 52 million years ago. Before our study, the Denali fault was thought to have moved ~370–400 km (230–250 mi.) since about

WALDIEN ET AL. 1 of 35



100 million years ago. Our improved estimates of timing and magnitude of motion on the Denali fault better bracket the former locations of rocks that make up western North America, which informs general questions about how continents grow, how fault systems evolve, and what geological processes lead to uplifted topography along continental margins.

#### 1. Introduction

Quantitative restoration of strike-slip deformation along obliquely convergent margins is commonly hindered by strike-slip localization within the arc (e.g., Busby-Spera & Saleeby, 1990; Lange et al., 2008) or forearc (Avé Lallemant, 1997; Jarrard, 1986), which translates sub-parallel elements of the margin relative to each other but may not cross-cut restorable features (Beck, 1986). Terrane accretion and associated geometric modification of the margin (e.g., Dominguez et al., 1998) form unique markers that may be used to track syn-collisional and post-collisional margin-parallel translation. Recognition, correlation, and restoration of such features requires identifying the suite of diagnostic characteristics by which they can be identified, knowledge of where/when the feature accreted to the margin, and how each part of the displaced feature has evolved since dismemberment.

Assembly of the North American Cordillera involved multiple episodes of strike-slip faulting and terrane accretion. Although both terrane accretion and translation have long been recognized as fundamental geologic processes shaping western North America (e.g., Coney et al., 1980; Moores, 1970), they persist as controversial topics. Shortening structures formed during terrane accretion are essential for reconstructing strike-slip deformation in the Cordillera because they have been found in multiple places to be cut by strike-slip faults and thus create reliable geological markers for estimating strike-slip separation (Gabrielse et al., 2006; Nokleberg et al., 1985). New views of the Mesozoic Cordilleran orogeny (Hildebrand, 2015; Johnston, 2008; Sigloch & Mihalynuk, 2017), however, call into question the timing and polarity of various terrane accretionary events (e.g., Pavlis et al., 2019). A detailed reappraisal of terrane accretionary rocks and structures is thus necessary to vet the various models of Cordilleran assembly and associated margin-parallel translation.

Metamorphic belts and structures formed during the closure of the ocean basin between the Wrangellia composite terrane and North America have been used to estimate total strike-slip displacement on the Denali fault between southern Alaska, USA and southwestern Yukon Territory, Canada. The purported correlative rock packages include schists, gneisses, and plutons in the Maclaren Glacier metamorphic belt<sup>1</sup> (Alaska) and Kluane metamorphic assemblage-Ruby Range batholith (Yukon) (Eisbacher, 1976; Nokleberg et al., 1985; Figure 1). Since the correlation between these two metamorphic belts was first proposed by Forbes et al. (1974), the tectono-metamorphic evolution of the Kluane metamorphic assemblage has been the focus of a number of detailed studies (e.g., Canil et al., 2015; Israel et al., 2011; Mezger, 1999, 2002; Mezger, Chacko, et al., 2001; Mezger, Creaser, et al., 2001; Stanley, 2012). In contrast, metamorphic and plutonic rocks near the Maclaren Glacier have mainly been studied as part of early regional mapping efforts (Nokleberg et al., 1985; Nokleberg, Aleinikoff, Lange, et al., 1992; Smith, 1981), other than detailed studies in a small accessible region (Beam & Fisher, 1999; Davidson & McPhillips, 2007; Davidson et al., 1992; Link, 2017). The difference in study resolution has led to doubt as to whether the rock units correlate (e.g., Mezger, Chacko, et al., 2001). Moreover, tectonic models describing the prograde metamorphic path of the Maclaren and Kluane belts have argued for opposing vergence directions for syn-collisional structures (cf., Csejtey et al., 1982; Erdmer & Mortensen, 1993; Johnston & Canil, 2007; Nokleberg et al., 1985). If the disparate tectonic models are correct, then the proposed correlation of the Maclaren and Kluane belts may be refutable and estimates of total displacement along the Denali fault system would require revision.

Here, we present a new regional synthesis map (Figure 2), zircon U-Pb age data from 9 metasedimentary and 13 plutonic samples, zircon Hf isotopic data from three metasedimentary samples, and  $^{40}\mathrm{Ar}/^{39}\mathrm{Ar}$  geochronology on four volcanic samples located south of the Denali fault in the eastern Alaska Range. Our data bear on the timing of initial burial and tectono-metamorphic evolution of the Maclaren and Clearwater metasedimentary belts in Alaska leading up to and after strike-slip separation. We compare our data to equivalent data sets from the Kluane metamorphic assemblage and argue that the metasedimentary/plutonic belts represent a single body that was cut and displaced by the Denali fault. By integrating our data

WALDIEN ET AL. 2 of 35



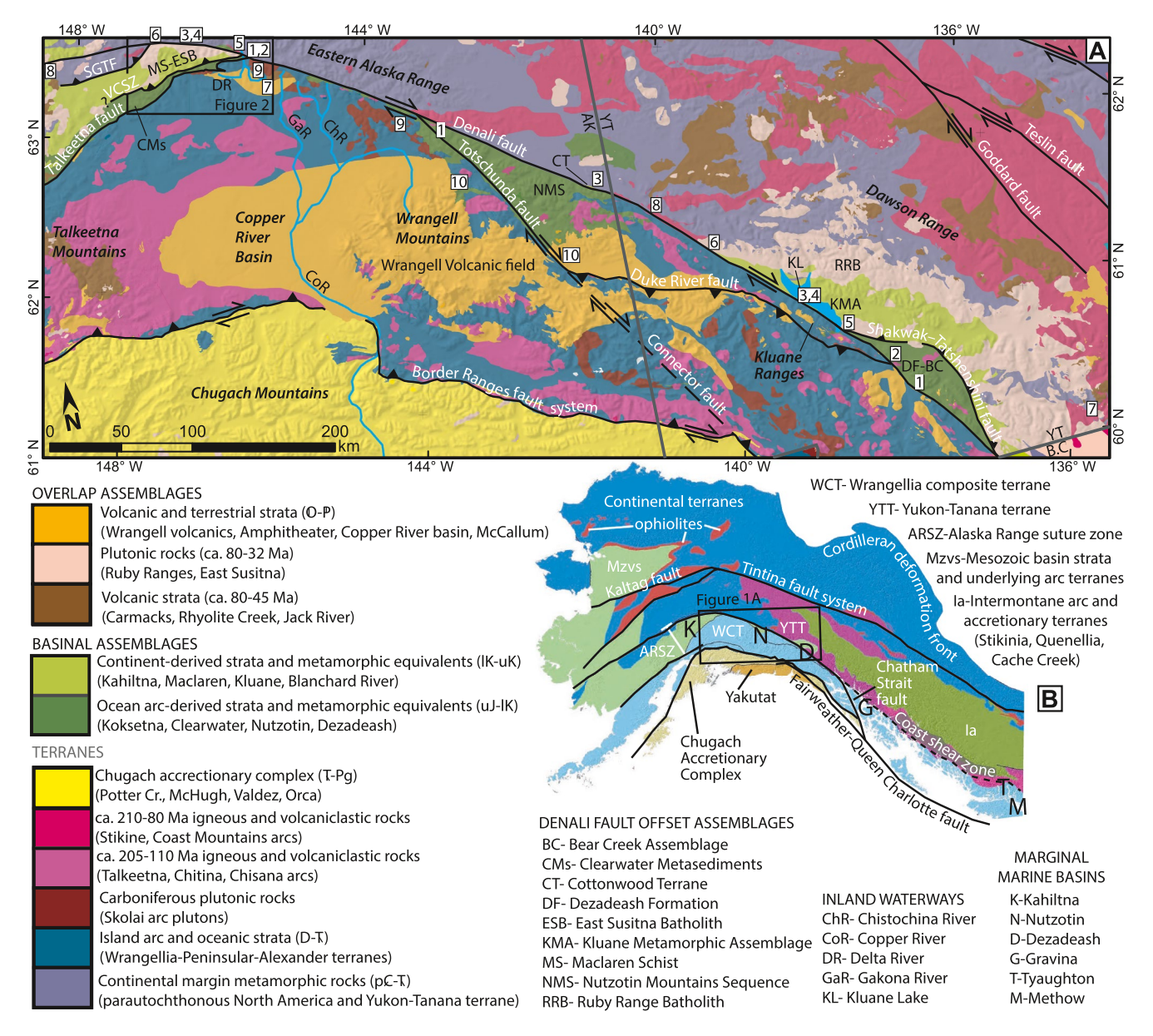


Figure 1. (a) Simplified geologic map of the southwestern Yukon and eastern Alaska region surrounding the Denali fault (modified from Wilson et al. [2015] and Colpron et al. [2016]). Basement geology is combined into the Wrangellia and Yukon composite terranes south and north of the Denali fault, respectively. Mesozoic-Cenozoic igneous belts and basinal assemblages are delineated as either pre-Wrangellia-collisional terranes and marginal marine strata (≥80 Ma) or overlap (<80 Ma). The legend contains regional formation, metamorphic belt, or plutonic suite names that are contained within the map area and are pertinent to the study. The location of Figure 2 is contained within the black box. Boxed numbers denote the locations of correlative geologic features that are listed in Table 1. SGTF—Susitna Glacier thrust fault; VCSZ—Valdez Creek shear zone; AK—Alaska; YT—Yukon Territory; B.C.—British Columbia. (b) Regional terrane map of the Canadian-Alaska Cordillera showing the location of Figure 1A and major strike-slip fault systems (black lines), modified from Colpron and Nelson (2011). Abbreviations denoting the marginal marine basins are shown in the general locations.

with other regional data sets, we are able to place the Maclaren-Kluane metamorphic belt into a regional tectonic framework during the final accretion of the Wrangellia composite terrane and arrive at more precise measurements and timing of subsequent strike-slip separation.

<sup>1</sup>Recent studies by Link (2017) and Waldien et al. (2021) have shown that the Maclaren Glacier metamorphic belt is a composite metamorphic belt wherein rocks at various structural positions have different protoliths, which experienced different metamorphic, magmatic, and structural histories before final juxtaposition by the Valdez Creek shear zone during Wrangellia composite terrane accretion to North America. The

WALDIEN ET AL. 3 of 35



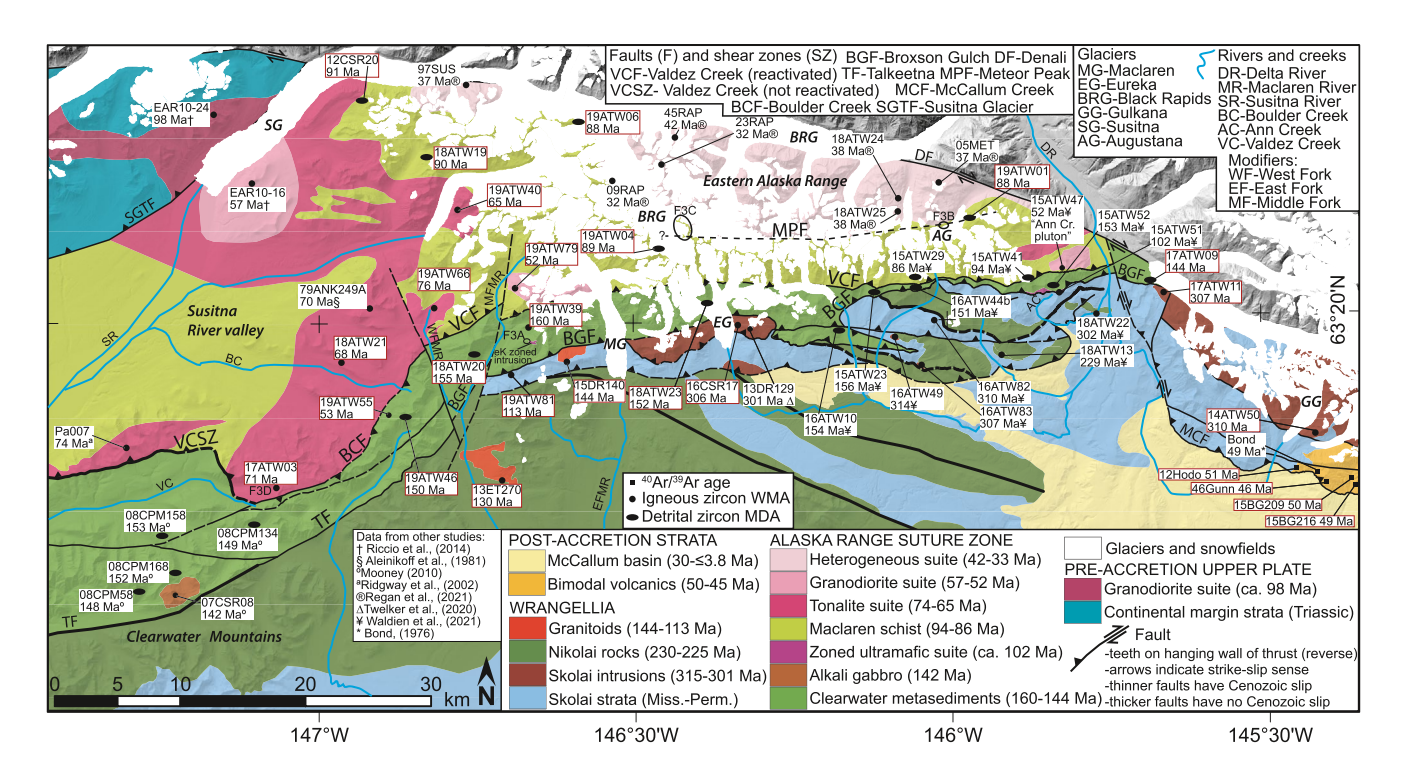


**Figure 2.** Regional geologic and age compilation map of the study area in the eastern Alaska Range. The map is compiled from Smith and Turner (1974), Mooney (2010), Waldien et al. (2018), Twelker et al. (2020), Waldien et al. (2021), and our new mapping near the headwaters of the Maclaren River. Previously published ages are annotated with a symbol corresponding to an author, whereas new ages are outlined by a red box. The locations of field photographs in Figure 3 are shown as "F3A-D." WMA—weighted mean age; MDA—maximum depositional age.

term "Maclaren Glacier metamorphic belt" as originally defined does not convey the disparate polyphase tectonic evolution of the metamorphic rocks in the area. We propose that the recent advances in understanding have rendered the term "Maclaren Glacier metamorphic belt" obsolete. We argue that parsing the metamorphic rocks into the Maclaren schist/gneiss (structurally above the Valdez Creek shear zone) and Clearwater metasediments (structurally below the Valdez Creek shear zone) is more informative and thus will be more useful for future studies in the region.

## 2. Geologic Background

## 2.1. Slip on the Modern Denali Fault

The Denali fault system is an arcuate set of structures that transect the Cordillera from northern British Columbia to western Alaska (St. Amand, 1957). Active dextral slip is likely routed to the Denali fault master strand from the plate boundary fault systems by way of the Connector fault (Brothers et al., 2018; Choi et al., 2021; Doser, 2014; Elliott & Freymueller, 2020; Figure 1). Published estimates of total offset on the Denali fault range from 370 to 400 km and are based on a variety of offset markers ranging from topography to terrane boundaries. Lowey (1998) provided a synopsis of strike-slip displacement estimates and Table 1 contains an updated list of separation estimates for the Denali fault, including those presented here for the first time. It is important to emphasize that the tabulated separation estimates consider only the active strand of the Denali fault. We recognize the likelihood of an older Denali fault system, which may have had multiple strands active during the Cretaceous (McDermott et al., 2019; Miller et al., 2002; Wahrhaftig et al., 1975). Herein, our use of the words Denali fault refers to the active strand of the fault, which appears to have been a single highly localized strand for much of the Cenozoic (Cole et al., 1999; Regan et al., 2021). When necessary for clarity, we distinguish the modern- or proto- Denali fault to refer to the Cenozoic and Cretaceous fault systems, respectively. Our use of the words Denali fault system includes the active Denali fault master strand, Totschunda fault, and thrust systems at the northern and southern flanks of the Alaska Range.

WALDIEN ET AL. 4 of 35

10.1029/2020TC006677



**Table 1**Offset Markers for the Modern Denali Fault System

Reference	Fault section	Offset markers	Separation and Timing	Number on Figure 1
Lowey (1998)	Eastern Denali	Dissected megaboulder channel in Dezadeash (YT)- Nutzotin (AK) strata	370 km since 52 Ma <sup>b</sup>	1
Waldien et al. (2021)	Eastern Denali	Clearwater metasediments (AK)-Dezadeash formation (YT)	465 km since 52 Ma <sup>b</sup>	1
Waldien et al. (2021)	Eastern Denali	Granodiorite and pyroxenite near Ann Creek (AK)- Shorty Creek granodiorite and Pyroxenite Cr. Pyroxenite (YT) <sup>a</sup>	≤505 km since 52 Ma <sup>b</sup>	2
Regan et al. (2021), This	Eastern Denali	Cottonwoodschist (AK)-Maclaren schist (AK)	305 km since 33 Ma	3
study		Cottonwood schist (AK)-Kluane schist (YT)	100–125 km, 52–33 Ma	
Nokleberg et al. (1985), Riccio et al. (2014)	Eastern Denali	Maclaren schist and East Susitna batholith (AK)-Kluane schist and Ruby Range batholith (YT)	445 km since 52 Ma <sup>b</sup>	4
Γhis Study	Eastern Denali	ca. 52 Ma Shakwak pluton (YT)-Ann Creek pluton (AK)	465 km since 52 Ma	5
		74-65 Ma intrusions within Kluane schist and Maclaren schist <sup>a</sup>	≥425 km since 52 Ma	6
		Eocene bimodal volcanic strata near Gakona Gl. (AK)- Bennett Lake igneous complex (YT) <sup>a</sup>	≤580 km since 52 Ma <sup>a</sup>	7
		Jack River igneous field (AK)-Rhyolite Creek volcanics $(YT)^a$	≤490 km since 52 Ma <sup>b</sup>	8
This Study; D. Murphy personal communication	Eastern Denali	Kluhini River Thrust (YT)-Susitna Glacier thrust (AK)	≥425 km post 52 Ma <sup>b</sup>	7
Waldien et al. (2018)	Totschunda-Eastern Denali	Strain compatibility with fault linkage	≤91 km since 7 Ma	9
Berkelhammer et al. (2019)	Totschunda	Wrangell volcanics and intrusions (AK)	≤85 km since 7 Ma <sup>b</sup>	10
Fasulo et al. (2020); This study	Totschunda-Eastern Denali	Nutzotin basin strata and associated ca. 120 Ma intrusions (AK)	>75 km since 7 Ma <sup>b</sup>	Similar to
Allen et al. (2016)	Totschunda-Eastern Denali	Transtensional lower McCallum basin (AK) to transtension zone at Denali-Totschunda intersection (AK)	<95 km since 7 Ma <sup>b</sup>	Similar to
Regan et al. (2021)	Central Denali	Schist Creek pluton-Foraker pluton (AK)	155 km since 37 Ma	Not Show
Trop et al. (2019)	Central Denali	Colorado Cr. basin detritus-eastern Alaska Range sources (AK)	150 km since 29 Ma	Not Show
Miller et al. (2002)	Western Denali	Algal Reef in Farewell terrane strata (AK)	134 km, post mid-K	Not Show

<sup>a</sup>Correlated features may be different bodies. <sup>b</sup>Separation re-measured and/or new timing inferred from our data.

## 2.2. Mesozoic Terrane Accretion and Strike-Slip Faulting in the Cordillera

The Mesozoic geologic evolution of the North American Cordillera is characterized by accretion and margin-parallel transport of allochthonous terranes (Colpron et al., 2015; Coney et al., 1980; Nelson & Colpron, 2007). The outboard belt of the Cordillera is largely composed of Paleozoic and Mesozoic arc rocks belonging to the Wrangellia, Peninsular, and Alexander terranes, which had accreted to each other before collision with the Cordilleran margin (Beranek et al., 2014; Gardner et al., 1988; Israel et al., 2014). Herein, we refer to the amalgamated terranes as the "Wrangellia composite terrane" and distinguish the individual terranes only when necessary. The structural polarity during accretion of the Wrangellia composite terrane to the Cordillera is disputed; some authors argue for west-dipping subduction (Hildebrand, 2015; Lowey, 2019; Sigloch & Mihalynuk, 2017), whereas others argue for east-dipping collisional structures and an unclear role of subduction during the collision (Pavlis et al., 2019; Trop & Ridgway, 2007). Regardless of structural polarity, the collision coincided with along-strike diachronous oblique closure of a marginal marine basin system from Late Jurassic to Late Cretaceous (Manselle et al., 2020; McClelland et al., 1992; Ridgway et al., 2002). Deformed and variably metamorphosed packages of clastic strata representing the

WALDIEN ET AL. 5 of 35



closed marginal marine basins are exposed over 3,000 km length of the Cordillera from southern British Columbia to western Alaska (Methow-Tyaughton-Gravina-Dezadeash-Nutzotin-Kahiltna basins—Figure 1b). In southern Alaska, the highly deformed region underlain by imbricated and metamorphosed Kahiltna basin strata, fragments of oceanic crust, and disparate continental terranes is referred to as the Alaska Range suture zone (Fitzgerald et al., 2014; Ridgway et al., 2002; Trop et al., 2019; ARSZ—Figure 1b).

Syn-collisional and post-collisional strike-slip faulting contributed to margin-parallel transport of the Wrangellia composite terrane and dismemberment of the basinal assemblages along the inboard margin of the composite terrane. The strike-slip faulting is generally taken to accommodate the margin-parallel component of oblique relative plate motion between western North America and outboard oceanic plates (e.g., Monger & Gibson, 2019). Regional deformation patterns are consistent with southward transport of outboard terranes along sinistral fault systems during the Late Jurassic and Early Cretaceous (Chardon et al., 1999; Cobbett et al., 2017; Evenchick, 1991; Israel et al., 2006; Mahoney et al., 2009; Monger et al., 1994). By the Late Cretaceous, widespread dextral shear in the Cordillera contributed to northward transport of the terranes relative to the North American craton, which continued into the Cenozoic (Avé Lallemant & Oldow, 1988; Wyld et al., 2006). Many paleomagnetic-based studies call for large-scale (>1,500 km) of Cretaceous-Cenozoic northward displacement of the Cordilleran terranes (e.g., Enkin, 2006; Hillhouse & Coe, 1994; Johnston, Jane Wynne, et al., 1996; Stamatakos et al., 2001). However, the sum of geology-based slip estimates does not reach the magnitude of translation inferred from the paleomagnetic estimates (e.g., Wyld et al., 2006), thus implying the potential for missing slip.

Much of the strike length of the Denali fault marks the boundary between rocks belonging to, or derived from, the Wrangellia composite terrane and rocks with peri-continental affinity. Thermochronological, structural, and stratigraphic data sets suggest that oblique closure of the Kahiltna basin, and associated development of the Alaska Range suture zone, involved slip on a potentially multi-stranded proto-Denali fault system along the paleo-eastern margin of the Wrangellia composite terrane, which may have translated the composite terrane relative to Mesozoic strata to the east (McDermott et al., 2019; Trop et al., 2020). In contrast, the modern Denali fault cuts obliquely through the Mesozoic basinal assemblages, continental margin rocks, and plutonic belts (Figure 1). The section of the Denali fault between the longitudes of the Delta River (~145.5°W—Alaska) and Kluane Lake (~139°W—Yukon) juxtaposes the Wrangellia terrane rocks directly against peri-Laurentian rocks, whereas Mesozoic basin strata and associated crystalline rocks are largely absent from that section of the fault system (Figure 1a). The similarities among Mesozoic-Paleogene rocks near the Delta River and Kluane Lake, and lack of similar rocks between the two areas, has made them a target for estimating offset on the modern Denali fault (e.g., Eisbacher, 1976; Nokleberg et al., 1985).

## 2.3. Geology South of the Denali Fault Near the Delta River in the Eastern Alaska Range

South of the Denali fault and west of the Delta River, a series of north-dipping thrust panels contain Triassic continental margin strata, Alaska Range suture zone metasedimentary and plutonic rocks, and Wrangellia terrane meta-igneous rocks. From north to south, important structures bounding the thrust panels are the Susitna Glacier thrust fault, Valdez Creek shear zone/fault, and the Talkeetna-Broxson Gulch fault (Figures 1a and 2).

The Triassic continental margin rocks in the northernmost and structurally highest panel south of the Denali fault comprise carbonate and clastic strata that are intruded by ca. 98–57 Ma plutons in the hanging wall of the Susitna Glacier thrust fault (Csejtey et al., 1992; Riccio et al., 2014). In the footwall south of the Susitna Glacier thrust fault, amphibolite facies pelitic-to-quartzofeldspathic schists and gneisses of the Maclaren schist are intruded by the East Susitna batholith (Davidson et al., 1992; Nokleberg et al., 1985; Waldien et al., 2021). Individual plutons within the East Susitna batholith have yielded crystallization ages ranging from ca. 74–33 Ma (Aleinikoff et al., 1981; Davidson & McPhillips, 2007; Regan et al., 2021; Ridgway et al., 2002; Turner & Smith, 1974). Across the Valdez Creek fault/shear zone to the south, the Clearwater metasediments comprise ca. 160–144 Ma generally arkosic-to-mafic metasedimentary strata with lesser argillaceous slate and phyllite, which are intruded by small volume intermediate-to-ultramafic intrusions with crystallization ages ranging from ca. 142–102 Ma (Mooney, 2010; Waldien et al., 2021). The Talkeetna-Broxson Gulch fault juxtaposes the metasedimentary and plutonic rocks in the north against the Wrangellia terrane to the south.

WALDIEN ET AL. 6 of 35



In the eastern Alaska Range, Wrangellia stratigraphy consists of Carboniferous volcanic and volcaniclastic strata overlain by lesser Permian carbonate strata and regionally extensive Triassic flood basalts. The Carboniferous strata in the area host generally intermediate composition intrusions dated at ca. 300–315 Ma (Waldien et al., 2021). Both the strata and the intrusions have been linked to the Skolai arc that forms the nucleus of the Wrangellia terrane in south-central Alaska (Bond, 1973; Beard and Barker, 1989). Carbonate strata containing Early Permian fossils unconformably overly the Skolai arc rocks (Bond, 1973, 1976; Nokleberg, Aleinikoff, Dutro, et al., 1992; Richter & Dutro, 1975) and may record cessation of Skolai arc magmatism in the Late Pennsylvanian (e.g., Beranek et al., 2014; Israel et al., 2014). Triassic Nikolai flood basalt strata unconformably overly the Paleozoic rocks in the region (Greene et al., 2008; 2010; Twelker et al., 2020). Nikolai strata and associated intrusions yield crystallization ages of 225–230 Ma (Bittenbender et al., 2007; Greene et al., 2010; Twelker et al., 2020; Waldien et al., 2021).

South of the Denali fault and east of the Delta River, a belt of Eocene felsic volcanic rocks with lesser basalt unconformably overlies and is faulted against pre-Cenozoic Wrangellia rocks between the Delta River in the west and the Chistochina River in the east (Nokleberg, Aleinikoff, Lange, et al., 1992; Gillis et al., 2019; Figures 1 and 2). The Eocene volcanic strata and Wrangellia rocks are carried in the hanging wall of the south-vergent McCallum-Slate Creek thrust system. The footwall south of the McCallum-Slate Creek thrust system contains the Oligocene-Pliocene fluvial-lacustrine McCallum basin strata (Allen et al., 2016; Waldien et al., 2018).

The tectono-metamorphic evolution of rocks south of the Denali fault near the Delta River records imbrication of North American-affinity and Wrangellia-affinity rocks during Late Cretaceous terrane accretion and Oligocene reactivation of the terrane accretionary structures. Before juxtaposition during terrane accretion, the Maclaren schist protolith was derived from, and deposited upon, the western margin of North America at ca. 94-86 Ma, whereas the Clearwater metasediments were deposited along the paleo-eastern margin of the Wrangellia terrane at ca. 150 Ma (Waldien et al., 2021). Initial juxtaposition of the Maclaren schist and Clearwater metasediments took place with the formation of the Valdez Creek shear zone, which is a south-vergent thrust shear zone intruded by a ca. 74 Ma syn-kinematic tonalite sill (Ridgway et al., 2002). Motion on the shear zone produced a well-preserved inverted metamorphic gradient in the footwall Clearwater metasediments, which records the Late Cretaceous history of prograde metamorphism related to Wrangellia terrane accretion (Davidson et al., 1992; Hollister, 1993; Smith, 1981). In the Alaska Range east of the Maclaren River, the Maclaren schist experienced a pervasive greenschist facies retrograde metamorphic overprint that has been linked to post-32 Ma reactivation of the Valdez Creek shear zone as the Valdez Creek fault (Waldien et al., 2021). Reactivation of the shear zone nucleated a south-vergent imbricate thrust system that includes the Broxson Gulch fault at the northern margin of the Wrangellia terrane and reverse faults within the Wrangellia terrane to the south (Waldien et al., 2021). The Denali fault truncates the Maclaren schist and associated rocks and structures near the Delta River (Figures 1 and 2).

#### 2.4. Geology Northeast of the Denali Fault Near Kluane Lake in Southwestern Yukon

Near Kluane Lake northeast of the Denali fault, a series of north-to-northeast-dipping thrust panels contain peri-Laurentian Yukon-Tanana terrane rocks, the Kluane Metamorphic assemblage, the Dezadeash Formation, and the Bear Creek Formation. Important structures in the region are the Kluhini River thrust and the Tatshenshini shear zone/Shakwak fault.

Rocks belonging to the Yukon-Tanana terrane occupy the highest structural panel, which consists of pre-Carboniferous quartzose metasedimentary rocks with lesser carbonate and amphibolite that host late Devonian and younger intrusions (Israel et al., 2011; Johnston, Mortensens, et al., 1996). South of the Yukon-Tanana terrane, the Ruby Range batholith is a ca. 77–57 Ma composite intrusive suite emplaced along the boundary between Yukon-Tanana terrane rocks to the north and the Kluane metamorphic assemblage to the south (Israel et al., 2011; Stanley, 2012). The Kluane metamorphic assemblage consists of Late Cretaceous amphibolite facies pelitic and quartzofeldspathic schist and gneiss (Mezger, Chacko, et al., 2001). For simplicity, we hereafter refer to these metasedimentary rocks as the Kluane schist. The batholith largely obscures the contact between the Kluane schist and Yukon Tanana terrane, yet vestiges of a Late Cretaceous west-vergent thrust shear zone (Kluhini River thrust-Vice et al., 2020) are preserved. Smaller intrusions within the 54–48 Ma Hayden Lake suite intruded the lowest structural position of the Kluane schist

WALDIEN ET AL. 7 of 35



(Colpron et al., 2016). Graben-bounded Paleogene volcanic strata unconformably overlie Yukon-Tanana terrane metamorphic assemblages and associated plutons throughout southwestern Yukon.

The southern margin of the Ruby Range batholith and Kluane schist are juxtaposed against Dezadeash and Bear Creek strata to the southwest along the Shakwak fault and Tatshenshini shear zone (Colpron et al., 2016; Lowey, 2000; Vice et al., 2020). The Bear Creek assemblage consists of Upper Triassic marine strata and lava flows (Israel et al., 2015). The Late Jurassic-Early Cretaceous Dezadeash Formation unconformably overlies the Bear Creek assemblage and consists of ≥1 km of marine turbidite strata (Eisbacher, 1976; Lowey, 1998). Both the Bear Creek and Dezadeash strata host the ca. 126–106 Ma (K-Ar dates) Shorty Creek and Pyroxenite Creek intermediate-ultramafic intrusive suite (Dodds & Campbell, 1988; Eisbacher, 1976). The northwest-striking Denali fault truncates the western margin of the entire package of north-dipping structural panels in southwestern Yukon.

The geologic evolution of rocks near Kluane Lake records the closure of an ocean basin during the Late Cretaceous (Mezger, Creaser, et al., 2001). Detrital zircon U-Pb data indicate that both schistose and gneissic Kluane rocks have ca. 95–90 Ma protolith ages and received sediment from Yukon-Tanana and other peri-Laurentian terranes (Israel et al., 2011; Stanley, 2012) before imbrication and prograde metamorphism along east-northeast-dipping convergent structures (Erdmer & Mortensen, 1993). In contrast, the Dezadeash Formation was likely sourced from the Mesozoic arcs built upon the Wrangellia composite terrane as indicated by paleo-current indicators and detrital zircon U-Pb age spectra (Lowey, 2019). Similarly, the Bear Creek Formation may correlate with similar age and composition rocks within the Alexander terrane (Israel et al., 2015). During Wrangellia composite terrane accretion, the Kluane schist experienced regional metamorphism as early as 82 Ma and was intruded by the Ruby Range batholith from ca. 77 to 57 Ma (Israel et al., 2011; Stanley, 2012). The ca. 57 Ma phase of the Ruby Range batholith displays regional plutonic-to-volcanic textural gradation that links it to the Rhyolite Creek volcanics to the north (Israel et al., 2011), which may record tilting of the crustal section following terrane accretion (Johnston & Canil, 2007).

#### 3. Methods

## 3.1. Geologic Mapping

We performed 1:20,000-scale bedrock geologic mapping during the summers of 2018 and 2019 on base maps constructed from IfSAR Alaska and ArcticDEM digital terrain models. Mapping focused on along-strike correlation of major structures and bedrock units between the eastern Alaska Range and Clearwater mountains. Here, we present a new bedrock geologic map (Figure 2), compiled from the new mapping and prior mapping by Turner and Smith (1974), Smith (1981), Mooney (2010), Waldien et al. (2018), Twelker et al. (2020), and Waldien et al. (2021).

## 3.2. Separation Measurements

We measured the strike-slip separation of correlative rock units along the Denali fault on a NAD83 Alaska Albers Conic equal area projection using the *ruler* tool in ESRI Arcmap. If the body of rock used for measurement is cut by the Denali fault, then measurements represent the distance between the midpoints of the cut faces of the correlative bodies. If the body is not mapped as cut by the Denali fault, then we measured from the location on the fault nearest to the body. Differences in deformation, rotation, and erosional exhumation of the correlative rocks on opposite sides of the fault introduce uncertainty into the separation measurements that are difficult to quantify. A simple trigonometric calculation accounting for the dip of reactivated structures near the Delta River ( $\sim$ 40–70°N), the inferred differential exhumation between the Maclaren and Kluane schist ( $\sim$ 5–10 km), and the timing of the differential exhumation relative to slip on the Denali fault (post-32 Ma exhumation of Maclaren schist; Waldien et al., 2021) suggests that separation measurements have associated uncertainties as great as  $\sim$ 8.5 km. Instead of measurement-specific uncertainties, we infer that the measurements of strike-slip separation presented and discussed herein have associated uncertainties of less than  $\pm$ 10 km.

WALDIEN ET AL. 8 of 35



## 3.3. Zircon U-Pb Dating

## 3.3.1. Sample Preparation and Data Collection

We performed single-grain zircon U-Pb geochronology by Laser Ablation Quadrupole Inductively Couple Mass Spectrometry (LA-Q-ICP-MS) with three primary goals: (a) to fingerprint metasedimentary rocks by determining the sediment source areas of the protolith, (b) to estimate the maximum depositional age of the protolith, and (c) to date igneous intrusions in the map area. Mineral separation at UC Davis involved standard crushing techniques, a miner's gold pan, Frantz isodynamic separator, and Lithium Polytungstate and/or Methylene Iodide heavy liquids to concentrate zircon grains. For detrital zircon samples, we concentrated zircon grains enough to mount them by pouring; for igneous samples we hand-picked relatively large, inclusion-sparse zircon grains. Before LA-Q-ICP-MS analysis, we mounted the zircon grains and reference materials into 1 in. epoxy rounds, polished the rounds to expose the grain surface, and imaged them using a Cameca SX-100 Electron Microprobe. High-contrast back-scattered electron images allowed us to identify zoning and/or inherited cores in individual zircon grains, which informed our laser spot placement on each grain. We collected isotopic data using an Agilent 7700 series Q-ICP-MS coupled to a Photon Machines 193 nm Excimer laser ablation system at UC Davis. By polishing the grain mounts until zircon surfaces are exposed, rather than grinding to the core of the crystal, we were in some cases able to ablate through metamorphic rims into detrital cores. We obtained dates on both the rim and core using the VizualAge plug-in as implemented with the *U\_Pb\_geochronology3* data reduction scheme in the Iolite program (Paton et al., 2010; Petrus & Kamber, 2012). Supporting Information S1 contains detailed mineral extraction, analytical, data reduction, and data filtering methods used in the LA-Q-ICP-MS analyses. Supporting Information S2 contains the single-grain U-Pb data.

#### 3.3.2. Data Presentation

Our fingerprinting of metasedimentary protoliths is based on identifying distinctive populations of detrital zircon single-grain U-Pb dates. Each multimodal detrital zircon age data set contains analyses on at least 117 grains (Vermeesch, 2004). One detrital sample displays a unimodal age spectrum that is defined by 50 single-grain analyses. We represent the detrital U-Pb data as Kernel Density Estimates using the DZStats and Density Plotter programs (Saylor & Sundell, 2016; Vermeesch, 2012, respectively). Because many of the rocks analyzed in our study experienced amphibolite and upper greenschist metamorphic temperatures and thus may have experienced metamorphic recrystallization and/or lead loss (e.g., Hoskin & Schaltegger, 2003), we screened each analysis from the youngest age population of each sample to parse detrital and post-depositional metamorphic grains based on U content (ppm), U/Th ratio, imaged zoning patterns, age relative to the known ages of intrusions within the rock unit, and presence of age zoning reveled by laser depth profiling (Supporting Information S1). After parsing detrital and metamorphic grains, we calculated a maximum depositional age for each sample using the age of the youngest statistical population of the detrital grains (e.g., Herriott et al., 2019).

We used Isoplot (Ludwig, 2008) to determine the ages of igneous zircon populations by calculating the weighted mean of single grain dates with internal 2 s errors. Reported uncertainties of weighted mean ages represent 95% confidence interval internal uncertainties and the quadratic addition of external uncertainties (e.g., Horstwood et al., 2016; Supporting Information S1).

## 3.3.3. Statistical Tests

To assess the similarities between metasedimentary assemblages across the Denali fault, we performed statistical tests on the detrital zircon U-Pb age data using the multidimensional scaling program DZmds from Saylor et al. (2018). We focused our multidimensional scaling approach on the cross-correlation of probability density distributions because that approach has been shown to work well with both simple and complex data sets that range in sample size (Saylor & Sundell, 2016).

## 3.4. Hf Isotopic Data

To refine sediment source areas of metasedimentary protoliths, we performed Hf isotopic analysis on Mesozoic detrital zircon grains from two samples of Clearwater metasediment and one sample of Maclaren schist. Hf analyses employed a Photon Machines 193 nm Analyte G2 excimer laser (40  $\mu$ m spot size)

WALDIEN ET AL. 9 of 35



coupled to a Nu High-Resolution Multicollector ICP-MS at the Arizona Laserchron Center. The analytical approach used the sample bracketing technique, wherein we performed at least one analysis on each of the six reference materials (FC, Mud Tank, 91500, Temora, Plesovice, R-33, and Sri Lanka natural zircon) between every 15–20 unknowns. U-Pb age data for the analyzed grains are published in Waldien et al. (2021). Complete Hf analysis methods and data are available in Supporting Information S1.

### 3.5. 40Ar/39Ar Dating Methods

To determine the age of faulted volcanic rocks, we conducted <sup>40</sup>Ar/<sup>39</sup>Ar analyses at the Geochronology Laboratory at the University of Alaska, Fairbanks, where we crushed, sieved, washed, and hand-picked samples to obtain a pure phase of phenocryst-free groundmass or biotite. The sample aliquots and monitor mineral MMhb-1 (Samson & Alexander, 1987), which has an age of 523.5 Ma (Renne et al., 1994), were irradiated at McMaster University in Hamilton, Ontario, Canada. Upon their return from the reactor, we loaded the samples and monitors into 2 mm diameter holes in a copper tray and then loaded them into an ultra-high vacuum extraction line. The monitors were fused, and samples heated, using a 6-W argon-ion laser following the technique described in York et al. (1981), Layer et al. (1987), and Benowitz et al. (2014). Ar isotope measurements in this system are made using a VG-3600 mass spectrometer.

Supporting Information S3 contains detailed  $^{40}$ Ar/ $^{39}$ Ar analytical methods and contains the  $^{40}$ Ar/ $^{39}$ Ar data, wherein all ages are reported at the  $1\sigma$  level and calculated using the constants of Renne et al. (2010). The integrated age is the age given by the total gas measured and is equivalent to a potassium-argon (K-Ar) age. The spectrum provides a plateau age if three or more consecutive gas fractions represent at least 50% of the total gas release and are within two standard deviations of each other (mean square weighted deviation <2.5).

## 4. Results

## 4.1. New Mapping and Synthesis With Existing Maps

Our new mapping and U-Pb geochronology (discussed below) link the two regions of previously detailed mapping to the west (Smith, 1981) and east (Waldien et al., 2021). Accordingly, the mapping presented herein addresses the correlation between Mesozoic structures in the Clearwater Mountains (bold faults on Figure 2) and reactivated versions of those structures to the east (thin faults on Figure 2). The transition between reactivated and non-reactivated structures broadly coincides with the Maclaren River, which is also the location of a 1:250,000-scale quadrangle boundary (147°W) (cf., Csejtey et al., 1992; Nokleberg, Aleinikoff, Lange, et al., 1992; Wilson et al., 1998, 2015). To our knowledge, our study is the first to attempt to correlate the geology across the region. Our along-strike correlation of structures from the Clearwater Mountains to the eastern Alaska Range relies on the continuity of distinct rock packages between the two regions (Figure 2).

## 4.1.1. Geology of the Maclaren River Corridor

The 10-km-wide region between the Maclaren Glacier in the east and west fork of the Maclaren River in the west exposes the Maclaren schist, Clearwater metasediments, and the Wrangellia terrane (Figure 2). The structurally highest panel contains the Maclaren schist and a cross-cutting granodiorite body carried in the hanging wall of the Valdez Creek fault. South of the Valdez Creek fault, the Clearwater metasediments in this region are dominated by fine-grained metagreywacke and slate. East of the middle fork of the Maclaren River, the metasediments host a volumetrically small zoned gabbro-diorite intrusion. Diorite dikes near the intrusion are folded with the foliation in the Clearwater slate (Figure 3a). Due to the composition of the intrusion, the zonal structure, and the deformation shared with the host rocks, we infer that the intrusion is Early Cretaceous in age, which has been documented within the Clearwater metasediments to both the east and southwest (Mooney, 2010; Waldien et al., 2021). The Clearwater metasediments and associated intrusions were thrust southward over Wrangellia terrane rocks, which in this region are predominantly composed of Nikolai rocks and lesser Permian carbonate strata in the north near the Broxson Gulch fault. The Wrangellia strata host zoned intermediate-mafic composition granitoids.

WALDIEN ET AL. 10 of 35



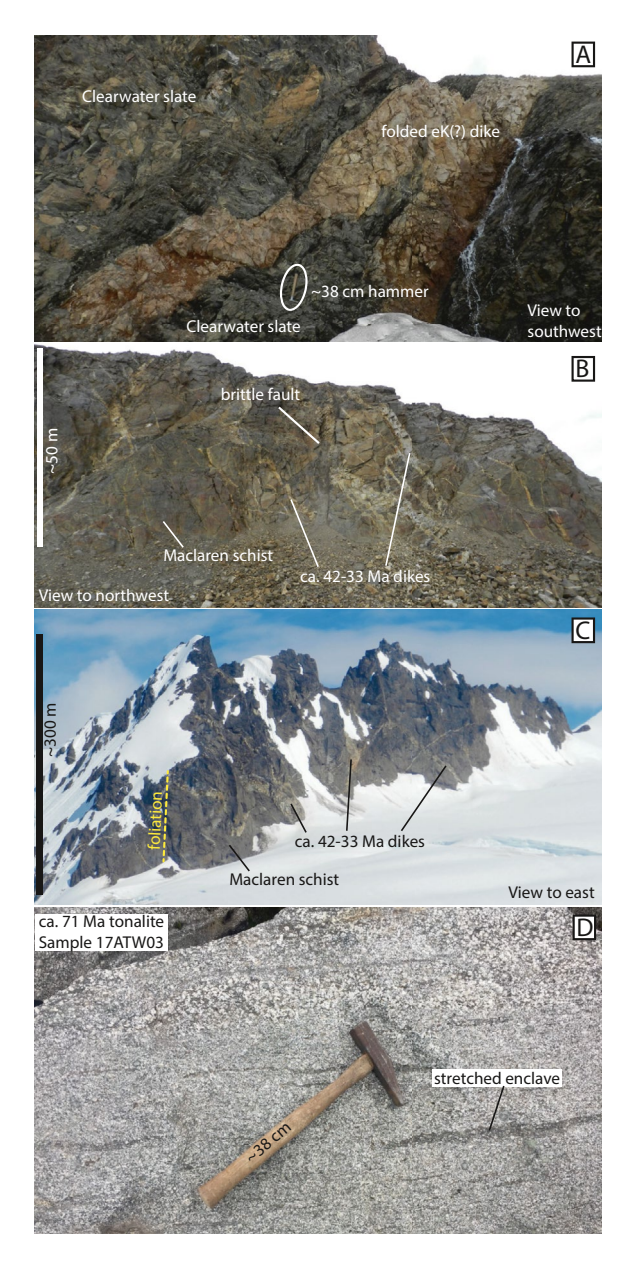


**Figure 3.** Field photos show key relationships in the area of Figure 2. (a) An intermediate dike associated with a zoned mafic-intermediate intrusion is folded with the foliation in the Clearwater slate. Photo is from an outcrop east of the middle fork of the Maclaren River. (b) Distributed brittle deformation is associated with the southern margin of the ca. 42–33 Ma plutonic suite. Nokleberg, Aleinikoff, Lange. et al. (1992) mapped this outcrop as an exposure of the Meteor Peak fault north of the Augustana Glacier. Dikes commonly cross-cut the metamorphic foliation in the Maclaren schist and are cut by small brittle faults. (c) Dikes associated with the ca. 42–33 Ma plutonic suite intersect the Maclaren schist foliation (yellow broken line) at multiple angles both south and north of the Meteor Peak fault. Photo is of an arête east of the Black Rapids Glacier. (d) Mafic enclaves in the ca. 74–65 Ma tonalite suite are highly stretched and commonly elongate in the down-dip direction. Photo is from sample location 17ATW03.

Along the west and middle forks of the Maclaren River, two approximately north-striking faults cut the dominant east-west structural fabric in the region. Although the faults are not exposed due to their location in the river valleys, their existence is implied by the misalignment of east-west-trending structures across the river valleys and the steep topographic gradient between the eastern Alaska Range and Susitna River valley.

A northeast-southwest-trending belt of topography separates the Maclaren River from the Susitna River valley (headwaters of Boulder Creek-Figure 2). Structures in the area include the Talkeetna fault and the herein-named Boulder Creek fault (BCF-Figure 2). The Talkeetna fault in the area is a steeply northwest-dipping structure exposed near the southeastern margin of the topography, which likely has limited Cenozoic slip, based on the modest offset of Late Cretaceous sedimentary rocks (Mooney, 2010; O'Neill et al., 2001). The map pattern suggests that the Boulder Creek fault dips steeply to the southeast and the topographic gradient across the fault trace marks the eastern boundary of the Susitna River valley. The Boulder Creek fault juxtaposes low-grade metagreywacke and slate of the Clearwater metasediments to the east against tonalite intrusions to the west (Figure 2). Thus, the southeast-side-up sense of slip on the Boulder Creek fault has cut out the higher-grade portion of the inverted metamorphic field gradient that is elsewhere present in the footwall of the Valdez Creek shear zone. Cataclastic deformation associated with the Boulder Creek fault overprints Late Cretaceous (e.g., Ridgway et al., 2002) ductile fabrics in the tonalite body, thus implying Cenozoic slip on the Boulder Creek fault. Although post-collisional brittle faults are present in the Clearwater Mountains to the southwest of the Boulder Creek fault (e.g., Mooney, 2010; Smith, 1981), the Valdez Creek shear zone does not appear to have experienced reactivation (e.g., Davidson et al., 1992) and is crosscut by the Boulder Creek fault (Figure 2).

#### 4.1.2. Along-Strike Correlation of Structures

Published synthesis maps of the eastern Alaska Range have correlated the Valdez Creek shear zone in the west with a structure east of the Maclaren Glacier named the Meteor Peak fault (Wilson et al., 1998, 2015). The correlation appears to have stemmed from the location of the two structures at the southern margin of plutons within the Maclaren schist and the inference that all of the plutons in the area intruded at ca. 70 Ma (e.g., Aleinikoff et al., 1981; Nokleberg, Aleinikoff, Dutro, et al., 1992; Nokleberg, Aleinikoff, Lange, et al., 1992).

Multiple lines of evidence indicate that the Valdez Creek shear zone and Meteor Peak fault are not correlative structures. Mainly, the Cenozoic evolution of structures east of the Maclaren River reveals that the Valdez Creek fault formed as a reactivation of the Valdez Creek shear zone during the Oligocene (Waldien et al., 2021). Moreover, our observations of the Meteor Peak fault between the Black Rapids and Augustana Glaciers (BRG and AG—Figure 2) show it to be an anastomosing brittle fault system that follows the southern margin of the 42-33 Ma phase of the East Susitna batholith. Dikes along the margin of the 42-33 Ma composite pluton are generally offset by fewer than 10 m and cataclasis associated with slip on strands of the Meteor Peak fault is poorly developed and restricted to discrete zones less than 5 m wide (Figure 3b). These

WALDIEN ET AL. 11 of 35



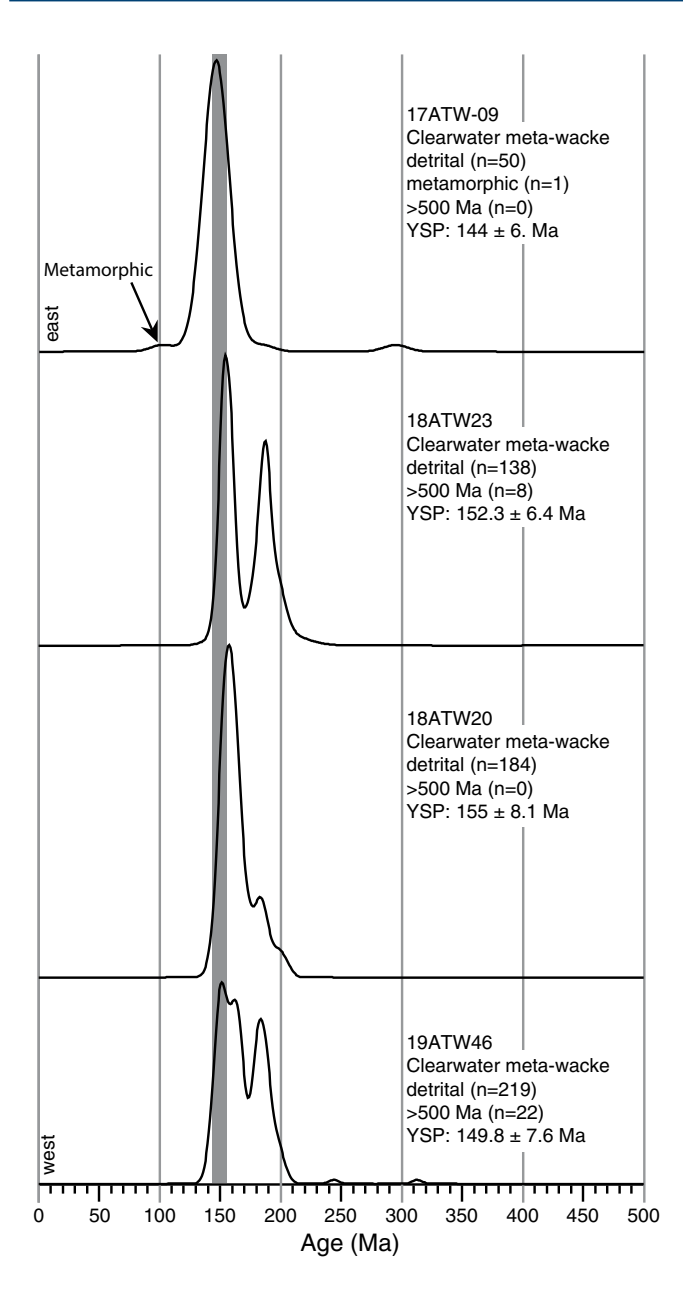


**Figure 4.** Kernel density estimate (KDE) plots of detrital zircon U-Pb age spectra (<500 Ma) for individual samples of Clearwater metagreywacke ordered from east (top) to west (bottom). The post-depositional metamorphic date is indicated for sample 17ATW-09. The dark gray bar at 155–144 Ma highlights the range of maximum depositional ages for individual samples. KDE plots were made using the DensityPlotter program (Vermeesch, 2012). YSP—weighted mean and 2 s uncertainty of the youngest statistical detrital population, interpreted as the maximum depositional age; n—number of analyses composing the plot.

observations together indicate that the Meteor Peak fault is a minor brittle fault that formed after ca. 33 Ma and thus is not related to the Late Cretaceous Valdez Creek shear zone.

After reconciling the structural complications near the headwaters of the Maclaren River described above, the along-strike continuity in metasedimentary belts reveals the transition between Cretaceous structures in the Clearwater Mountains and reactivated versions of those structures nearer to the Denali fault in the eastern Alaska Range (Figure 2). The Talkeetna-Broxson Gulch fault marks the boundary between the Wrangellia terrane and the Wrangellia-affiliated Clearwater metasediments. The Talkeetna fault in the Clearwater Mountains is a steeply dipping to sub-vertical crustal-scale fault with limited evidence for Cenozoic slip (Brennan et al., 2011; O'Neill et al., 2001). The Broxson Gulch fault in the Alaska Range is a moderately north-dipping reverse fault that is part of the post-32 Ma thrust system along the south flank of the Alaska Range (Waldien et al., 2021). The boundary between the Maclaren schist and Clearwater metasediments is the Valdez Creek shear zone in the west and Valdez Creek fault to the east. Late Cretaceous syn-collisional ductile thrusting is preserved in the Valdez Creek shear zone in the Clearwater Mountains (Davidson et al., 1992), whereas the shear zone has been reactivated as a brittle fault in the eastern Alaska Range (Waldien et al., 2021). The Meteor Peak fault appears to have no correlative structure in the Clearwater Mountains.

## 4.2. Zircon U-Pb Dating

## 4.2.1. Metasedimentary Rocks

Detrital zircon U-Pb age spectra from four samples of Clearwater metagreywacke (621 grains, Figure 4) are dominated by Jurassic grains. Three of the samples (18ATW20, 18ATW23, and 19ATW46) display bimodal distributions with modes at ca. 155 and 185 Ma. Pre-Jurassic grains in two of the samples define subordinate populations at ca. 550 Ma, 1,100–1,800 Ma, and 2,500–2,800 Ma. Sample 17ATW09 yielded a unimodal age peak centered at ca. 150 Ma. Maximum depositional ages of the samples range from ca. 155–144 Ma. Near the middle fork of the Maclaren River, sample 19ATW39 is a quartz-muscovite phyllite interfoliated with the Clearwater slate, which we interpret as a metamorphosed felsic tuff based on the composition and unimodal distribution of single-grain zircon dates, yielded a weighted mean age of  $160.4 \pm 1.5 \, \text{Ma}$  (Table 2).

Detrital zircon U-Pb age spectra from five samples of Maclaren schist (1,094 grains; Figure 5) display: (a) dominant Mesozoic age populations at ca. 110–85, 160–145, and 200–180 Ma, although the relative proportions vary; (b) a subordinate population of ca. 370–330 Ma grains; (c) Proterozoic and Archean grains in all samples, although abundances are low; (d) post-depositional metamorphic rims or recrystallized domains with dates of ca. 84–55 Ma (Supporting Information S1); and (e) mid-Cretaceous maximum depositional ages of ca. 91–88 Ma.

#### 4.2.2. Plutonic Rocks

Multiple intrusive phases are present in the study area, each of which has a distinctive age-composition relationship that is unique to the thrust panels that host them. Here, we present the ages of the plutonic suites from structurally highest (youngest) to structurally lowest (oldest) level. The new ages are reported in Table 2 and Supporting Information S4 contains additional details.

WALDIEN ET AL. 12 of 35

 Table 2

 Igneous Zircon U-Pb Analytical Results

Host rocks	Sample name	Latitude (°N)	Longitude (°W)	Rock type	Weighted mean 206Pb/238U Age (Ma) <sup>a</sup>	MSWD	Number of acceptable grains in age calculation <sup>b</sup>	Total number of zircons analyzed <sup>c</sup>
Clearwater metasediments	19ATW39	63.3318	146.6695	Meta-felsic Tuff	160.4 ± 1.5	0.74	22	22
Maclaren schist	19ATW79	63.3548	146.6812	Quartz Monzonite	$51.9 \pm 0.6$	3.2	45	53
Maclaren schist	19ATW40	63.4155	146.7800	Tonalite	$64.6 \pm 0.7$	1.9	46	49
Maclaren schist	18ATW21	63.3070	146.9629	Tonalite	$68.3 \pm 1.3$	3.7	33	40
Maclaren schist	17ATW03	63.2163	147.0698	Tonalite	$70.5 \pm 1.0$	2.6	28	35
Maclaren schist	19ATW66	63.3473	146.8130	Biotite-garnet leucogranite	$75.8 \pm 1.9$	1.14	$9^{d}$	29
Clearwater metasediments	19ATW55	63.2699	146.8861	Diorite	$53.1 \pm 0.6$	0.71	16	21
Wrangellia terrane	14ATW50	63.2483	145.4092	Granodiorite	$309.8 \pm 3.9$	3.2	30	32
Wrangellia terrane	17ATW11	63.3498	145.6523	Granodiorite	$307.2 \pm 6.1$	0.9	12	14
Wrangellia terrane	16CSR17	63.3330	146.3319	Granite	$306.3 \pm 4.0$	0.48	14	16
Wrangellia terrane	15DR140	63.3054	146.6025	Quartz syenite	$144.1 \pm 2.3$	1.9	15	17
Wrangellia terrane	13ET270	63.2216	146.7085	Diorite	$129.8 \pm 2.4$	1.5	31	31
Wrangellia terrane	19ATW81	63.2986	146.6962	Tonalite	$112.9 \pm 1.3$	1.7	31	31

Note. MSWD, mean square weighted deviation.

<sup>a</sup>Weighted mean uncertainties represent quadratic addition of internal and external uncertainties at 2s. <sup>b</sup>The number of analyses that passed the filtering criteria. <sup>c</sup>The total number of analyzed grains. <sup>d</sup>Rim analyses: Filtering criteria relaxed to allow more analyses in age calculation.

Maclaren schist: The Maclaren schist hosts three intrusive suites that are distinguishable based on age and petrographic features. The youngest phase intruded the structurally highest portion of the Maclaren schist adjacent to the Denali fault. Compositions in this plutonic suite vary and include biotite tonalite, horn-blende-biotite granodiorite, and biotite-muscovite granite. The margins of the bodies are zones of mutually crosscutting dikes that crosscut the metamorphic foliation in the Maclaren schist (Figure 3c). Many samples from the suite display a high-temperature fabric defined by the alignment of amphibole and plagioclase grains. Some samples display sub-solidus mylonitic fabrics. Samples from this suite yielded U-Pb zircon dates ranging from ca. 42 to 33 Ma (Benowitz et al., 2011; Regan et al., 2021).

An intermediate-age plutonic suite intruded the structurally lowest portion of the Maclaren schist in the Alaska Range and is cut by the Valdez Creek fault (Waldien et al., 2021). Plutons in this suite consist of non-foliated biotite or hornblende granodiorite with late biotite-muscovite-K-feldspar pegmatite veins. The margins of the plutons crosscut the Maclaren schist foliation (Waldien et al., 2021). One sample from this suite near the middle fork of the Maclaren River (19ATW79) yielded a U-Pb zircon weighted mean date of  $51.9 \pm 0.6$  Ma.

The oldest intrusions in the Maclaren schist are tonalitic, found in the western portion of the study area near Boulder and Valdez Creeks (Figure 2), and generally contain a well-developed, high-temperature foliation defined by strained mafic enclaves and aligned biotite, plagioclase, and amphibole (Davidson et al., 1992; Figure 3d). The tonalite bodies display reaction textures wherein primary clinopyroxene has reacted to amphibole and then to biotite. Three samples from the tonalite suite yielded U-Pb zircon weighted mean dates of  $64.6 \pm 0.7$  (19ATW40),  $68.3 \pm 1.3$  (18ATW21), and  $70.5 \pm 1.0$  Ma (17ATW03). In the headwaters of the west fork of the Maclaren River, the tonalite suite is associated with a garnet-and-biotite-bearing leucocratic body. The leucocratic body generally lacks internal structure and forms a series of disseminated veins and dikelets into the Maclaren schist along the margins. Zircon crystals separated from the leucocratic body (sample 19ATW66) display core-rim textures wherein the cores yield ages common of detrital zircons within the Maclaren schist and the rims yielded a weighted mean date of  $75.8 \pm 1.9$  Ma.

Clearwater metasediments: Sample 19ATW55 came from a small (<50 m across) body of non-foliated horn-blende diorite, which intrudes the Clearwater metasediments east of Boulder Creek and yielded a weighted

WALDIEN ET AL. 13 of 35



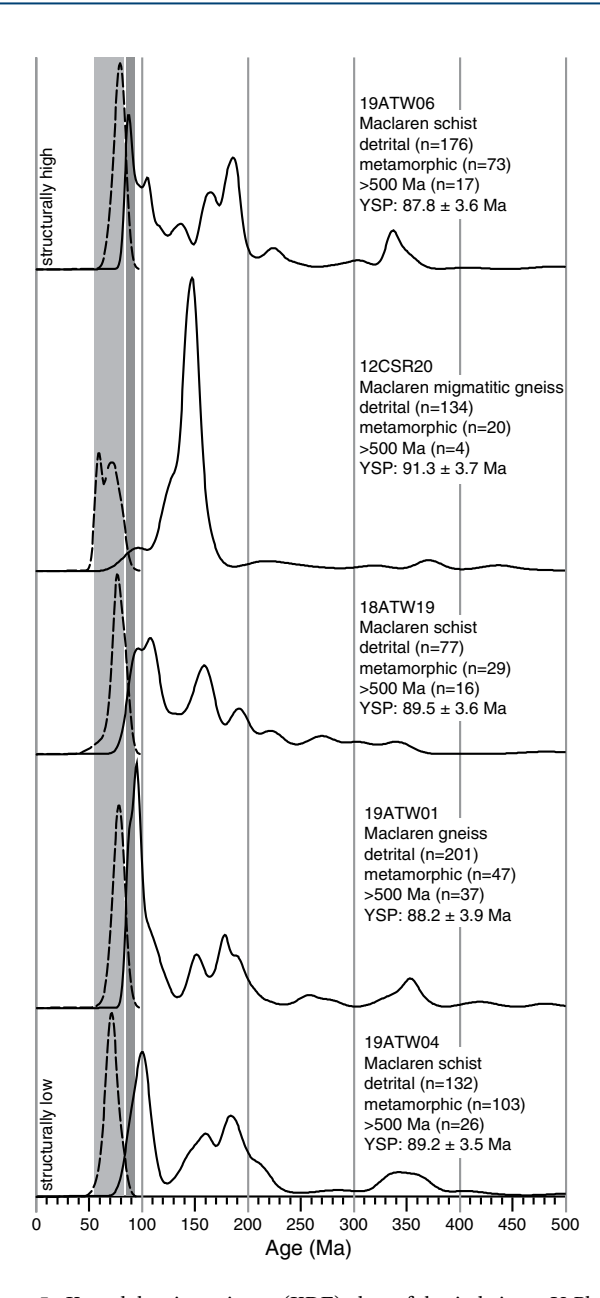


**Figure 5.** Kernel density estimate (KDE) plots of detrital zircon U-Pb age spectra (<500 Ma) for individual samples of Maclaren schist ordered from structurally highest (top) to structurally lowest (bottom). Post-depositional metamorphic dates are shown as a dashed line KDE curve and are outlined by a light gray bar at ca. 84–55 Ma. The dark gray bar at 91–87 Ma indicates the range of maximum depositional ages for individual samples in this study. KDE plots were made using the DensityPlotter program (Vermeesch, 2012). YSP—weighted mean and 2 s uncertainty of the youngest statistical detrital population, interpreted as the maximum depositional age; n—number of analyses in the plot.

mean date of 53.1  $\pm$  0.6 Ma. The new date on sample 19ATW55 expands the known age range of small volume intrusions within the Clearwater metasediments, which elsewhere have been dated at ca. 142, 102, and 63–68 Ma (Davidson & McPhillips, 2007; Mooney, 2010; Waldien et al., 2021).

Wrangellia terrane: Our zircon U-Pb dating of plutonic rocks bears on two phases of magmatism within the Wrangellia terrane (Figure 2). The oldest dates come from a tabular granodiorite body east of the Delta River, which yielded weighted mean dates of 309.8  $\pm$  3.9 Ma (14ATW50) and 307.2  $\pm$  6.1 Ma (17ATW11). Similarly, a composite granodiorite-granite body near the Eureka Glacier (16CSR17) yielded a weighted mean date of 306.3  $\pm$  4.0 Ma. Younger dates come from the Maclaren River corridor, where concentric diorite-granodiorite bodies with marginal diorite-gabbro dike systems intrude Skolai and Nikolai rocks. Samples from these bodies yielded weighted mean dates of 144.1  $\pm$  2.3 Ma (15DR140—hornblende diorite body), 129.8  $\pm$  2.4 Ma (13ET270—biotite granodiorite body), and 112.9  $\pm$  1.3 Ma (19ATW81—hornblende diorite dike).

## 4.3. Hf Isotopic Signatures of Mesozoic Detrital Zircon Grains

Detrital zircon grains from both age populations in the Clearwater meta-sediments (ca. 155 and 185 Ma) display juvenile  $\epsilon Hf$  isotopic signatures (Figure 6). Zircon grains belonging to the Early Jurassic age population in sample 16ATW10 display  $\epsilon Hf$  values ranging from +4 to +11, whereas Early Jurassic grains in sample 15ATW23 have values of +5 to +16. Late Jurassic zircon grains in sample 16ATW10 yielded  $\epsilon Hf$  values ranging from +6 to +10 and sample 15ATW23 contains grains with values of +8 to +15.

Hf isotopic signatures from detrital zircon grains in the Maclaren schist (sample 15ATW29) show a range of juvenile and evolved  $\epsilon$ Hf compositions (Figure 6). Early Jurassic zircon grains display  $\epsilon$ Hf values ranging from -10 to +12. Late Jurassic grains are more juvenile and display  $\epsilon$ Hf values ranging from +2 to +15. The small population (three grains) of ca. 100 Ma zircon grains display a spread of  $\epsilon$ Hf values ranging from -18 to +13. Circa 90 Ma detrital zircon grains have more juvenile  $\epsilon$ Hf compositions ranging from +8 to +13.

## 4.4. 40Ar/39Ar Dates on Volcanic Strata

Volcanic strata overlap and are faulted against Paleozoic Wrangellia rocks along the southern margin of the Alaska Range east of the Delta River. The volcanic strata are generally felsic in composition, yet mafic flows, mafic dikes, and conglomeratic strata are found locally (Bond, 1976; Gillis et al., 2019; Hults & Athey, 2011; Waldien et al., 2018). Four felsic extrusive samples southeast of the Gulkana Glacier in our study area (Figure 2) yielded  $^{40}\mathrm{Ar}/^{39}\mathrm{Ar}$  dates of 50.9  $\pm$  0.5 Ma (12HODO—rhyodacite tuff, biotite plateau age), 45.5  $\pm$  0.2 Ma (46GUNN—dacite flow, whole rock plateau age), 49.3  $\pm$  0.7 Ma (15BG216—dacite flow, whole

rock weighted mean age), and  $49.8 \pm 0.3$  Ma (15BG209—rhyodacite tuff, whole rock weighted mean age) (Table 3; Supporting Information S3).

WALDIEN ET AL. 14 of 35



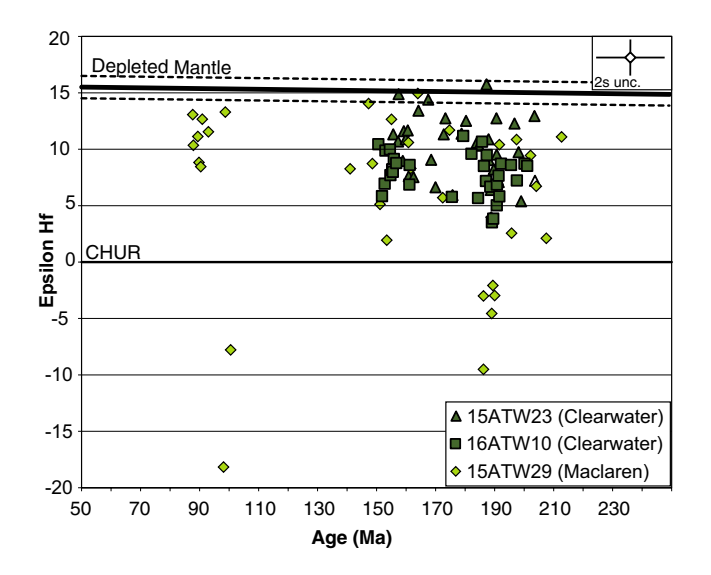


**Figure 6.** Epsilon  $(\varepsilon)$  Hf-versus-age plot of single grain analyses from the Maclaren schist and Clearwater metasediments (colored as in Figure 1). The maximum 2 s uncertainties (unc.) associated with the data points are represented by the data symbol in the upper right. CHUR—chondritic uniform reservoir.

#### 5. Discussion

# **5.1. Protolith Provenance and Paleogeographic Setting for Metasedimentary Assemblages**

#### 5.1.1. Clearwater Metasediments

Detrital zircon U-Pb age spectra and Hf isotopic signatures suggest that the Clearwater metasedimentary rocks formed along the paleo-eastern margin of the Wrangellia composite terrane during the Late Jurassic-Early Cretaceous. Although terranes along the Laurentian margin contain Jurassic rocks that could have supplied Jurassic zircon grains to the Clearwater metasediment protolith (e.g., Allan et al., 2013; Gehrels et al., 2009; Sack et al., 2020), the general scarcity of pre-Mesozoic grains and juvenile εHf values of the Jurassic grains together suggest that the protolith sediment was derived from juvenile arc crust within the Wrangellia composite terrane (Figures 4 and 7). Jurassic source areas within the Wrangellia composite terrane include Chitina arc rocks (ca. 160-140 Ma: Beranek et al., 2017; Day et al., 2016; Roeske et al., 2003) and Talkeetna arc rocks (ca. 205-150 Ma: Amato et al., 2007; Rioux et al., 2007; Roeske et al., 1989). The maximum depositional ages of the Clearwater metasediments and the ages of inter-bedded volcanics indicate that the strata were deposited from ca. 160-144 Ma (Mooney, 2010; Table 2). Intrusion of a ca. 142 Ma alkali gabbro in the Clearwater Mountains post-dates deposition of the Clearwater protolith strata (Mooney, 2010; Figure 2).

Depositional ages, interpreted sediment source areas, detrital zircon Hf signatures, and stratigraphic features place the Clearwater metasediments among a suite of Late Jurassic-Early Cretaceous basinal assemblages that span the inboard (north and east in present coordinates) margin of the Wrangellia composite terrane from western Alaska to British Columbia. From west to southeast, these basinal assemblages include the Koksetna River sequence (Box et al., 2019; Hults et al., 2013; Wallace et al., 1989), Clearwater metasediments (Mooney, 2010; Waldien et al., 2021; this study), Nutzotin Mountains sequence (Fasulo et al., 2020; Manuszak et al., 2007; Trop et al., 2020), Dezadeash Formation (Lowey, 2019), Vand Creek assemblage (Vice, 2017), and western Gravina belt (Yokelson et al., 2015). It is not necessary that these basinal assemblages were linked as a single basin system at the time of deposition (e.g., Hults et al., 2013); however, the similarities in depositional setting and interpreted provenance within the Wrangellia composite terrane do suggest that they together represent a regionally extensive clastic marine sequence linked to the paleo-eastern margin of the Wrangellia composite terrane. An Early-to-mid-Cretaceous phase of strike-slip faulting may have translated the marine sequence relative to the Wrangellia composite terrane (e.g., Gehrels et al., 2009; McDermott et al., 2019; Mooney, 2010; Yokelson et al., 2015), yet the displacement history for that structure remains unclear.

**Table 3**<sup>40</sup>Ar/<sup>39</sup>Ar Analytical Results for Volcanic Rocks

Sample name	Latitude (°N)	Longitude (°W)	Rock type	Phase analyzed	Grain size analyzed (um)	Integrated age (Ma) <sup>a</sup>	Plateau age (Ma) <sup>a</sup>	Plateau information
12HODO	63.2233	145.4485	Rhyodacite tuff	Biotite	500-1000	$50.9 \pm 0.3$	$50.9 \pm 0.5$	6 of 12 steps 91.8% 39Ar release MSWD = 1.91
46GUNN	63.2108	145.4025	Dacite flow	Whole rock	212-500	$45.1 \pm 0.1$	$45.5 \pm 0.2$	3 of 8 fractions 49.7% 39Ar release MSWD = $1.55$
15BG216	63.2098	145.3516	Dacite flow	Whole rock	212-500	$48.8 \pm 0.4$	$49.3 \pm 0.7^{b}$	7 of 8 fractions 94% 39Ar release MSWD = $3.34$
15BG209	63.2123	145.3635	Rhyodacite tuff	Whole rock	212-500	$49.6 \pm 0.4$	$49.8 \pm 0.3^{b}$	2 of 8 fractions 50.8% 39Ar release MSWD = $3.18$

Note. MSWD, mean square weighted deviation.

<sup>a</sup>Uncertainties are 1s. <sup>b</sup>Did not meet all the criteria of a plateau age, hence a weighted average age is presented.

WALDIEN ET AL. 15 of 35



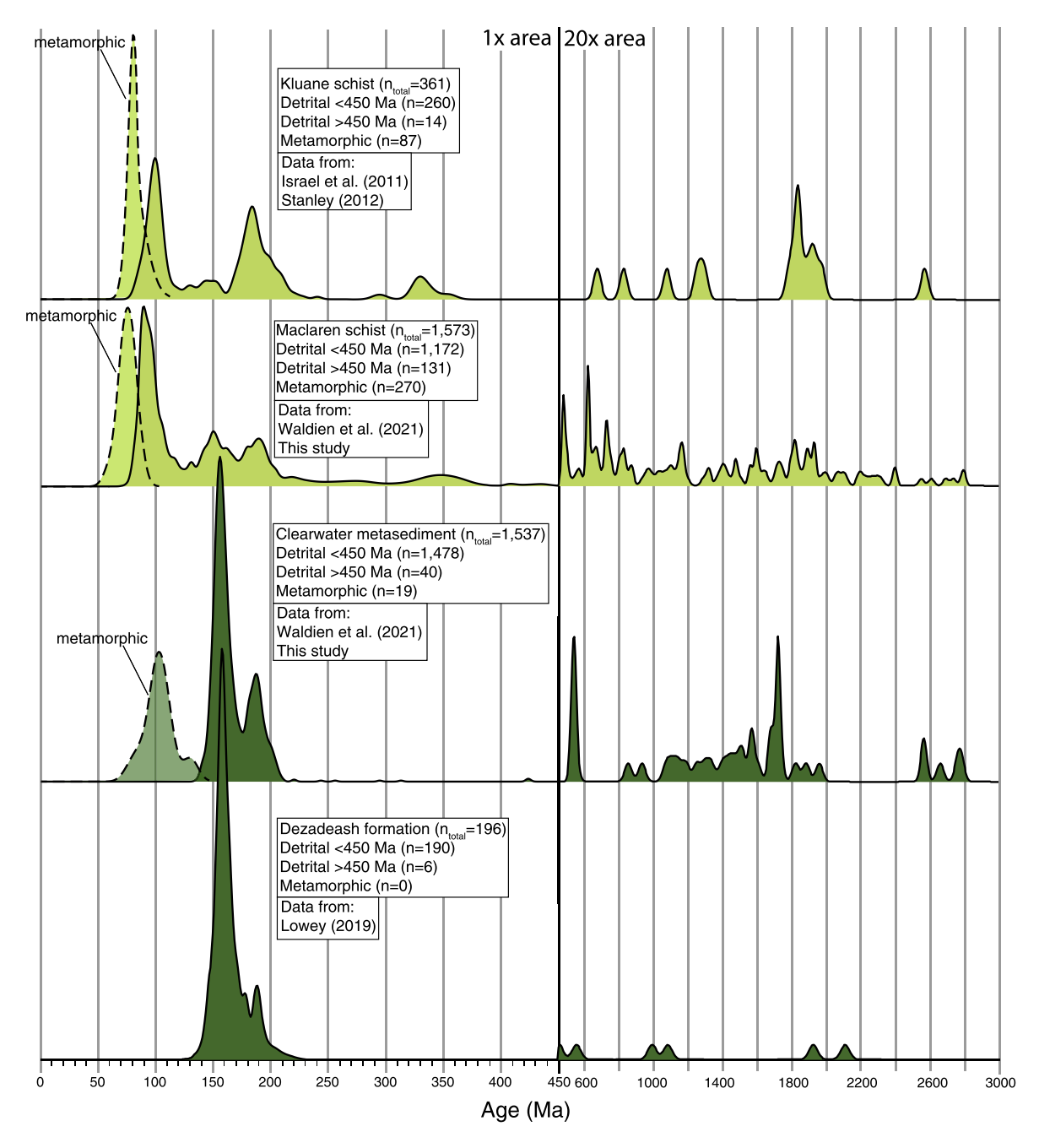


**Figure 7.** Kernel density estimate (KDE) plots of compiled detrital zircon U-Pb age spectra for the Maclaren schist, Kluane schist, Clearwater metasediments, and Dezadeash Formation, colored as in Figure 1. Note the change in horizontal scale and the 20× increase in area under the curves at 450 Ma. The dashed line KDE curves represent post-depositional metamorphic grains, which are plotted at half the vertical scale of the <450 Ma detrital age spectra. KDE plots were made using the DZStats and Density Plotter programs (Vermeesch, 2012; Saylor & Sundell, 2016).

#### 5.1.2. Maclaren Schist

Detrital zircon U-Pb age spectra indicate that the protolith of the Maclaren schist was deposited into a basin between previously accreted Cordilleran terranes to the east and the Wrangellia composite terrane to the west at ca. 94–86 Ma. As with other detrital zircon U-Pb studies of the Maclaren schist (Link, 2017; Waldien et al., 2021), the samples presented herein comprise dominant detrital age populations at ca. 100–85, 200–145, and 370–330 Ma (Figures 5 and 7). The ubiquitous presence of pre-Mesozoic grains suggests that the protolith strata received sediment from regions within the Yukon-Tanana terrane and paratautochthonous

WALDIEN ET AL. 16 of 35



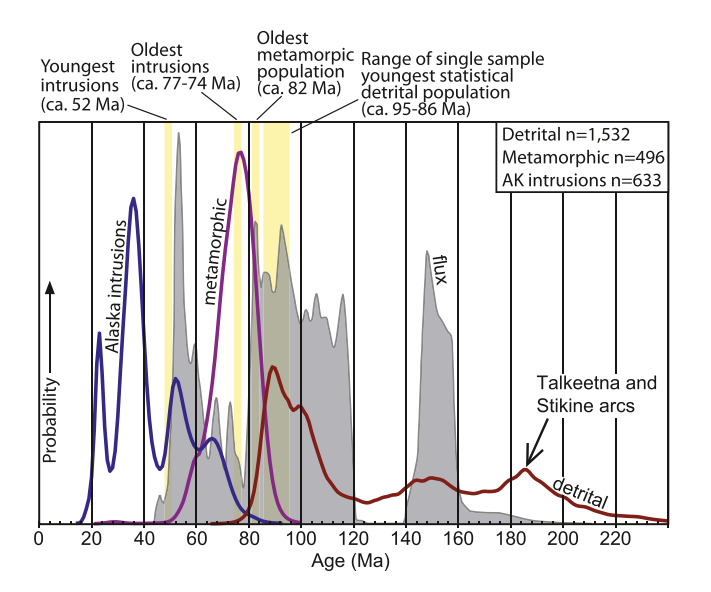


Figure 8. Probability density plot comparing ≤240 Ma detrital (dark red curve) and metamorphic (purple curve) U-Pb zircon dates from the Maclaren-Kluane schist (this study; Israel et al., 2011; Stanley, 2012; Waldien et al., 2021) with the 240–40 Ma magmatic flux curve of the central Coast Mountains arc (filled gray curve; from Gehrels et al., 2009). LA-ICPMS dates from plutonic rocks within the Maclaren and Cottonwood schists constitute the blue curve (this study; Regan et al., 2021). The vertical yellow bars highlight important time periods that are shared in the evolution of the Maclaren-Kluane schist and associated batholithic rocks. Note how magmatism within the Maclaren and Cottonwood schists (Alaska intrusions) outlasts the shared magmatism. n—number of grains used to generate each curve.

North America (e.g., Dusel-Bacon & Williams, 2009; Dusel-Bacon et al., 2017; Gehrels & Pecha, 2014; Pecha et al., 2016; Piercey & Colpron, 2009). The overlap between periods of high magmatic flux in the Coast Mountains arc and the populations of detrital zircon grains in the Maclaren schist further suggests that the protolith sediment was sourced from rocks along the western margin of North America (Figure 8). Hf isotopic compositions from Mesozoic zircon grains in the Maclaren schist display a range of juvenile and evolved &Hf values that may record either isotopic heterogeneity in the peri-continental source area (e.g., Cecil et al., 2011; Piercy et al., 2003; Sack et al., 2020), sediment sourced from igneous belts built upon both the Wrangellia composite terrane and the North American margin, and/or sediment recycling from the Clearwater metasediments. All samples presented in this study display a population of metamorphic growth rims dated at ca. 84–55 Ma, which we interpret to post-date deposition (Figures 5 and 7; Supporting Information S1).

The Maclaren schist displays both similarities and differences compared to other Mesozoic basinal assemblages in the suture zone between the Wrangellia composite terrane and the Mesozoic North American margin. Ca. 110–90 Ma strata are exposed in the northern domain of the Kahiltna assemblage throughout the central and western Alaska Range (Box et al., 2019; Hampton et al., 2007, 2010; Hults et al., 2013; Kalbas et al., 2007; Romero et al., 2020). The eastern Gravina belt of southeastern Alaska contains similar continental-derived strata, yet detrital zircon age spectra and available biostratigraphic information suggest the strata were deposited at ca. 120–110 Ma (Berg et al., 1972; Kapp & Gehrels, 1998; Yokelson et al., 2015). The Maclaren schist, northern Kahiltna, and eastern Gravina assemblages all share a ca. 120–100 Ma detrital zircon age population that, in addition to Precambrian grains, likely records a sediment source from igneous belts corresponding to the Teslin, Whitehorse, and Coffee Creek plutonic suites built upon the western margin of North

America (Allan et al., 2013; Tempelman-Kluit & Wanless, 1975). The additional presence of Jurassic age populations with juvenile & Hf signatures in these basin assemblages permits sediment input from approaching outboard terranes as the marine basin closed. The Maclaren schist, however, differs from much of the northern Kahiltna and eastern Gravina strata in that it is 10–30 Myr younger and experienced amphibolite facies metamorphism during the collision of the Wrangellia composite terrane. The sum of information suggests that the protolith of the Maclaren schist formed in one of the youngest, if not the youngest, known syn-collisional marine basins between the Wrangellia composite terrane and North American margin.

## 5.2. Correlative Rock Packages and Strike-Slip Separation

Our restoration of the Denali fault system relies on the correlation of metasedimentary, plutonic, and volcanic belts across the fault. The correlative rock packages are listed in Table 1, located as boxed numbers in Figure 1, and described below.

#### 5.2.1. Clearwater-Nutzotin-Dezadeash (Meta)Sedimentary Strata

Our new data from the Clearwater metasediments suggest that they correlate with the Nutzotin Mountains sequence and Dezadeash Formation. Presently, the Clearwater metasediments are exposed south of the Denali fault in the eastern Alaska Range, the Nutzotin Mountains sequence is exposed south of the Denali fault and east of the Totschunda fault in eastern Alaska, and the Dezadeash Formation is exposed the northeast of the Denali fault in southwestern Yukon (Figure 1). A correlation between the Dezadeash and Nutzotin strata was initially proposed based on age and sedimentological features that are shared between the two successions (Eisbacher, 1976). Later work by Lowey (1998) documented the existence of a paleochannel carrying distinctive limestone boulders incised into the Dezadeash and Nutzotin strata, which has been offset ~370 km by the Denali fault. More recent studies involving detrital zircon U-Pb

WALDIEN ET AL. 17 of 35



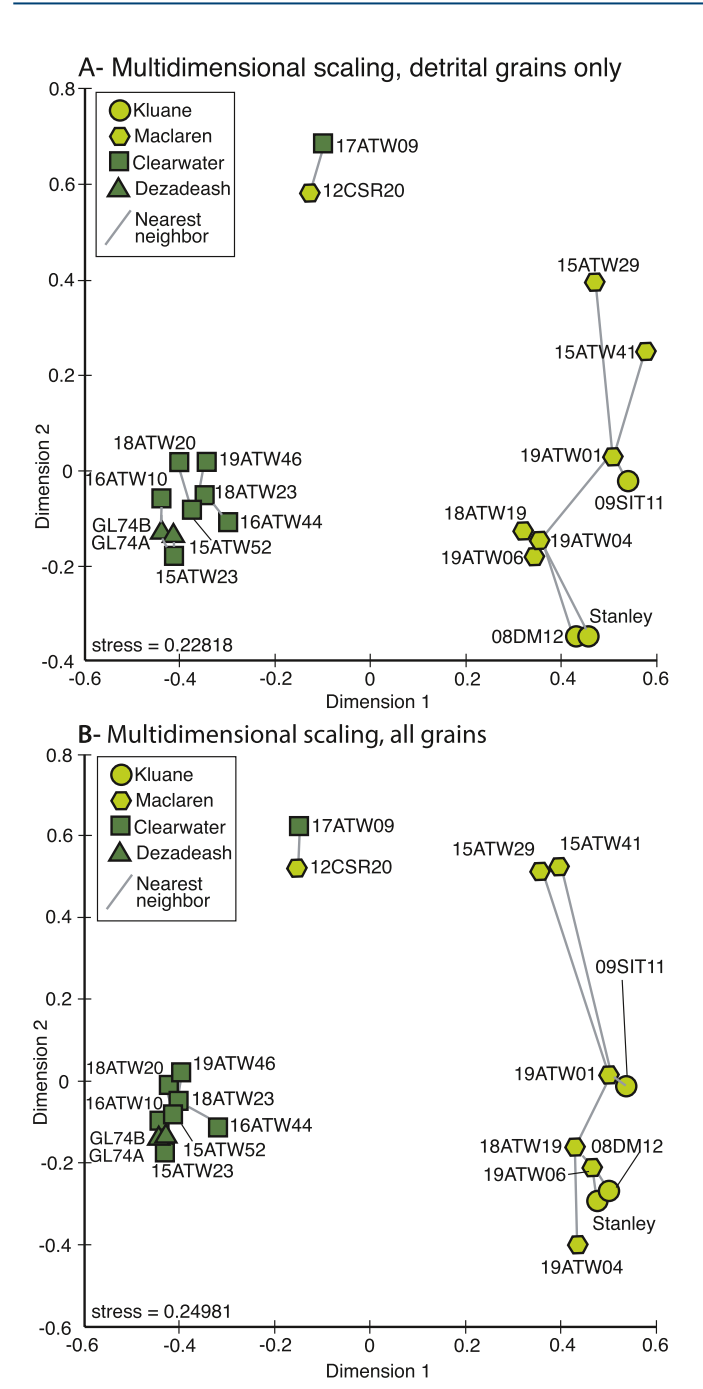


**Figure 9.** Multidimensional scaling (MDS) plots of U-Pb age spectra from individual samples of Maclaren schist (hexagons), Kluane schist (circles), Clearwater metasediments (squares), and Dezadeash Formation (triangles). All symbols are colored to match map units in Figure 1. (a) MDS of U-Pb age spectra excluding post-depositional metamorphic grains. (b) MDS of U-Pb age spectra including post-depositional metamorphic grains. MDS plots were made using the DZmds program of Saylor et al. (2018). Maclaren and Clearwater data are from this study and Waldien et al. (2021); Kluane data are from Israel et al. (2011) and Stanley (2012); Dezadeash data are from Lowey (2019).

dating show similar age populations and distribution of Jurassic and Early Cretaceous zircon grains within the Dezadeash Formation, Nutzotin Mountains sequence, and Clearwater metasediments, which are interpreted to be sourced from Jurassic arcs built upon the Wrangellia composite terrane (Fasulo et al., 2020; Link, 2017; Lowey, 2019; Manuszak et al., 2007; Mooney, 2010; Trop et al., 2020; Waldien et al., 2021). Among the dated samples, the Dezadeash Formation and Clearwater metasediments of the Alaska Range show the greatest similarity because they both include a ca. 185 Ma age population that is absent from the Nutzotin strata and Clearwater metasediments of the Clearwater mountains (cf., Fasulo et al., 2020; Lowey, 2019; Mooney, 2010; Trop et al., 2020; Figures 7 and 9). Hf isotopic signatures from detrital zircon grains in the Clearwater metasediments show juvenile &Hf values (Figure 6), which compare well with juvenile whole rock ENd values from the Dezadeash Formation (Lowey, 2011) and juvenile zircon EHf values from age-equivalent detrital zircon grains in the Nutzotin Mountains sequence (Fasulo et al., 2020). Biostratigraphic and U-Pb radioisotopic ages indicate that Clearwater-Nutzotin-Dezadeash rocks were deposited from ca. 160 to 135 Ma (Fasulo et al., 2020; Lowey, 2011; Mooney, 2010; Trop et al., 2020; Figure 4).

Because the Clearwater, Nutzotin, and Dezadeash rocks are presently separated from each other along the Denali fault system, their restoration requires slip on both the Denali fault and Totschunda fault. The incised paleochannel records ~370 km of dextral separation between the Dezadeash Formation and Nutzotin Mountains sequence (Lowey, 1998). The measured 80–90 km of separation between the Clearwater and Nutzotin strata likely resulted from right-lateral slip transfer from the Totschunda fault to the Denali fault (e.g., Berkelhammer et al., 2019; Brueseke et al., 2019; Waldien et al., 2018). Cumulative translation and dissection of the Clearwater, Nutzotin, and Dezadeash assemblages record at least 465 km of separation on the Denali fault.

## 5.2.2. Alaska-Type Ultramafic Intrusions

Ultramafic-to-intermediate intrusive bodies within the Clearwater metasediments (AK) and Dezadeash Formation (YT) correlate based on petrography and possibly age. Early workers in both the Clearwater metasediments and Dezadeash Formation had described pegmatitic biotite-hornblende clinopyroxenite cumulate bodies associated with granodiorite (Eisbacher, 1976; Stout, 1965). Subsequent work established that these bodies display geochemical characteristics that classify them as Alaska-type zoned ultramafic suites (Sturrock et al., 1980; Waldien et al., 2021). In Yukon, the Pyroxenite Creek ultramafite and associated Shorty Creek granodiorite hosted within the Dezadeash Formation yielded amphibole and biotite K-Ar dates ranging from ca. 126 to 106 Ma (Eisbacher, 1976). In the Alaska Range, petrographically similar biotite-hornblende clinopyroxenite cumulates and associated granodiorite bodies intrude the Clearwater metasediments north of Ann Creek and have been dated at ca. 102 Ma (Stout, 1965; Waldien et al., 2021). Due to similarities in petrography, structural position, host rocks, proximity to the Denali fault, and general age information, it is possible that the Pyroxenite Creek and Ann Creek zoned ultramafic bodies represent a single body that was dissected by the Denali fault. If correlative, the bodies would record up to 505 km of dextral separation across the Denali fault.

WALDIEN ET AL. 18 of 35



#### 5.2.3. Maclaren-Kluane Schist

The Maclaren schist (AK) and Kluane schist (YT) correlate based on petrography, metamorphic history, and detrital zircon U-Pb age spectra (Figures 7 and 9). Both schist bodies display a dominant foliation that dips toward North America (north or northeast). The foliation in both bodies contains porphyroclasts of garnet and distinctive "black" plagioclase, both of which contain curved inclusion trails defined by rutile and graphite (Mezger, Chacko, et al., 2001; Stanley, 2012; Waldien et al., 2021). The shared metamorphic history involves an early Barrovian series path that peaked at Temperature (T)  $\sim 500^{\circ}$ C and Pressure (P)  $\geq 7$  kbar, followed by a phase of isothermal decompression, and subsequent Buchan series conditions of T ~550-750°C and  $P \le 5$  kbar (Davidson & McPhillips, 2007; Mezger, Chacko, et al., 2001). In the Alaska Range, the eastern portion of the Maclaren schist experienced a post-32 Ma retrograde metamorphic event that has been linked to the reactivation of adjacent structures (Waldien et al., 2021). The absence of the retrograde event in the Kluane schist does not preclude the correlation because the retrogression took place after the bodies were separated by the Denali fault (see Section 5.3). Detrital zircon age spectra from the Maclaren and Kluane schists both contain a predominance of Mesozoic grains accompanied by smaller Paleozoic and Precambrian populations and metamorphic overgrowth rims ranging in age from ca. 84 to 55 Ma (Figures 7 and 9). All published detrital zircon U-Pb data sets yield maximum depositional ages between 95 and 86 Ma (Figure 5; Supporting Information S2). Because each schist body is cut obliquely by the Denali fault and no discrete diagnostic feature within the schists has been found for correlation, the measurement of strike-slip separation between the bodies is approximate. However, measuring from center to center of the cut face of each body yields ~445 km of dextral separation.

#### 5.2.4. East Susitna-Ruby Range Batholith (74-57 Ma Phase)

Late Cretaceous and Paleocene plutonic belts within the Maclaren and Kluane schists have similar ages and compositions. Both comprise predominantly Late Cretaceous tonalite and Paleocene granodiorite, although their proportions differ. In the East Susitna batholith (AK), syn-collisional tonalite bodies dated at ca. 74–65 Ma represent the oldest phase of magmatism within the Maclaren schist (Aleinikoff et al., 1981; Ridgway et al., 2002; this study). The oldest dated rocks within the Ruby Range batholith (YT) come from intermediate and mafic intrusions dated at 72–68 Ma (Israel et al., 2011), and possibly as old as 77 Ma (Stanley, 2012). Voluminous ca. 64–57 Ma granodiorite-to-granite plutons compose the main phase of the Ruby Range batholith (Israel et al., 2011). Granodiorite bodies dated at ca. 57 Ma represent a volumetrically minor portion of the East Susitna batholith (Riccio et al., 2014; Figure 2), but are present throughout the Talkeetna Mountains to the west (Csejtey et al., 1992). Although the proportions of each magmatic phase do not appear to be equal within the East Susitna and Ruby Range batholiths, the range of ages and compositions of the intrusions are nearly identical. It remains unclear if there are individual bodies in the dissected 74–57 Ma batholith that can be matched across the Denali fault, yet correlating the easternmost 57 Ma pluton south of the Denali fault in Alaska to the northwestern margin of the Ruby Range batholith in Yukon results in a minimum dextral separation of 425 km.

#### 5.2.5. Shakwak-Ann Creek Pluton (52-48 Ma)

Early Eocene plutonic rocks hosted within the Maclaren and Kluane schists correlate based on structural position, composition, and age. In Yukon, the Hayden Lake plutonic suite comprises ca. 55–48 Ma felsic plutons intruded into the structurally lowest portion of the Kluane schist (Colpron et al., 2016; Stanley, 2012). Similar plutons in Alaska include the ca. 52 Ma biotite granodiorite-monzonite plutons north of Ann Creek and in the west fork of the Maclaren River (Figure 2). The westernmost pluton within the Hayden Lake suite (Shakwak pluton) is a >54-to-46 Ma (K-Ar biotite cooling and U-Pb zircon crystallization dates, respectively) composite body consisting of unfoliated biotite tonalite, biotite granodiorite, and quartz diorite (Yukon Geological Survey, 2020). Due to the overlap in age, identical structural position, overlapping rock types, and proximity to the Denali fault, we propose a correlation between the Shakwak pluton and the ca. 52 Ma biotite quartz monzonite body north of Ann Creek. Matching these two igneous bodies results in ~465 km of dextral separation along the Denali fault. We regard this correlation as our highest quality match across the Denali fault and the most accurate measurement of strike-slip separation.

WALDIEN ET AL. 19 of 35



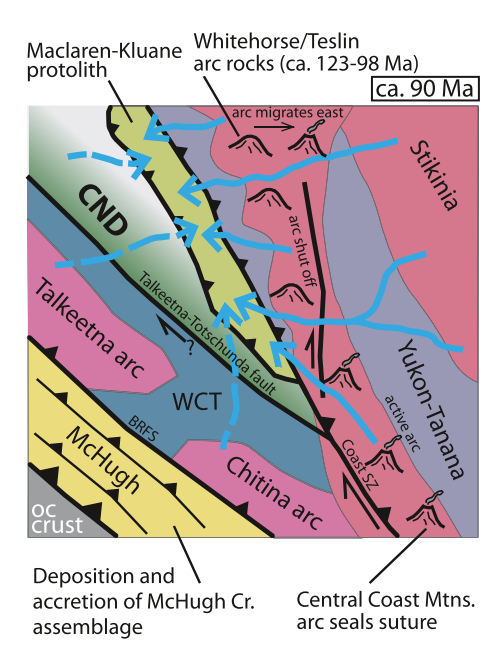


Figure 10. Schematic map view diagram illustrating the interpreted tectonic setting of the Maclaren-Kluane protolith basin. Sediment was delivered to the basin by drainage systems (blue lines/arrows; dashed lines where uncertain) that sourced uplifted terranes to the east, south, and possibly the west. Strike-slip fault systems in the Coast shear zone (Coast SZ) and on both sides of the Maclaren-Kluane basin have been documented to be active at this time. Deposition and accretion of the McHugh Creek assemblage record ongoing subduction along the outboard margin of the Wrangellia composite terrane. Map unit colors are the same as Figure 1. WCT—Wrangellia composite terrane; CND—Clearwater-Nutzotin-Dezadeash assemblage; oc—oceanic; BRFS—Border Ranges fault system.

#### 5.2.6. Paleogene Volcanic Rocks

Post-collisional volcanic strata may correlate based on composition, structural setting, and general age information. South of the Denali fault, ca. 51-46 Ma volcanic strata between the Delta and Chistochina Rivers (Figure 1) in Alaska consist predominantly of syn-extensional felsic tuffs with lesser basalt-to-andesite flows and dikes (Bond, 1976; Gillis et al., 2019; Waldien et al., 2018; Figure 2 and Table 3). The volcanic rocks near the Chistochina River appear to be the eastern-most isolated extent of the Paleogene volcanic belt that covers much of the Talkeetna Mountains (Csejtey et al., 1978, 1992; Nokleberg, Aleinikoff, Lange, et al., 1992). Potentially correlative rocks northeast of the Denali fault in southwestern Yukon include graben-bounded rhyolite tuffs with lesser andesite and basalt (Colpron et al., 2016; Miskovic and Francis, 2004). Field relationships and radiometric ages link the volcanic rocks to the ca. 57-55 Ma plutonic suite throughout southwestern Yukon (Israel et al., 2011; Miskovic & Francis, 2004; Morris & Creaser, 2003). The Bennett Lake igneous complex near the Yukon-British Columbia border, however, contains lava flows as young as ca. 50 Ma (Morrison et al., 1979; Morris & Creaser, 2003). Although no unique correlation between Eocene volcanic complexes across the Denali fault has yet been identified, we propose that the ca. 50 Ma volcanic strata and intrusions in the eastern Alaska Range may be a displaced portion of the Bennett Lake igneous complex or a suite of distal channelized flows. Moreover, the northern Talkeetna Mountains west of our study area contain a suite of ca. 63-50 Ma bimodal volcanic strata and associated intrusions (Cole et al., 2007; Csejtey et al., 1992), which may correlate with the Rhyolite Creek volcanics and associated intrusions north of the Ruby Range batholith in Yukon. If correlative, the volcanic fields could record up to 580 km of separation on the Denali fault, yet the combined likelihood that the flows were channelized and uncertainties in Eocene geomorphology of the region make this measurement speculative. The potential correlation raises the possibility that mineralization associated with the Eocene volcanic strata in Canada may

also be present in the Alaskan volcanic rocks (e.g., Light et al., 1990), but more field-based geochemical and geochronological studies of Paleogene volcanic rocks in the Alaska Range and Talkeetna Mountains will be necessary to vet these hypotheses.

#### 5.3. Palinspastic Reconstruction

The Maclaren-Kluane schist and associated rocks record nearly 100 Myr of tectonic evolution in the North American Cordillera. Our palinspastic reconstruction of the Denali fault begins with deposition of the Maclaren-Kluane protolith in the mid-Cretaceous and culminates with historic dextral slip in the Denali fault system. In addition to our data highlighting the total offset history on the modern Denali fault, we use markers established by Regan et al. (2021) to restore the post-33 Ma slip (Table 1).

Ca. 95-82 Ma (Figure 10): The protolith of the Maclaren-Kluane schist was deposited into a marine basin west of the Coast Mountains arc. Sediment was delivered to the basin from uplifted regions to the east, south, and possibly the west. Due to stratigraphic, structural, and thermochronological evidence for Early-to-mid-Cretaceous oblique shortening in the region (e.g., Johnston, 1999; Mair et al., 2006; McDermott et al., 2019; Ridgway et al., 2002), it is likely that the Maclaren-Kluane protolith was deposited in a contractional setting. We infer that syn-depositional imbrication of the Maclaren-Kluane protolith took place along east-dipping structures because the prograde structures within the Maclaren-Kluane schist dip north and east toward the North American continent (Davidson et al., 1992; Erdmer & Mortensen, 1993; Johnston & Canil, 2007; Lowey, 2000) and the timing of protolith deposition overlaps with an eastward migration of arc magmatism across the present-day southwestern Yukon (cf. Allan et al., 2013; Hart et al., 2004;

WALDIEN ET AL. 20 of 35



Tempelman-Kluit & Wanless, 1975). Taken together, these data suggest that the Maclaren-Kluane protolith sediment formed in a contractional forearc position during the waning stage of the west-facing mid-Cretaceous arc built upon the Yukon-Tanana terrane. Maximum depositional ages from the Maclaren schist require that final closure of the forearc basin and associated tectonic underplating of the Maclaren-Kluane schist took place after ca. 86 Ma.

It remains unclear whether Late Cretaceous syn-collisional underplating of the Maclaren-Kluane schist requires a subduction zone between the Wrangellia composite terrane and the North American margin at that time. Hypotheses regarding the nature of the crust along the inboard margin of the Wrangellia terrane in the mid-to-Late Cretaceous include oceanic crust, a thickened oceanic(?) plateau, or a combination of these end-member scenarios (e.g., Lowey, 2019; Trop & Ridgway, 2007; Waldien et al., 2021). The presence of oceanic crust is implied by the apparently disparate geologic histories between the paleo-eastern margin of the Wrangellia composite terrane and western margin of North America prior to collision in the mid-Cretaceous (Trop et al., 2020). Alternatively, it has been suggested that the Early Cretaceous collision of the Wrangellia composite terrane with western North America was followed by transtensional rifting that reopened the marine basin (McClelland et al., 1992), yet it is not clear if the rift basins evolved to full seafloor spreading. An argument against the presence of a wide marginal seaway between the Wrangellia terrane and North America draws on the presence of an Early-to-mid-Cretaceous magmatic belt in Yukon (Whitehorse, Dawson Range, Tombstone suites) and lack of mid-Cretaceous arc rocks south of the Maclaren schist in southern Alaska. Because deposition and accretion of the McHugh Creek Assemblage record paleo-eastdipping subduction along the western margin of the Wrangellia composite terrane from ca. 100-90 Ma (Amato & Pavlis, 2010; Amato et al., 2013), the singular magmatic belt in Yukon could be explained by that subduction zone alone, and eastward migration of the arc magmatism across Yukon could be attributed changes in the geometry of that slab leading up to underplating of the Maclaren-Kluane schist and cessation of arc magmatism between ca. 83 and 78 Ma (e.g., Gehrels et al., 2009; Figure 8). If a second subduction zone were present between the Wrangellia composite terrane and the North American margin, then two sub-parallel mid-Cretaceous igneous belts should be present. Acknowledging the aforementioned uncertainties regarding the nature of the crust beneath the mid-to-late Cretaceous marginal seaway between the Wrangellia composite terrane and western North America, we drafted Figure 11 to include queried oceanic crust along the eastern margin of the Wrangellia composite terrane.

Ca. 82–65 Ma (Figure 11a): Tectonic underplating of the Maclaren-Kluane schist beneath the western margin of North America resulted in Barrovian series metamorphism that began shortly after deposition. During underplating, the schist experienced kyanite grade conditions (e.g., Davidson et al., 1992; Mezger, Chacko, et al., 2001) and growth of ca. 82 Ma metamorphic zircon rims.

In Yukon, the structure responsible for burial and metamorphism of the Kluane schist is largely overprinted by the Ruby Ranges batholith (e.g., Israel et al., 2011). Along strike to the south of Kluane Lake, the Kluhini River shear zone has been described as an east-dipping shear zone that thrusts the Yukon-Tanana terrane and related igneous belts over pelitic gneiss with an Early Cretaceous protolith age (Vice, 2017). In Alaska, a structure beneath the Susitna Glacier (SGTF—Figure 2) places pre-Jurassic continental margin rocks hosting ca. 98 Ma plutons in the north against the Maclaren schist and East Susitna batholith in the south (Figure 2). We infer that historic and Neogene slip on the Susitna Glacier thrust fault reactivated a Mesozoic collisional structure correlative with the Kluhini River shear zone.

Following underplating, shortening continued by the formation of the Valdez Creek-Tatshenshini shear zone along the former plate boundary between the Maclaren-Kluane schist to the northeast and the Clearwater-Nutzotin-Dezadeash strata to the southwest (Waldien et al., 2021). Our date of ca. 76 Ma on the garnet-biotite leucocratic body within the Maclaren schist suggests that initiation of slip on the Valdez Creek shear zone may have facilitated decompression partial melting in the schist or served as a conduit for melt migration (e.g., Hollister, 1993). Shortening along the Valdez Creek-Tatshenshini shear zone developed an inverted metamorphic field gradient preserved in the footwall Clearwater-Dezadeash metasediments, which reached peak upper greenschist-lower amphibolite facies conditions at ca. 65 Ma (Lowey, 2000; Waldien et al., 2021).

WALDIEN ET AL. 21 of 35



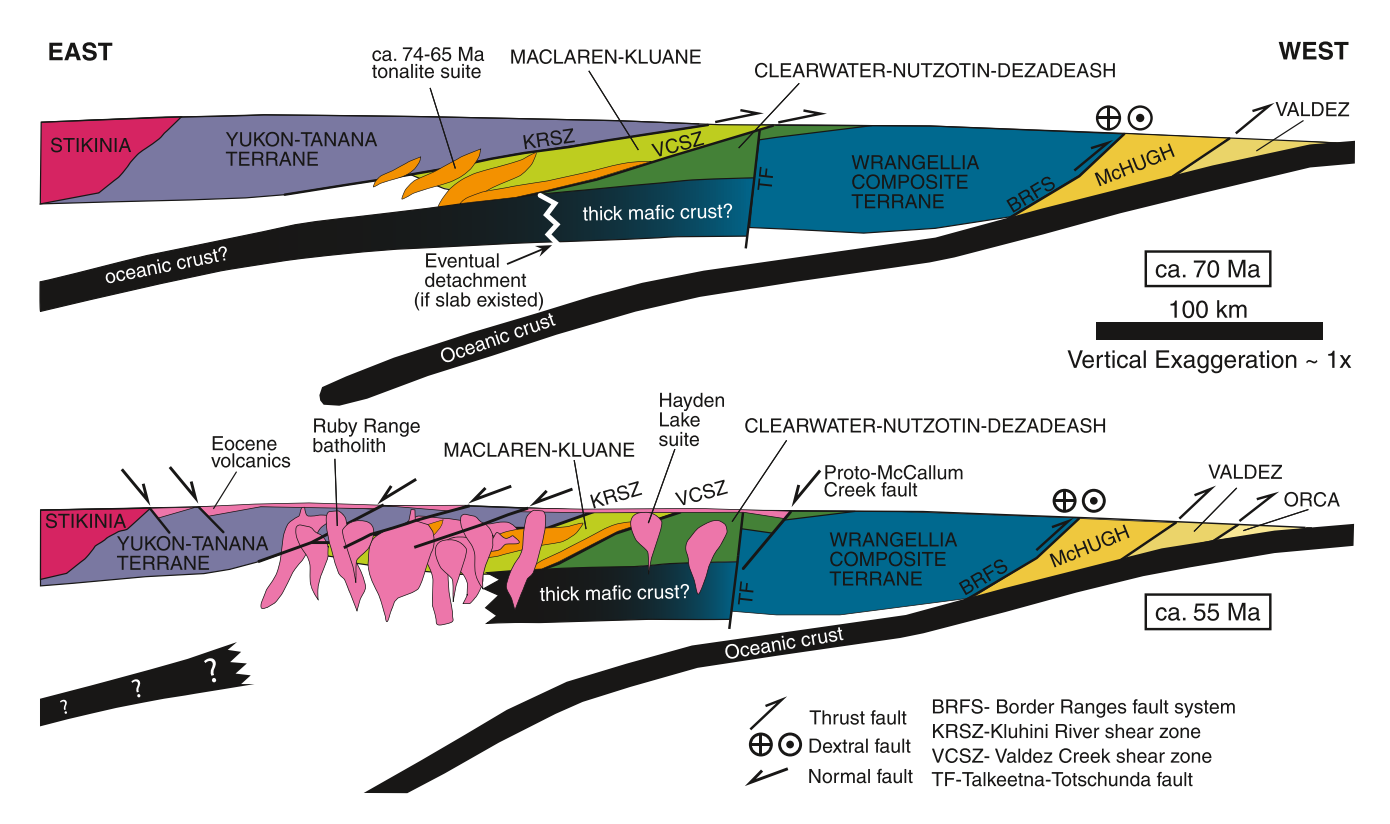


Figure 11. Schematic cross-sections illustrating generalized crustal structure during syn-collisional metamorphism of the Maclaren-Kluane schist. Colors are the same as Figure 1. (a) From ca. 74 to 65 Ma the Maclaren-Kluane schist underwent regional amphibolite facies metamorphism contemporaneous with slip on the Valdez Creek shear zone and syn-kinematic intrusion of tonalite bodies. Oceanic lithosphere may have been attached to the inboard margin of the Wrangellia composite terrane, but subduction in the marginal seaway is not necessary to explain regional magmatism. Deposition and accretion of the Valdez Group record ongoing subduction along the outboard margin of the Wrangellia composite terrane. (b) From ca. 60 to 50 Ma the Maclaren-Kluane schist experienced regional high temperature-low pressure metamorphic conditions contemporaneous with regional extension and intrusion of the main voluminous phase of the Ruby Range batholith. If oceanic lithosphere were attached to the inboard margin of the Wrangellia composite terrane, it likely would have detached by this time. Deposition and accretion of the Orca Group record ongoing subduction along the outboard margin of the Wrangellia composite terrane.

Ca. 60–50 Ma (Figure 11b): Cessation of slip on the Valdez Creek-Tatshenshini shear zone was followed by isothermal decompression throughout much of the Maclaren-Kluane schist (Mezger, Chacko, et al., 2001), local cooling near the Valdez Creek shear zone in the Clearwater Mountains (AK) (Ridgway et al., 2002), and reheating associated with voluminous magmatism in the Ruby Range batholith in Yukon (Israel et al., 2011; Mezger, Chacko, et al., 2001). The magmatism was accompanied by regional extension, which preserved volcanic strata within grabens throughout eastern Alaska, southwestern Yukon, and northern British Columbia (Bacon et al., 1990; Miskovic and Francis, 2004; Morris & Creaser, 2003). South of the Denali fault in Alaska, syn-extensional volcanic strata and intrusions near the Gulkana Glacier record formation of the McCallum Creek fault as part of the Paleogene extensional system (Gillis et al., 2019; Terhune et al., 2015; Figure 12a). Despite the regional importance of Paleogene extension, eastern Alaska and southwestern Yukon appear not to have experienced the high magnitude of extension that occurred in coeval extensional systems farther south in the Cordillera (e.g., Parrish et al., 1988). The ca. 60-50 Ma syn-extensional volcanism may record the initiation of dextral motion along the modern Denali fault in concert with dextral-slip on the Tintina and Border Ranges fault systems during oblique subduction of a spreading center along the outboard margin of the Wrangellia composite terrane (Davidson & Garver, 2017; Gabrielse et al., 2006; Roeske et al., 2003). However, our correlation of the Shakwak and Ann Creek plutons asserts that localization of the modern Denali fault and subsequent dissection of the Maclaren-Kluane schist and the associated batholith is restricted to post-52 Ma (Figure 12a).

Ca. 33 Ma (Figure 12b): The ca. 42–33 Ma phase of the East Susitna batholith (AK) and absence of age-equivalent plutons in the Ruby Range batholith (YT) support our hypothesis of localized dextral slip on the Denali fault by ca. 42 Ma (see also Figure 8). The 42–33 Ma plutons within the Maclaren schist constitute

WALDIEN ET AL. 22 of 35



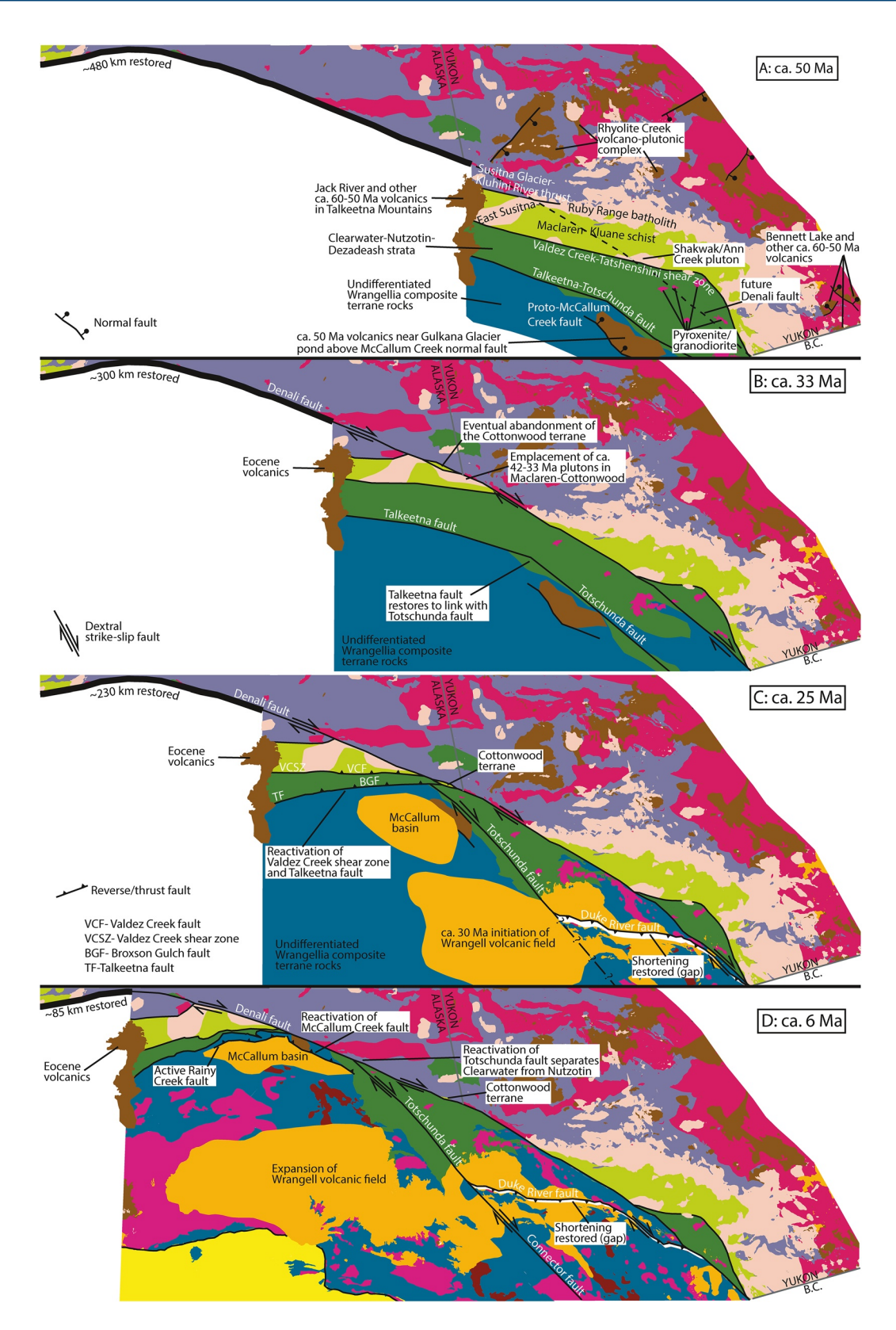


Figure 12.

WALDIEN ET AL. 23 of 35



the eastern-most extent of a suite of plutons emplaced along the Denali fault as far west as Mt. Foraker in the Central Alaska Range (Regan et al., 2020, 2021). Rapid post-emplacement cooling and thermal resetting of the Ar isotopic system in biotite and muscovite only within ~3 km of the plutons (e.g., Benowitz et al., 2014, 2019; Benowitz, Roeske, & Layer, 2011; Waldien et al., 2021) indicate that this phase of the batholith was emplaced at a relatively shallow crustal level.

Ca. 30-20 Ma (Figure 12c): The Oligocene and Early Miocene marks a major change in the geology of southern Alaska and southwestern Yukon, which involves the onset of exhumation in the Alaska Range and the Kluane Ranges (Benowitz et al., 2011, 2012, 2014; Lease et al., 2016; McDermott et al., 2019), drainage reorganization (Benowitz et al., 2019; Brennan & Ridgway, 2015; Finzel et al., 2011, 2015), onset of Wrangell volcanism (Berkelhammer et al., 2019; Brueseke et al., 2019), and development of the St. Elias fold-andthrust belt (Bruhn et al., 2004; Pavlis et al., 2012). Contemporaneous events in our study area include the post-32 Ma reactivation of the Valdez Creek shear zone indicated by cooling ages and brittle deformation features, development of an imbricate thrust system along the southern flank of the eastern Alaska Range (Valdez Creek, Broxson Gulch, Airstrip, and Rainy Creek faults), and retrograde metamorphism of the Maclaren schist (Waldien et al., 2021). The onset of transpressional deformation in the Denali fault system may have nucleated a short-lived structural complexity (e.g., a restraining bend), which resulted in abandonment of the Cottonwood terrane, a fragment of the Maclaren schist and ca. 33 Ma orthogneiss, on the north side of the active Denali fault strand near the present-day Yukon-Alaska border (Nokleberg & Richter, 2007; Regan et al., 2021; see also Figure 12b). The widespread ca. 30-25 Ma tectonic modification of southern Alaska is generally regarded as an upper plate response to increased plate coupling and progressive flat-slab subduction of the Yakutat oceanic plateau beneath southern Alaska (Enkelmann et al., 2008, 2010; Haynie & Jadamec, 2017; Jadamec et al., 2013).

Late Miocene to Present (Figure 12d): Southern Alaska experienced pulses in bedrock cooling and basin development beginning in the late Miocene. Regional events at this time include uplift and exhumation of the Denali massif (Burkett et al., 2016; Fitzgerald et al., 1993, 1995), exhumation in the western Alaska Range (Benowitz et al., 2012; Haeussler et al., 2008; Lease, 2018), a transition from lacustrine to alluvial facies in basins north and south of the Denali fault (Allen et al., 2016; Ridgway et al., 2002, 2007), development of the Northern Foothills fold and thrust belt (Bemis & Wallace, 2007; Ridgway et al., 2007), reactivation of shortening structures along the southern flank of the Alaska Range (Waldien et al., 2018), expansion of the Wrangell volcanic field (Preece & Hart, 2004), and a regional shift in precipitation related to topographic development (Bill et al., 2018; Otiniano et al., 2020).

One aspect of the late Miocene tectonic event that is integral to the development of the Denali fault system is post-18 Ma dextral slip on the Totschunda fault (Berkelhammer et al., 2019; Milde, 2014). Although it is plausible that the Totschunda fault was part of the proto-Denali fault system before 114 Ma (Trop et al., 2020), the present data only imply linkage with the modern Denali fault since the Late Miocene. Contemporaneous dextral slip on the Totschunda and Denali faults feeds slip from the Totschunda fault onto the Denali fault west of their intersection (Haeussler et al., 2017), which produces transpression west of the junction (Bemis et al., 2015). Due to these observations and the similarity in magnitudes (~80–90 km) of post-7 Ma separation on the Denali fault west of the Denali-Totschunda juncture and post-18 Ma separation

**Figure 12.** Schematic map-view diagrams illustrating the ca. 50 Ma-Present evolution of the Denali fault system. The diagrams focus on correlative rock units and thus do not account for eroded material. The geology north and east of the Denali fault is not modified from Figure 1 and modern political borders are retained as reference markers. The geology south and west of the Denali fault becomes increasingly schematic further back in time. Eocene volcanic rocks presently in the Talkeetna Mountains (brown map unit south of the Denali fault) may be used to track restoration of the Denali fault. Kinematics are shown only on faults that are active during the time frame. Colors are the same as Figure 1. See text and map annotations for key events in each time frame and Figure 1 for a Present-day time frame. (a) By ca. 50 Ma, all correlative rock packages between the Delta River region and Kluane Lake region had formed. Upon localization, the Denali fault will cut obliquely through the geology (dashed line). (b) By ca. 33 Ma, the Denali fault had begun slipping as a localized dextral fault. The ca. 42–33 Ma intrusions that are shared among the Maclaren and Cottonwood schists are not present in the Kluane schist (see also Figure 8). A structural complexity, probably a restraining step-over, in the Denali fault abandons the Cottonwood schist near the present-day Alaska-Yukon border between 33 and 25 Ma. (c) By ca. 25 Ma, slip on the Valdez Creek fault had nucleated the imbricate thrust system along the south flank of the eastern Alaska Range. Deposition into the McCallum basin records sediment input from uplifted regions of the surrounding Alaska Range (Allen et al., 2016). The Totschunda fault was likely active at this time (Milde, 2014). (d) By ca. 6 Ma dextral slip transfer from the Totschunda fault to the Denali fault was ongoing, which resulted in transpression in the eastern Alaska Range and separation of the Clearwater metasediments from the Nutzotin Mountains sequence. Shortening on the Duke River fault acts t

WALDIEN ET AL. 24 of 35



on the Totschunda fault, it is likely that both separations accumulated entirely since ca. 7 Ma. Restoring ~85 km of Late Miocene to Present separation on the Totschunda and Denali faults places the Clearwater metasediments adjacent to the Nutzotin Mountains sequence and would also match the Talkeetna fault to the Totschunda fault (see also Figures 11, 12a–12c). Such a restoration is supported both by the rock types near these structures and by crustal tomography revealing nearly identical contrasts in crustal seismic properties across them (Allam et al., 2017). Incorporating the ~85 km of dextral separation on the Totschunda fault is a key component of our palinspastic reconstruction of the Denali fault system because it allows both the ~370 km of separation recorded by correlation of the Dezadeash and Nutzotin strata and the ~465 km of separation recorded by the correlation of the Clearwater metasediments and Dezadeash Formation to be correct.

Transpressional deformation in the Denali fault system during the Neogene was highly partitioned between dextral strike-slip on the Denali fault master strand and Totschunda fault and shortening on thrust systems at the northern and southern flanks of the Alaska Range. The record of long-term cooperation between strike-slip and shortening structures is also reflected in historic seismicity, including the  $2002\ M_w$  7.9 Denali earthquake, which indicates that both strike-slip and shortening structures remain active components of the Denali fault system (Doser, 2004; Eberhart-Phillips et al., 2003; Ratchkovski et al., 2004; Vallage et al., 2014).

## 5.4. Implications for Strike-Slip Faulting in the North American Cordillera

#### 5.4.1. Separation Versus Slip on the Denali Fault

Cenozoic shortening on structures in the Alaska Range causes the measurements of strike-slip separation to underestimate the magnitude of slip on the Denali fault between the offset markers. Our favored correlation of the ca. 52 Ma Shakwak and Ann Creek plutons yields 465 km of dextral separation. Post-32 Ma reactivation of the Valdez Creek shear zone nucleated the southeast-vergent thrust system that carried the Maclaren schist, Clearwater metasediments, and associated intrusive rocks in the hanging wall (Waldien et al., 2021). Synchronous slip between the thrust system and Denali fault resulted in slip transfer from the Denali fault to the thrusts. As a result of the slip transfer, translation of the Ann Creek pluton relative to the Shakwak pluton took place at a rate lower than the slip rate on the Denali fault. Over time, the accumulated shortening led to a discrepancy in the separation of the offset features relative to the amount of slip on the section of the Denali fault between the correlative plutons. It is not entirely clear how much slip has taken place on the Valdez Creek or Broxson Gulch faults, yet detailed mapping paired with thermochronological and geophysical data sets suggest that these structures accommodated at least 15 km of shortening during the Oligocene and Miocene (Allam et al., 2017; Waldien et al., 2021). Incorporating the Cenozoic shortening into our model of Denali fault evolution reveals that the 465 km of strike-slip separation corresponds to a total slip estimate of ~480 km.

## 5.4.2. Timing of Strike-Slip Displacement

In agreement with other recent studies (e.g., Murphy, 2018), our review of the ages and separation of features displaced by the Denali fault requires that the ~480 km of displacement on the fault system took place entirely during the Cenozoic. There are two major implications of this outcome.

First, formation and localization of slip on the modern Denali fault appear to have begun as slip on other major strike-slip faults in the Cordillera was decreasing. Both the Border Ranges and Tintina fault systems were active dextral fault systems during the Paleogene, but appear to have experienced minor dextral slip since the Late Eocene (Gabrielse et al., 2006; Little, 1990; Roeske et al., 2003; Ryan et al., 2017; Till et al., 2007). In contrast, we have documented that localization and major slip on the modern Denali fault took place after ca. 52 Ma. This time period corresponds to major changes in the tectonic configuration along the entire margin of western North America, which may be related to changes in the obliquity, rates, and physical properties of incoming oceanic plates (e.g., Atwater, 1989; Doubrovine & Tarduno, 2008; McCrory & Wilson, 2013). The prevalence of Paleogene extensional complexes from British Columbia, Canada into the northern contiguous United States may partially correspond to the coexistence of multiple dextral fault systems that were active at that time (e.g., Andronicos et al., 2003; Foster et al., 2007; Gabrielse et al., 2006). Likewise, the apparent decline of widespread extension in the Late Eocene may record an

WALDIEN ET AL. 25 of 35



increase in localized slip on the Denali fault and a decrease in major slip on neighboring strike-slip fault systems in concert with changing plate boundary conditions.

Second, the recognition of Cenozoic slip on the modern Denali fault allows for larger cumulative margin-parallel displacement of the Wrangellia composite terrane relative to inboard terranes since the Early Cretaceous. Recently published geology-based data sets bear on long-standing hypotheses that the Cordilleran terranes experienced large magnitude (>1,500 km) northward transport along dextral fault systems in the mid- and Late Cretaceous (Coutts et al., 2020; Garver & Davidson, 2015; Matthews et al., 2017; Rusmore et al., 2013; Sauer et al., 2019). Our review of slip in the Denali fault system reveals that the oft-cited ~370-400 km of slip that was inferred to have taken place since the Early Cretaceous is not an accurate assessment of Denali fault slip. We have shown herein that ~480 km of slip on the modern Denali fault took place entirely since ca. 52 Ma. Thus, the modern Denali fault should not be grouped with other fault systems contributing to large-scale margin-parallel displacement in the Cretaceous. Rather, thermochronological data and regional geologic correlations suggest the existence of a proto-Denali strike-slip fault system that was likely active during the Early-to-mid-Cretaceous (McDermott et al., 2019; Miller et al., 2002; Wahrhaftig et al., 1975). The amount of displacement and the sense of motion on the proto-Denali fault system are presently not well understood. Finding and interrogating the rock packages that record the slip history of the proto-Denali fault will undoubtedly help reconcile disputes regarding margin-parallel transport of Cordilleran terranes during the Cretaceous. If the proto-Denali fault experienced a phase of dextral slip, northward displacement of the Wrangellia composite terrane along the Denali fault system relative to the North American margin would exceed the ~480 km of Cenozoic displacement established herein.

#### 5.4.3. Lithospheric Strength Heterogeneity Following Terrane Accretion

The key feature that allows offset on the modern Denali fault to be determined is the presence of correlative syn-collisional rock packages on both sides of the fault. Thermochronological and thermobarometric data indicate that the Maclaren-Kluane schist and associated batholithic rocks were in the upper ~15 km of the crust when the modern Denali fault formed. Because these rock packages, and fabrics within them, were cut obliquely by the fault, it is implied that their mechanical properties did not influence the localization of the fault. Instead, we propose that the mechanical properties of the lower crust and/or lithospheric mantle were more important for controlling the formation and localization of the modern Denali fault. Elements of the post-collisional lower crust and lithospheric mantle in the Cordillera that may have guided localization of the modern Denali fault include a thick mafic root within the Wrangellia composite terrane, differences in mantle hydration as a result of subduction-related magmatism, and/or differences in the thickness of the mantle lithosphere. Such inferences are supported by a variety of geophysical data sets, all of which indicate a fundamental change in the properties of the lower crust and upper mantle across the eastern Denali fault (Allam et al., 2017; Audet et al., 2016; Berg et al., 2020; Miller et al., 2018; O'Driscoll & Miller, 2015; Rasendra et al., 2014; Saltus & Hudson, 2007). The sum of geophysical and geological data from the Denali fault, together with thermochronological and geophysical data sets from other regions of the Cordillera (Enkelmann et al., 2019; Estève et al., 2020), challenge the hypothesis of an active Cordillera-wide weak lower crustal décollement (e.g., Hyndman et al., 2005).

Instead, the contrasting mechanical properties of individual terranes may cause terrane-bounding structures to penetrate the lithosphere. Such a scenario is highly likely for southern Alaska, where the thermal structure of the lithosphere is strongly controlled by the shape of the subducting plate, and lithospheric-scale weaknesses along terrane boundaries (i.e., the Denali fault) are required to accurately model active deformation (Haynie & Jadamec, 2017; Jadamec et al., 2013).

## 6. Conclusions

Integration of new geologic mapping and geochronology data from the eastern Alaska Range with existing data sets from southwestern Yukon reveals five distinct rock packages that record Cenozoic displacement on the Denali fault: (a) ca. 94–86 Ma Maclaren schist and Kluane schist; (b) the 74–57 Ma phase of the East Susitna batholith and the Ruby Range batholith; (c) ca. 52 Ma granodiorite bodies in the Maclaren schist and the Hayden Lake intrusive suite within the Kluane schist; (d) the ca. 160–144 Ma Clearwater metasediments, Nutzotin Mountains sequence, and Dezadeash Formation strata and ca. 120–100 Ma zoned

WALDIEN ET AL. 26 of 35

27 of 35



pyroxenite-granodiorite bodies that intrude those strata; and (e) Eocene extension-related volcanic rocks and associated shallow intrusions. Restoring these offset features results in ~465 km of dextral separation, and accounting for Neogene shortening in the eastern Alaska Range results in ~480 km of dextral slip in the Denali fault system. All of this slip accumulated since ca. 52 Ma, following the main phase of slip on other major Cordilleran strike-slip faults.

Before offset by the Denali fault system, protolith deposition and prograde metamorphism of the Maclaren-Kluane schist records the closure of a marine basin between the Wrangellia composite terrane and the Cordilleran margin at ca. 95-86 Ma. Underplating and regional metamorphism of the schist took place along east-dipping ductile thrusts (Kluhini River and Valdez Creek-Tatshenshini shear zones) between ca. 82 and 65 Ma. The data presented and summarized herein provide additional evidence for diachronous accretion of the Wrangellia composite terrane along east-dipping structures.

## **Data Availability Statement**

Data presented in this publication are included as supporting information files and have been uploaded to the Geochron database, which is accessible at https://www.geochron.org/dataset/html/ geochron\_dataset\_2020\_12\_21\_7SR8l.

#### References Acknowledgments

This study was funded by grants from

Geologists, Alaska Geological Society,

UC Davis Durrell fund (Waldien), U.S.

Geological Survey National Cooperative

Geological Society of America, and

Geologic Mapping Program Award

#G16AC00206 (Roeske and Waldien),

NSF Tectonics Award #EAR-1828737

(Roeske), and #EAR-1828023 (Benow-

Laserchron Center were partially sup-

ported by NSF Award #EAR-1649254

to that facility. The authors are grateful

to Wing Air, Alaska Land Exploration,

and from the field areas. Waldien appre-

ciates assistance in the field from Cait

Livsey, Jordan Carey, Michael Chen,

and Jack Foran. Jim Stout graciously

advice upon starting this project. Steve

Israel is thanked for sharing Kluane

schist detrital zircon U-Pb data. The

authors appreciate feedback and discus-

sions with Richard Lease, Eric Cowgill,

Jonathan Caine, and Don Murphy. The

manuscript benefited from reviews by

Cam Davidson, Eric Cowgill, Robinson

Cecil, and an anonymous reviewer,

and editorial handling by Margaret

WALDIEN ET AL.

Rusmore.

shared thin sections and words of

and 40 Mile Air for transportation to

itz). Lu/Hf analyses at the Arizona

the American Association of Petroleum

Aleinikoff, J. N., Nokleberg, W. J., & Herzon, P. L. (1981). Age of intrusion and metamorphism of the East Susitna batholith. Mount Hayes B-6 quadrangle, eastern Alaska Range, Alaska. U.S. Geological Survey Circular, 844, 100-102.

Allam, A. A., Schulte-Pelkum, V., Ben-Zion, Y., Tape, C., Ruppert, N., & Ross, Z. E. (2017). Ten kilometer vertical Moho offset and shallow velocity contrast along the Denali fault zone from double-difference tomography, receiver functions, and fault zone head waves. Tectonophysics, 721, 56-69. https://doi.org/10.1016/j.tecto.2017.09.003

Allan, M. M., Mortensen, J. K., Hart, C. J. R., Bailey, L. A., Sanchez, M. G., Ciolkiewicz, W., et al. (2013). Magmatic and metallogenic framework of west-central Yukon and eastern Alaska. In M. Colpron, T. Bissig, B. G. Rusk, & J. F. H. Thomposon (Eds.), Tectonics, metallogeny, and discovery: The North American Cordillera and similar accretionary settings (Vol. 17, pp. 111-168). Littleton, CO: Society of Economic Geologists Special Publication, Society of Economic Geologists. https://doi.org/10.5382/SP.1710.5382/sp.17.04

Allen, W. K., Ridgway, K. D., Benowitz, J. A., Waldien, T. S., Roeske, S. M., & Roeske, S. M. (2016). Sedimentary and volcanic record of Neogene transpressional foreland basin development along the central Denali Fault system, Eastern Alaska Range. (Vol. 48). Geological Society of America Abstracts with Programs. https://doi.org/10.1130/abs/2016AM-284817

Amato, J. M., & Pavlis, T. L. (2010). Detrital zircon ages from the Chugach terrane, southern Alaska, reveal multiple episodes of accretion and erosion in a subduction complex.  $\textit{Geology}, \textit{38} (5), 459-462. \ \text{https://doi.org/} 10.1130/G30719.1$ 

Amato, J. M., Pavlis, T. L., Clift, P. D., Kochelek, E. J., Hecker, J. P., Worthman, C. M., & Day, E. M. (2013). Architecture of the Chugach accretionary complex as revealed by detrital zircon ages and lithologic variations: Evidence for Mesozoic subduction erosion in south-central Alaska. GSA Bulletin, 125(11–12), 1891–1911. https://doi.org/10.1130/b30818.1

Amato, J. M., Rioux, M. E., Kelemen, P. B., Gehrels, G. E., Clift, P. D., Pavlis, T. L., & Draut, A. E. (2007). U-Pb geochronology of volcanic rocks from the Jurassic Talkeetna Formation and detrital zircons from prearc and postarc sequences: Implications for the age of magmatism and inheritance in the Talkeetna arc. In K. D. Ridgway, J. M. Trop, J. M. G. Glen, & J. M. O'Neill (Eds.), Special Paper 431: Tectonic growth of a collisional continental margin: Crustal evolution of Southern Alaska (Vol. 431, pp. 253–271). Boulder, CO: Geological Society of America. https://doi.org/10.1130/2007.2431(11)

Andronicos, C. L., Chardon, D. H., Hollister, L. S., Gehrels, G. E., & Woodsworth, G. J. (2003). Strain partitioning in an obliquely convergent orogen, plutonism, and synorogenic collapse: Coast Mountains Batholith, British Columbia, Canada. Tectonics, 22(2). https://doi. org/10.1029/2001tc001312

Atwater, T. (1989). Plate tectonic history of the northeast Pacific and western North America. In E. L. Winterer, D. M. Hussong, & R. W. Decker (Eds.), Geology of North America: Volume N, the Eastern Pacific Ocean and Hawaii (pp. 21-72), Boulder, CO: Geological Society of America. https://doi.org/10.1130/DNAG-GNA-N.21

Audet, P., Sole, C., & Schaeffer, A. J. (2016). Control of lithospheric inheritance on neotectonic activity in northwestern Canada? Geology, 44(10), 807-810. https://doi.org/10.1130/G38118.1

Avé Lallemant, H. G. (1997). Transpression, displacement partitioning, and exhumation in the eastern Caribbean/South American plate boundary zone. Tectonics, 16(2), 272-289. https://doi.org/10.1029/96tc03725

Avé Lallemant, H. G., & Oldow, J. S. (1988). Early Mesozoic southward migration of Cordilleran transpressional terranes. Tectonics, 7(5), 1057-1075. https://doi.org/10.1029/tc007i005p01057

ib095ib13p21451

Beam, E. C., & Fisher, D. M. (1999). An estimate of kinematic vorticity from rotated elongate porphyroblasts. Journal of Structural Geology, 21(11), 1553-1559. https://doi.org/10.1016/s0191-8141(99)00110-8

Beck, M. E., Jr (1986). Model for late Mesozoic-early Tertiary tectonics of coastal California and western Mexico and speculations on the origin of the San Andreas fault. Tectonics, 5(1), 49-64. https://doi.org/10.1029/tc005i001p00049

Bemis, S. P., & Wallace, W. K. (2007). Neotectonic framework of the north-central Alaska Range foothills. In K. D. Ridgway, J. M. Trop, J. M. G. Glen, & J. M. O'Neill (Eds.), Special Paper 431: Tectonic growth of a collisional continental margin: Crustal evolution of Southern Alaska (Vol. 431, pp. 549-572). Boulder, CO: Geological Society of America. https://doi.org/10.1130/2007.2431(21)

Bacon, C. R., Foster, H. L., & Smith, J. G. (1990). Rhyolitic calderas of the Yukon-Tanana Terrane, east central Alaska: Volcanic remnants of a Mid-Cretaceous magmatic arc. Journal of Geophysical Research: Solid Earth, 95(B13), 21451-21461. https://doi.org/10.1029/



- Benowitz, J. A., Davis, K., & Roeske, S. (2019). A river runs through it both ways across time: 40Ar/39Ar detrital and bedrock muscovite geochronology constraints on the Neogene paleodrainage history of the Nenana River system, Alaska Range. *Geosphere*, 15(3), 682–701. https://doi.org/10.1130/GES01673.1
- Benowitz, J. A., Haeussler, P. J., Layer, P. W., O'Sullivan, P. B., Wallace, W. K., & Gillis, R. J. (2012). Cenozoic tectono-thermal history of the Tordrillo Mountains, Alaska: Paleocene-Eocene ridge subduction, decreasing relief, and late Neogene faulting. *Geochemistry, Geophysics, Geosystems*, 13(4). https://doi.org/10.1029/2011GC003951
- Benowitz, J. A., Layer, P. W., Armstrong, P., Perry, S. E., Haeussler, P. J., Fitzgerald, P. G., & VanLaningham, S. (2011). Spatial variations in focused exhumation along a continental-scale strike-slip fault: The Denali fault of the eastern Alaska Range. *Geosphere*, 7(2), 455–467. https://doi.org/10.1130/GES00589.1
- Benowitz, J. A., Layer, P. W., & Vanlaningham, S. (2014). Persistent long-term (c. 24 Ma) exhumation in the Eastern Alaska Range constrained by stacked thermochronology. *Geological Society, London, Special Publications, 378*(1), 225–243. https://doi.org/10.1144/SP378.12
- Benowitz, J. A., Roeske, S. M., & Layer, P. W. (2011). Deep exhumation, neotectonics, and constraints on the Denali fault system long-term off-set history: The Totschunda strand and the south-eastern Alaska Range. *Geological Society of America Abstracts with Programs*. 43(5), 438.
- Beranek, L. P., McClelland, W. C., van Staal, C. R., Israel, S., & Gordee, S. M. (2017). Late Jurassic flare-up of the Coast Mountains arc system, NW Canada, and dynamic linkages across the northern Cordilleran orogen: Flare-Up of the Coast Mountains Arc. *Tectonics*, 36(5), 877–901. https://doi.org/10.1002/2016TC004254
- Beranek, L. P., van Staal, C. R., McClelland, W. C., Joyce, N., & Israel, S. (2014). Late Paleozoic assembly of the Alexander-Wrangellia-Peninsular composite terrane, Canadian and Alaskan Cordillera. *Geological Society of America Bulletin*. 20. https://doi.org/10.1130/31066.1
- Berg, E. M., Lin, F., Allam, A., Schulte-Pelkum, V., Ward, K. M., & Shen, W. (2020). Shear velocity model of Alaska via joint inversion of Rayleigh wave ellipticity, phase velocities, and receiver functions across the Alaska transportable array. *Journal of Geophysical Research: Solid Earth*, 125(2). https://doi.org/10.1029/2019JB018582
- Berg, H. C., Jones, D. L., & Richter, D. H. (1972). Gravina-Nutzotin belt: Tectonic significance of an upper Mesozoic sedimentary and volcanic sequence in southern and southeastern Alaska. U. S. Geological Survey Professional Paper 800D. D1–D24.
- Berkelhammer, S. E., Brueseke, M. E., Benowitz, J. A., Trop, J. M., Davis, K., Layer, P. W., & Weber, M. (2019). Geochemical and geochronological records of tectonic changes along a flat-slab arc-transform junction: Circa 30 Ma to ca. 19 Ma Sonya Creek volcanic field, Wrangell Arc, Alaska. *Geosphere*, 15(5), 1508–1538. https://doi.org/10.1130/GES02114.1
- Bill, N. S., Mix, H. T., Clark, P. U., Reilly, S. P., Jensen, B. J. L., & Benowitz, J. A. (2018). A stable isotope record of late Cenozoic surface uplift of southern Alaska. Earth and Planetary Science Letters, 482, 300–311. https://doi.org/10.1016/j.epsl.2017.11.029
- Bittenbender, P. E., Bean, K. W., Kurtak, J. M., & Deininger, J. (2007). Mineral assessment of the delta river mining District Area, East-Central Alaska. U.S. Bureau of Land Management Alaska Technical Report. 57, 697.
- Bond, G. C. (1973). A late Paleozoic volcanic arc in the Eastern Alaska Range, Alaska. *The Journal of Geology*, 81(5), 557–575. https://doi.org/10.1086/627907
- Bond, G. C. (1976). Geology of the Rainbow Mountain-Gulkana Glacier Area, Eastern Alaska Range, with Emphasis on Upper Paleozoic Strata. State of Alaska Geologic Division of Geological & Geophysical Surveys Geologic Report, 45, p. 47. Scale 1:40:000, 3 sheets. https://doi.org/10.14509/373
- Box, S. E., Karl, S. M., Jones, J. V., III, Bradley, D. C., Haeussler, P. J., & O'Sullivan, P. B. (2019). Detrital zircon geochronology along a structural transect across the Kahiltna assemblage in the western Alaska Range: Implications for emplacement of the Alexander-Wrangellia-Peninsular terrane against North America. *Geosphere*, 15(6), 1774–1808. https://doi.org/10.1130/GES02060.1
- Brennan, P. R., & Ridgway, K. D. (2015). Detrital zircon record of Neogene exhumation of the central Alaska Range: A far-field upper plate response to flat-slab subduction. GSA Bulletin, 127(7–8), 945–961. https://doi.org/10.1130/b31164.1
- Brennan, P. R. K., Gilbert, H., & Ridgway, K. D. (2011). Crustal structure across the central Alaska Range: Anatomy of a Mesozoic collisional zone. *Geochemistry, Geophysics, Geosystems*, 12(4). https://doi.org/10.1029/2011GC003519
- Brothers, D. S., Elliott, J. L., Conrad, J. E., Haeussler, P. J., & Kluesner, J. W. (2018). Strain partitioning in Southeastern Alaska: Is the Chatham Strait Fault active? *Earth and Planetary Science Letters*, 481, 362–371. https://doi.org/10.1016/j.epsl.2017.10.017
- Brueseke, M. E., Benowitz, J. A., Trop, J. M., Davis, K. N., Berkelhammer, S. E., Layer, P. W., & Morter, B. K. (2019). The Alaska Wrangell Arc: ~30 Ma of subduction-related magmatism along a still active arc-transform junction. *Terra Nova*, 31(1), 59–66. https://doi.org/10.1111/ter.12369
- Bruhn, R. L., Pavlis, T. L., Plafker, G., & Serpa, L. (2004). Deformation during terrane accretion in the Saint Elias orogen, Alaska. *The Geological Society of America Bulletin*, 116(7–8), 771–787. https://doi.org/10.1130/b25182.1
- Burkett, C. A., Bemis, S. P., & Benowitz, J. A. (2016). Along-fault migration of the Mount McKinley restraining bend of the Denali fault defined by late Quaternary fault patterns and seismicity, Denali National Park & Preserve, Alaska. *Tectonophysics*, 693, 489–506. https://doi.org/10.1016/j.tecto.2016.05.009
- Busby-Spera, C. J., & Saleeby, J. B. (1990). Intra-arc strike-slip fault exposed at batholithic levels in the southern Sierra Nevada. *Geology*, 18(3), 255–259. https://doi.org/10.1130/0091-7613(1990)018<0255:iassfe>2.3.co;2
- Canil, D., Johnston, S. T., D'Souza, R. J., & Heaman, L. M. (2015). Protolith of ultramafic rocks in the Kluane Schist, Yukon, and implications for arc collisions in the northern Cordillera. *Canadian Journal of Earth Sciences*, 52(7), 431–443. https://doi.org/10.1139/cjes-2014-0138
- Cecil, M. R., Gehrels, G., Ducea, M. N., & Patchett, P. J. (2011). U-Pb-Hf characterization of the central Coast Mountains batholith: Implications for petrogenesis and crustal architecture. *Lithosphere*, 3(4), 247–260. https://doi.org/10.1130/L134.1
- Chardon, D., Andronicos, C. L., & Hollister, L. S. (1999). Large-scale transpressive shear zone patterns and displacements within magmatic arcs: The Coast Plutonic Complex, British Columbia. *Tectonics*, 18(2), 278–292. https://doi.org/10.1029/1998TC900035
- Choi, M., Eaton, D. W., & Enkelmann, E. (2021). Is the Eastern Denali fault still active? Geology.
- Cobbett, R., Israel, S., Mortensen, J., Joyce, N., & Crowley, J. (2017). Structure and kinematic evolution of the Duke River fault, southwestern Yukon. Canadian Journal of Earth Sciences, 54(3), 322–344. https://doi.org/10.1139/cjes-2016-0074
- Cole, R. B., Layer, P. W., Hooks, B., Cyr, A., & Turner, J. (2007). Magmatism and deformation in a terrane suture zone south of the Denali Fault, northern Talkeetna Mountains, Alaska. In K. D. Ridgway, J. M. Trop, J. M. G. Glen, & J. M. O'Neill (Eds.), Special Paper 431: Tectonic growth of a collisional continental margin: Crustal evolution of Southern Alaska (Vol. 431, pp. 477–506). Geological Society of America. https://doi.org/10.1130/2007.2431(19)

WALDIEN ET AL. 28 of 35



- Cole, R. B., Ridgway, K. D., Layer, P. W., & Drake, J. (1999). Kinematics of basin development during the transition from terrane accretion to strike-slip tectonics. Late Cretaceous-early Tertiary Cantwell Formation, south central Alaska. *Tectonics*, 18(6), 1224–1244. https://doi.org/10.1029/1999tc900033
- Colpron, M., Crowley, J. L., Gehrels, G., Long, D. G. F., Murphy, D. C., Beranek, L., & Bickerton, L. (2015). Birth of the northern Cordilleran orogen, as recorded by detrital zircons in Jurassic synorogenic strata and regional exhumation in Yukon. *Lithosphere*, 7(5), 541–562. https://doi.org/10.1130/L451.1
- Colpron, M., Israel, S., Murphy, D., Pigage, L., & Moynihan, D. (2016). Yukon bedrock geology map. Yukon geological Survey, open file 2016-1, 1:1,000,000 scale map and legend.
- Colpron, M., & Nelson, J. L. (2011). A digital Atlas of terranes for the northern Cordillera. British Columbia Ministry of Energy and Mines. BCGS GeoFile 2011-11.
- Coney, P. J., Jones, D. L., & Monger, J. W. (1980). Cordilleran suspect terranes. *Nature*, *288*(5789), 329–333. https://doi.org/10.1038/288329a0 Coutts, D. S., Matthews, W. A., Englert, R. G., Brooks, M. D., Boivin, M. P., & Hubbard, S. M. (2020). Along-strike variations in sediment provenance within the Nanaimo basin reveal mechanisms of forearc basin sediment influx events. *Lithosphere*, *12*(1), 180–197. https://doi.org/10.1130/l1138.1
- Csejtey, B., Cox, D. P., Evarts, R. C., Stricker, G. D., & Foster, H. L. (1982). The Cenozoic Denali Fault System and the Cretaceous accretionary development of southern Alaska. *Journal of Geophysical Research*, 87(B5), 3741. https://doi.org/10.1029/JB087iB05p03741
- Csejtey, B., Mullen, M. W., Cox, D. P., & Stricker, G. D. (1992). Geology and geochronology of the Healy Quadrangle, south-central Alaska, U.S. Geological Survey Miscellaneous Investigations, Series Map 1961, 63 p., 2 sheets, scale 1:250,000. https://doi.org/10.3133/i1961
- Csejtey, B., Nelson, W. H., Jones, D. L., Silberling, N.J., Dean, R. M., Morris, M. S., et al. (1978). Reconnaissance geologic map and geochronology, Talkeetna Mountains Quadrangle, northern part of Anchorage Quadrangle, and southwest corner of Healy Quadrangle, Alaska. U.S. Geological Survey Open-File Report 78-558-A, 60 p., 1 sheet, scale 1:250,000. https://doi.org/10.3133/ofr78558a
- Davidson, C., & Garver, J. I. (2017). Age and origin of the resurrection ophiolite and associated turbidites of the Chugach–Prince William Terrane, Kenai Peninsula, Alaska. *The Journal of Geology*, 125(6), 681–700. https://doi.org/10.1086/693926
- Davidson, C., Hollister, L. S., & Schmid, S. M. (1992). Role of melt in the formation of a deep-crustal compressive shear zone: The Maclaren Glacier Metamorphic Belt, south central Alaska. *Tectonics*, 11(2), 348–359. https://doi.org/10.1029/91TC02907
- Davidson, C., & McPhillips, D. (2007). Along strike variations in metamorphism and deformation of the strata of the Kahiltna basin, south-central Alaska. In K. D. Ridgway, J. M. Trop, J. M. G. Glen, & J. M. O'Neill (Eds.), Special Paper 431: Tectonic growth of a collisional continental margin: Crustal evolution of Southern Alaska (Vol. 431, pp. 439–453). Geological Society of America. https://doi.org/10.1130/2007.2431(17)
- Day, E. M., Pavlis, T. L., & Amato, J. M. (2016). Detrital zircon ages indicate an Early Cretaceous episode of blueschist-facies metamorphism in southern Alaska: Implications for the Mesozoic paleogeography of the northern Cordillera. *Lithosphere*, 8(5), 451–462. https://doi.org/10.1130/L525.1
- Dodds, C. J., & Campbell, R. B. (1988). Potassium-argon ages of mainly intrusive rocks in the Saint Elias mountains, Yukon and British Columbia. Geological Survey of Canada Paper 87-16.
- Dominguez, S., Lallemand, S. E., Malavieille, J., & von Huene, R. (1998). Upper plate deformation associated with seamount subduction. *Tectonophysics*, 293(3–4), 207–224. https://doi.org/10.1016/s0040-1951(98)00086-9
- Doser, D. I. (2004). Seismicity of the Denali-Totschunda Fault Zone in Central Alaska (1912-1988) and its relation to the 2002 Denali Fault Earthquake Sequence. *Bulletin of the Seismological Society of America*, 94(6B), S132–S144. https://doi.org/10.1785/0120040611
- Doser, D. I. (2014). Seismicity of Southwestern Yukon, Canada, and its relation to slip transfer between the Fairweather and Denali fault systems. *Tectonophysics*, 611, 121–129. https://doi.org/10.1016/j.tecto.2013.11.018
- Doubrovine, P. V., & Tarduno, J. A. (2008). A revised kinematic model for the relative motion between Pacific oceanic plates and North America since the Late Cretaceous. *Journal of Geophysical Research*, 113(B12), B12101. https://doi.org/10.1029/2008JB005585
- Dusel-Bacon, C., Holm-Denoma, C. S., Jones, J. V., Aleinikoff, J. N., & Mortensen, J. K. (2017). Detrital zircon geochronology of quart-zose metasedimentary rocks from parautochthonous North America, east-central Alaska. *Lithosphere*, 9(6), 927–952. https://doi.org/10.1130/l672.1
- Dusel-Bacon, C., & Williams, I. S. (2009). Evidence for prolonged mid-Paleozoic plutonism and ages of crustal sources in east-central Alaska from SHRIMP U-Pb dating of syn-magmatic, inherited, and detrital zircon. *Canadian Journal of Earth Sciences*, 46(1), 21–39. https://doi.org/10.1139/e09-005
- Eberhart-Phillips, D., Haeussler, P. J., Freymueller, J. T., Frankel, A. D., Rubin, C. M., Craw, P., & Dawson, T. E. (2003). The 2002 Denali fault earthquake, Alaska: A large magnitude, slip-partitioned event. Science, 300(5622), 1113–1118. https://doi.org/10.1126/science.1082703
- Eisbacher, G. H. (1976). Sedimentology of the Dezadeash flysch and its implications for strike-slip faulting along the Denali Fault, Yukon Territory and Alaska. Canadian Journal of Earth Sciences, 13(11), 1495–1513. https://doi.org/10.1139/e76-157
- Elliott, J., & Freymueller, J. T. (2020). A block model of present-day kinematics of Alaska and Western Canada. *Journal of Geophysical Research: Solid Earth*, 125(7), e2019JB018378. https://doi.org/10.1029/2019jb018378
- Enkelmann, E., Finzel, E., & Arkle, J. (2019). Deformation at the eastern margin of the Northern Canadian Cordillera: Potentially related to opening of the North Atlantic. *Terra Nova*, 31(3), 151–158. https://doi.org/10.1111/ter.12374
- Enkelmann, E., Garver, J. I., & Pavlis, T. L. (2008). Rapid exhumation of ice-covered rocks of the Chugach–St. Elias orogen, Southeast Alaska. *Geology*, 36(12), 915–918. https://doi.org/10.1130/g2252a.1
- Enkelmann, E., Zeitler, P. K., Garver, J. I., Pavlis, T. L., & Hooks, B. P. (2010). The thermochronological record of tectonic and surface process interaction at the Yakutat-North American collision zone in southeast Alaska. *American Journal of Science*, 310(4), 231–260. https://doi.org/10.2475/04.2010.01
- Enkin, R. J. (2006). Paleomagnetism and the case for Baja British Columbia. In J. W. Haggart, R. J. Enkin, & J. W. H. Monger (Eds.), Paleogeography of the North American Cordillera: Evidence for and against large-scale displacements. Geological Association of Canada Special Paper 46, pp. 233–254. St. Johns, Newfoundland: Geological Association of Canada.
- Erdmer, P., & Mortensen, J. K. (1993). A 1200-km-long Eocene metamorphic-plutonic belt in the northwestern Cordillera: Evidence from southwest Yukon. *Geology*, 21(11), 1039–1042. https://doi.org/10.1130/0091-7613(1993)021<1039:aklemp>2.3.co;2
- Estève, C., Audet, P., Schaeffer, A. J., Schutt, D. L., Aster, R. C., & Cubley, J. F. (2020). Seismic evidence for craton chiseling and displacement of lithospheric mantle by the Tintina fault in the northern Canadian Cordillera. *Geology*, 48. https://doi.org/10.1130/g47688.1
- Evenchick, C. A. (1991). Geometry, evolution, and tectonic framework of the Skeena Fold Belt, north central British Columbia. *Tectonics*, 10(3), 527–546. https://doi.org/10.1029/90TC02680

WALDIEN ET AL. 29 of 35



- Fasulo, C. R., Ridgway, K. D., & Trop, J. M. (2020). Detrital zircon geochronology and Hf isotope geochemistry of Mesozoic sedimentary basins in south-central Alaska: Insights into regional sediment transport, basin development, and tectonics along the NW Cordilleran margin. Geosphere. 16(5), 1125–1152. https://doi.org/10.1130/ges02221.1
- Finzel, E. S., Ridgway, K. D., & Trop, J. M. (2015). Provenance signature of changing plate boundary conditions along a convergent margin: Detrital record of spreading-ridge and flat-slab subduction processes, Cenozoic forearc basins, Alaska. *Geosphere*, 11(3), 823–849. https://doi.org/10.1130/ges01029.1
- Finzel, E. S., Trop, J. M., Ridgway, K. D., & Enkelmann, E. (2011). Upper plate proxies for flat-slab subduction processes in southern Alaska. Earth and Planetary Science Letters, 303(3–4), 348–360. https://doi.org/10.1016/j.epsl.2011.01.014
- Fitzgerald, P. G., Roeske, S. M., Benowitz, J. A., Riccio, S. J., Perry, S. E., & Armstrong, P. A. (2014). Alternating asymmetric topography of the Alaska range along the strike-slip Denali fault: Strain partitioning and lithospheric control across a terrane suture zone. *Tectonics*, 33(8), 1519–1533. https://doi.org/10.1002/2013TC003432
- Fitzgerald, P. G., Sorkhabi, R. B., Redfield, T. F., & Stump, E. (1995). Uplift and denudation of the central Alaska Range: A case study in the use of apatite fission track thermochronology to determine absolute uplift parameters. *Journal of Geophysical Research: Solid Earth*, 100(B10), 20175–20191. https://doi.org/10.1029/95JB02150
- Fitzgerald, P. G., Stump, E., & Redfield, T. F. (1993). Late Cenozoic uplift of Denali and its relation to relative plate motion and fault morphology. Science, 259(5094), 497–499. https://doi.org/10.1126/science.259.5094.497
- Forbes, R. B., Smith, T. E., & Turner, D. L. (1974). Comparative petrology and structure of the Maclaren, Ruby Range, and Coast Range belts: Implications for offset along the Denali fault system. *Geological Society of America Abstracts with Programs*. 6, 177.
- Foster, D. A., Doughty, P. T., Kalakay, T. J., Fanning, C. M., Coyner, S., Grice, W. C., & Vogl, J. (2007). Kinematics and timing of exhumation of metamorphic core complexes along the Lewis and Clark fault zone, northern Rocky Mountains, USA. In A. B. Till, S. M. Roeske, J. C. Sample, & D. A. Foster (Eds.), Special Paper 434: Exhumation associated with continental strike-slip fault systems (pp. 207–232). Geological Society of America. https://doi.org/10.1130/2007.2434(10)
- Gabrielse, H., Murphy, D. C., & Mortensen, J. K. (2006). Cretaceous and Cenozoic dextral orogen-parallel displacements, magmatism, and paleogeography, north-central Canadian Cordillera. In J. W. Haggart, R. J. Enkin, & J. W. H. Monger (Eds.), *Paleogeography of the north American Cordillera: Evidence for and against large-scale displacements. Geological Association of Canada Special Paper 46* (pp. 255–276). Geological Association of Canada.
- Gardner, M. C., Bergman, S. C., Cushing, G. W., MacKevett, E. M., Jr, Plafker, G., Campbell, R. B., et al. (1988). Pennsylvanian pluton stitching of Wrangellia and the Alexander terrane, Wrangell Mountains, Alaska. *Geology*, 16(11), 967–971. https://doi.org/10.1130/009 1-7613(1988)016<0967:ppsowa>2.3.co;2
- Garver, J. I., & Davidson, C. M. (2015). Southwestern Laurentian zircons in upper Cretaceous flysch of the Chugach-Prince William terrane in Alaska. American Journal of Science, 315(6), 537–556. https://doi.org/10.2475/06.2015.02
- Gehrels, G., & Pecha, M. (2014). Detrital zircon U-Pb geochronology and Hf isotope geochemistry of Paleozoic and Triassic passive margin strata of western North America. *Geosphere*, 10(1), 49–65.
- Gehrels, G., Rusmore, M., Woodsworth, G., Crawford, M., Andronicos, C., Hollister, L., et al. (2009). U-Th-Pb geochronology of the Coast Mountains batholith in north-coastal British Columbia: Constraints on age and tectonic evolution. *The Geological Society of America Bulletin*, 121(9–10), 1341–1361. https://doi.org/10.1130/B26404.1
- Gillis, R. J., Fitzgerald, P. G., Ridgway, K. D., Keough, B. M., Benowitz, J. A., & Allen, W. K. (2019). Overview of the new 1:25,000-scale geologic mapping of the McCallum-Slate Creek fault system, eastern Alaska Range, Alaska, Alaska Division of Geological & Geophysical Surveys Preliminary Interpretive Report 2018-3, 10 p. https://doi.org/10.14509/30136
- Greene, A. R., Scoates, J. S., & Weis, D. (2008). Wrangellia flood basalts in Alaska: A record of plume-lithosphere interaction in a Late Triassic accreted oceanic plateau. *Geochemistry, Geophysics, Geosystems*, 9(12). https://doi.org/10.1029/2008gc002092
- Greene, A. R., Scoates, J. S., Weis, D., Katvala, E. C., Israel, S., & Nixon, G. T. (2010). The architecture of oceanic plateaus revealed by the volcanic stratigraphy of the accreted Wrangellia oceanic plateau. *Geosphere*, 6(1), 47–73. https://doi.org/10.1130/ges00212.1
- Haeussler, P. J., Matmon, A., Schwartz, D. P., & Seitz, G. G. (2017). Neotectonics of interior Alaska and the late Quaternary slip rate along the Denali fault system. *Geosphere*, 13(5), 1445–1463. https://doi.org/10.1130/ges01447.1
- Haeussler, P. J., O'sullivan, P., Berger, A. L., & Spotila, J. A. (2008). Neogene exhumation of the Tordrillo Mountains, Alaska, and correlations with Denali (Mount Mckinley). In J. T. Freymueller, P. J. Haeussler, R. L. Wesson, & G. Ekström (Eds.), Geophysical Monograph Series (pp. 269–285). American Geophysical Union. https://doi.org/10.1029/179GM15
- Hampton, B. A., Ridgway, K. D., & Gehrels, G. E. (2010). A detrital record of Mesozoic island arc accretion and exhumation in the North American Cordillera: U-Pb geochronology of the Kahiltna basin, southern Alaska. *Tectonics*, 29(4). https://doi.org/10.1029/2009TC002544
- Hampton, B. A., Ridgway, K. D., O'Neill, J. M., Gehrels, G. E., Schmidt, J., & Blodgett, R. B. (2007). Pre-, syn-, and postcollisional stratigraphic framework and provenance of Upper Triassic-Upper Cretaceous strata in the northwestern Talkeetna Mountains, Alaska. In Ridgway, K. D., Trop, J. M., Glen, J. M. G., O'Neill, J. M. (Eds.). Special Paper 431: Tectonic growth of a collisional continental margin: Crustal evolution of Southern Alaska (Vol. 431, pp. 401–438). Geological Society of America. https://doi.org/10.1130/2007.2431(16)
- Hart, C. J., Mair, J. L., Goldfarb, R. J., & Groves, D. I. (2004). Source and redox controls on metallogenic variations in intrusion-related ore systems, Tombstone-Tungsten Belt, Yukon Territory, Canada. Earth and Environmental Science Transactions of The Royal Society of Edinburgh, 95(1–2), 339–356. https://doi.org/10.1130/0-8137-2389-2.339
- Haynie, K. L., & Jadamec, M. A. (2017). Tectonic drivers of the Wrangell block: Insights on fore-arc sliver processes from 3-D geodynamic models of Alaska. *Tectonics*, 36(7), 1180–1206. https://doi.org/10.1002/2016tc004410
- Herriott, T. M., Crowley, J. L., Schmitz, M. D., Wartes, M. A., & Gillis, R. J. (2019). Exploring the law of detrital zircon: LA-ICP-MS and CA-TIMS geochronology of Jurassic forearc strata, Cook Inlet, Alaska, USA. *Geology*, 47(11), 1044–1048. https://doi.org/10.1130/G46312.1
- Hildebrand, R. S. (2015). Dismemberment and northward migration of the Cordilleran orogen: Baja-BC resolved. *Geological Society of America Today*, 4–11. https://doi.org/10.1130/GSATG255A.1
- Hillhouse, J. W., & Coe, R. S. (1994). Paleomagnetic data from Alaska. In G. Plafker, & H. C. Berg (Eds.), *The geology of Alaska: Geology of North America* (Vol. G-1, pp. 797–812). Boulder, CO: Geological Society of America.
- Hollister, L. S. (1993). The role of melt in the uplift and exhumation of orogenic belts. *Chemical Geology*, 108(1-4), 31-48. https://doi.org/10.1016/0009-2541(93)90316-B
- Horstwood, M. S. A., Košler, J., Gehrels, G., Jackson, S. E., McLean, N. M., Paton, C., et al. (2016). Community-derived standards for LA-ICP-MS U-(Th-)Pb geochronology—Uncertainty propagation, age interpretation and data reporting. *Geostandards and Geoanalytical Research*, 40(3), 311–332. https://doi.org/10.1111/j.1751-908X.2016.00379.x

WALDIEN ET AL. 30 of 35



- Hoskin, P. W., & Schaltegger, U. (2003). The composition of zircon and igneous and metamorphic petrogenesis. In J. M Hanchar, & P. W. O Hoskin (Eds.), *Reviews in mineralogy and geochemistry: Zircon* (Vol. 53, pp. 27–62). Chantilly, VI: Mineralogical Society of America. https://doi.org/10.1515/9781501509322-005
- Hults, C. P., & Athey, J. E. (2011). Similarities between early Tertiary conglomerates along the Slate Creek and Duke River faults, Alaska and Yukon. 2011 Cordilleran Tectonics Workshop. Yukon Geological Survey Miscellaneous Report, 3, 11–12.
- Hults, C. P., Wilson, F. H., Donelick, R. A., & O'Sullivan, P. B. (2013). Two flysch belts having distinctly different provenance suggest no stratigraphic link between the Wrangellia composite terrane and the paleo-Alaskan margin. *Lithosphere*, 5(6), 575–594. https://doi.org/10.1130/l310.1
- Hyndman, R. D., Currie, C. A., & Mazzotti, S. P. (2005). Subduction zone backarcs, mobile belts, and orogenic heat. *Geological Society of America Today*, 15(2), 4–10. https://doi.org/10.1130/1052-5173(2005)015<4:szbmba>2.0.co;2
- Israel, S., Beranek, L., Friedman, R. M., & Crowley, J. L. (2014). New ties between the Alexander terrane and Wrangellia and implications for North America Cordilleran evolution. *Lithosphere*, 6(4), 270–276. https://doi.org/10.1130/L364.1
- Israel, S., Colpron, M., Cubley, J., Moynihan, D., Murphy, D. C. & Relf, C. (2015). The Bear Creek assemblage: A latest Triassic volcano-sed-imentary succession in southwest Yukon. In K. E. MacFarlane, M. G. Nordling, & P. J. Sack (Eds.), *Yukon exploration and geology 2014* (pp. 99–112). Yukon Geological Survey.
- Israel, S., Murphy, D., Bennett, V., Mortensen, J., & Crowley, J. (2011). New insights into the geology and mineral potential of the Coast Belt in southwestern Yukon. *Yukon exploration and geology* (pp. 101–123).
- Israel, S., Schiarizza, P., Kennedy, L. A., Friedman, R. M., & Villeneuve, M. (2006). Evidence for Early to Late Cretaceous sinistral deformation in the Tchaikazan River area, southwestern British Columbia: Implications for the tectonic evolution of the southern Coast belt. In J. W. Haggart, R. J. Enkin, & J. W. H. Monger (Eds.), *Paleogeography of the North American Cordillera: Evidence for and against large-scale displacements. Geological Association of Canada Special Paper 46* (pp. 331–350). Geological Association of Canada.
- Jadamec, M. A., Billen, M. I., & Roeske, S. M. (2013). Three-dimensional numerical models of flat slab subduction and the Denali fault driving deformation in south-central Alaska. Earth and Planetary Science Letters, 376, 29–42. https://doi.org/10.1016/j.epsl.2013.06.009
  Jarrard, R. D. (1986). Terrane motion by strike-slip faulting of forearc slivers. Geology, 14(9), 780–783. https://doi.org/10.1130/0091-7613(1986)14<780:tmbsfo>2.0.coi2
- Johnston, S. T. (1999). Large-scale coast-parallel displacements in the Cordillera: A granitic resolution to a paleomagnetic dilemma. *Journal of Structural Geology*, 21(8–9), 1103–1108. https://doi.org/10.1016/s0191-8141(99)00015-2
- Johnston, S. T. (2008). The Cordilleran ribbon continent of North America. *Annual Review of Earth and Planetary Sciences*, 36(1), 495–530. https://doi.org/10.1146/annurev.earth.36.031207.124331
- Johnston, S. T., & Canil, D. (2007). Crustal architecture of SW Yukon, northern Cordillera: Implications for crustal growth in a convergent
- margin orogen. *Tectonics*, 26(1). https://doi.org/10.1029/2006tc001950

  Johnston, S. T., Jane Wynne, P., Francis, D., Hart, C. J., Enkin, R. J., & Engebretson, D. C. (1996). Yellowstone in Yukon: The late Cretaceous
- Carmacks group. Geology, 24(11), 997–1000. https://doi.org/10.1130/0091-7613(1996)024<0997:yiytlc>2.3.co;2 Johnston, S. T., Mortensens, J. K., & Erdmer, P. (1996). Igneous and metaigneous age constraints for the Aishihik metamorphic suite,
- southwest Yukon. Canadian Journal of Earth Sciences, 33(11), 1543–1555. https://doi.org/10.1139/e96-117

  Kalbas, J. L., Ridgway, K. D., & Gehrels, G. E. (2007). Stratigraphy, depositional systems, and provenance of the Lower Cretaceous Kahiltna assemblage, western Alaska Range: Basin development in response to oblique collision. In Ridgway, K. D., Trop, J. M., Glen, J. M. G., O'Neill, J. M. (Eds.). Special Paper 431: Tectonic growth of a collisional continental margin: Crustal evolution of Southern Alaska (Vol. 431, pp. 307–343). Geological Society of America. https://doi.org/10.1130/2007.2431(13)
- Kapp, P. A., & Gehrels, G. E. (1998). Detrital zircon constraints on the tectonic evolution of the Gravina belt, southeastern Alaska. Canadian Journal of Earth Sciences, 35(3), 253–268. https://doi.org/10.1139/e97-110
- Lange, D., Cembrano, J., Rietbrock, A., Haberland, C., Dahm, T., & Bataille, K. (2008). First seismic record for intra-arc strike-slip tectonics along the Liquiñe-Ofqui fault zone at the obliquely convergent plate margin of the southern Andes. *Tectonophysics*, 455(1–4), 14–24. https://doi.org/10.1016/j.tecto.2008.04.014
- Layer, P. W., Hall, C. M., & York, D. (1987). The derivation of <sup>40</sup>Ar/<sup>39</sup>Ar age spectra of single grains of hornblende and biotite by laser step-heating. *Geophysical Research Letters*, 14(7), 757–760. https://doi.org/10.1029/gl014i007p00757
- Lease, R. O. (2018). Pliocene erosional pulse and glacier-landscape feedbacks in the western Alaska Range. Earth and Planetary Science Letters, 497, 62–68. https://doi.org/10.1016/j.epsl.2018.06.009
- Lease, R. O., Haeussler, P. J., & O'Sullivan, P. (2016). Changing exhumation patterns during Cenozoic growth and glaciation of the Alaska Range: Insights from detrital thermochronology and geochronology. *Tectonics*, 35(4), 934–955. https://doi.org/10.1002/2015TC004067
- Light, T. D., Tripp, R. B., & King, H. D. (1990). Interpretation of reconnaissance geochemical data from the Healy quadrangle, Alaska. US Geological Survey Bulletin 1894. https://doi.org/10.3133/b1894
- Link, B. J. (2017). From deposition to deformation within an accretionary suture zone: An example from the clearwater and Talkeetna mountains, Alaska range suture zone. (Unpublished master's thesis). West Lafayette, IN. Purdue University.
- Little, T. A. (1990). Kinematics of wrench and divergent-wrench deformation along a central part of the Border Ranges Fault System, Northern Chugach Mountains, Alaska. *Tectonics*, 9(4), 585–611. https://doi.org/10.1029/tc009i004p00585
- Lowey, G. W. (1998). A new estimate of the amount of displacement on the Denali fault system based on the occurrence of carbonate megaboulders in the Dezadeash Formation (Jura-Cretaceous), Yukon, and the Nutzotin Mountains sequence (Jura-Cretaceous), Alaska. Bulletin of Canadian Petroleum Geology, 46(3), 379–386.
- Lowey, G. W. (2000). The Tatshenshini shear zone (new) in southwestern Yukon, Canada: Comparison with the Coast shear zone in British Columbia and southeastern Alaska and implications regarding the Shakwak suture. *Tectonics*, 19(3), 512–528. https://doi.org/10.1029/1999TC001119
- Lowey, G. W. (2011). Volcaniclastic gravity flow deposits in the Dezadeash Formation (Jura-Cretaceous), Yukon, Canada: Implications regarding the tectonomagmatic evolution of the Chitina arc in the northern Cordillera of North America. *Lithos*, 125(1–2), 86–100. https://doi.org/10.1016/j.lithos.2011.01.014
- Lowey, G. W. (2019). Provenance analysis of the Dezadeash Formation (Jurassic–Cretaceous), Yukon, Canada: Implications regarding a linkage between the Wrangellia composite terrane and the western margin of Laurasia. *Canadian Journal of Earth Sciences*, 56(1), 77–100. https://doi.org/10.1139/cjes-2017-0244
- Ludwig, K. R. (2008). User's manual for Isoplot 3.70 (Vol. 4, pp. 76–80). Berkeley Geochronology Center Special Publication. https://doi.org/10.1111/j.1439-0272.2007.00823.x

WALDIEN ET AL. 31 of 35



- Mahoney, J. B., Gordee, S. M., Haggart, J. W., Friedman, R. M., Diakow, L. J., & Woodsworth, G. J. (2009). Magmatic evolution of the eastern Coast Plutonic Complex, Bella Coola region, west-central British Columbia. *The Geological Society of America Bulletin*, 121(9–10), 1362–1380. https://doi.org/10.1130/B26325.1
- Mair, J. L., Hart, C. J., & Stephens, J. R. (2006). Deformation history of the northwestern Selwyn Basin, Canada: Implications for orogen evolution and mid-Cretaceous magmatism. *The Geological Society of America Bulletin*, 118(3–4), 304–323. https://doi.org/10.1130/b25763.1
- Manselle, P., Brueseke, M. E., Trop, J. M., Benowitz, J. A., Snyder, D. C., & Hart, W. K. (2020). Geochemical and stratigraphic analysis of the Chisana Formation, Wrangellia terrane, eastern Alaska: Insights into Early Cretaceous magmatism and tectonics along the northern Cordilleran margin. *Tectonics*, e2020TC006131. https://doi.org/10.1029/2020tc006131
- Manuszak, J. D., Ridgway, K. D., Trop, J. M., & Gehrels, G. E. (2007). Sedimentary record of the tectonic growth of a collisional continental margin: Upper Jurassic-Lower Cretaceous Nutzotin Mountains sequence, eastern Alaska Range, Alaska. In K. D. Ridgway, J. M. Trop, J. M. G. Glen, & J. M. O'Neill (Eds.), Special Paper 431: Tectonic growth of a collisional continental margin: Crustal evolution of Southern Alaska (Vol. 431, pp. 345–377). Boulder, CO: Geological Society of America. https://doi.org/10.1130/2007.2431(14)
- Matthews, W. A., Guest, B., Coutts, D., Bain, H., & Hubbard, S. (2017). Detrital zircons from the Nanaimo basin, Vancouver Island, British Columbia: An independent test of Late Cretaceous to Cenozoic northward translation. *Tectonics*, 36(5), 854–876. https://doi.org/10.1002/2017tc004531
- McClelland, W. C., Gehrels, G. E., & Saleeby, J. B. (1992). Upper Jurassic-Lower Cretaceous basinal strata along the Cordilleran Margin: Implications for the accretionary history of the Alexander-Wrangellia-Peninsular Terrane. *Tectonics*, 11(4), 823–835. https://doi.org/10.1029/92TC00241
- McCrory, P. A., & Wilson, D. S. (2013). A kinematic model for the formation of the Siletz-Crescent forearc terrane by capture of coherent fragments of the Farallon and Resurrection plates. *Tectonics*, 32(3), 718–736. https://doi.org/10.1002/tect.20045
- McDermott, R. G., Ault, A. K., Caine, J. S., & Thomson, S. N. (2019). Thermotectonic history of the Kluane ranges and evolution of the Eastern Denali Fault Zone in Southwestern Yukon, Canada. *Tectonics*, 38(8), 2983–3010. https://doi.org/10.1029/2019TC005545
- Mezger, J. E. (1999). Alpine-type'ultramafic rocks of the Kluane metamorphic assemblage, southwest Yukon: Oceanic crust fragments of a late Mesozoic back-arc basin along the northern Coast Belt. Yukon exploration and geology (pp. 127–138).
- Mezger, J. E. (2002). Geology of the Dezadeash Range and adjacent northern Coast Mountains (115A), southwestern Yukon: Re-examination of a terrane boundary. Yukon exploration and geology (pp. 149–163).
- Mezger, J. E., Chacko, T., & Erdmer, P. (2001). Metamorphism at a late Mesozoic accretionary margin: A study from the Coast Belt of the North American Cordillera. *Journal of Metamorphic Geology*, 19(2), 121–137. https://doi.org/10.1046/j.0263-4929.2000.00300.x
- Mezger, J. E., Creaser, R. A., Erdmer, P., & Johnston, S. T. (2001). A Cretaceous back-arc basin in the Coast Belt of the northern Canadian Cordillera: Evidence from geochemical and neodymium isotope characteristics of the Kluane metamorphic assemblage, southwest Yukon. Canadian Journal of Earth Sciences, 38(1), 91–103. https://doi.org/10.1139/e00-076
- Milde, E. R. (2014). Using low-temperature thermochronology to constrain the role of the Totschunda Fault in Southeastern Alaskan tectonics (Unpublished master's thesis). Syracuse, NY: Syracuse University.
- Miller, M. L., Bradley, D. C., Bundtzen, T. K., & McClelland, W. (2002). Late Cretaceous through Cenozoic Strike-Slip Tectonics of Southwestern Alaska. *The Journal of Geology*, 110(3), 247–270. https://doi.org/10.1086/339531
- Miller, M. S., O'Driscoll, L. J., Porritt, R. W., & Roeske, S. M. (2018). Multiscale crustal architecture of Alaska inferred from P receiver functions. Lithosphere, 10(2), 267–278. https://doi.org/10.1130/L701.1
- Miskovic, A., & Francis, D. (2004). The early tertiary sifton range volcanic complex, southwestern Yukon. Yukon exploration and geology (pp. 143–155).
- Monger, J. W. H., & Gibson, H. D. (2019). Mesozoic-Cenozoic deformation in the Canadian Cordillera: The record of a "Continental Bull-dozer"? *Tectonophysics*, 757, 153–169. https://doi.org/10.1016/j.tecto.2018.12.023
- Monger, J. W. H., Van Der Heyden, P., Journeay, J. M., Evenchick, C. A., & Mahoney, J. B. (1994). Jurassic-Cretaceous basins along the Canadian Coast Belt: Their bearing on pre-mid-Cretaceous sinistral displacements. *Geology*, 22(2), 175–178. https://doi.org/10.1130/0091-7613(1994)022<0175;jcbatc>2.3.co;2
- Mooney, P.R. (2010). Geology of the clearwater mountains and southern boundary of the Alaska range suture zone. (Unpublished master's thesis). Davis, CA: University of California.
- Moores, E. (1970). Ultramafics and orogeny, with models of the US Cordillera and the Tethys. *Nature*, 228(5274), 837–842. https://doi.org/10.1038/228837a0
- Morris, G. A., & Creaser, R. A. (2003). Crustal recycling during subduction at the Eocene Cordilleran margin of North America: A petrogenetic study from the southwestern Yukon. Canadian Journal of Earth Sciences, 40(12), 1805–1821. https://doi.org/10.1139/e03-063
- Morrison, G. W., Godwin, C. I., & Armstrong, R. L. (1979). Interpretation of isotopic ages and 87Sr/86Sr initial ratios for plutonic rocks in the Whitehorse map area, Yukon. *Canadian Journal of Earth Sciences*, 16(10), 1988–1997. https://doi.org/10.1139/e79-185
- Murphy, D. C. (2018). Latest Cretaceous–early Eocene Pacific-Arctic?—Atlantic connection: Co-evolution of strike-slip fault systems, oroclines, and transverse fold-and-thrust belts in the northwestern North American Cordillera. In K. Piepjohn, J. V. Strauss, L. Reinhardt, & W. C. McClelland (Eds.), Special Paper 541: Circum-Arctic structural events: Tectonic evolution of the Arctic margins and Trans-Arctic links with adjacent Orogens. Boulder, CO: Geological Society of America. https://doi.org/10.1130/2018.2541(28)
- Nelson, J., & Colpron, M. (2007). Tectonics and metallogeny of the British Columbia, Yukon and Alaskan Cordillera, 1.8 Ga to the present. In Mineral deposits of Canada: A synthesis of major deposit-types, district metallogeny, the evolution of geological provinces, and exploration methods (Vol. 5, pp. 755–791). Geological Association of Canada, Mineral Deposits Division, Special Publication.
- Nokleberg, W. J., Aleinikoff, J. N., Dutro, J. T., Jr, Lanphere, M. A., Silberling, N.J., Silva, S. R., et al. (1992). Map, tables, and summary of fossil and isotopic age data, Mount Hayes quadrangle, eastern 1789 Alaska Range, Alaska. U.S. Geological Survey Miscellaneous Field Studies map 1996-D, 43 p., 1 sheet, scale 1:250,000. https://doi.org/10.3133/mf1996d
- Nokleberg, W. J., Aleinikoff, J. N., Lange, I. M., Silva, S. R., Miyaoka, R. T., Schwab, C. E., & Zehner, R. E. (1992). Preliminary geologic map of the Mount Hayes quadrangle, eastern Alaska Range, Alaska. U.S. Geological Survey Open File Report 92-594, 39p., 1 sheet, scale 1:250,000. https://doi.org/10.3133/ofr92594
- Nokleberg, W. J., Jones, D. L., & Silberling, N. J. (1985). Origin and tectonic evolution of the Maclaren and Wrangellia terranes, eastern Alaska Range, Alaska. The *Geological Society of America Bulletin*, 96(10), 1251–1270. https://doi.org/10.1130/0016-7606(1985)96<125
- Nokleberg, W. J., & Richter, D. H. (2007). Origin of narrow terranes and adjacent major terranes occurring along the Denali fault in the Eastern and Central Alaska Range, Alaska. In K. D. Ridgway, J. M. Trop, J. M. G. Glen, & J. M. O'Neill (Eds.), Special Paper 431: Tectonic

WALDIEN ET AL. 32 of 35



- growth of a collisional continental margin: Crustal evolution of southern Alaska (Vol. 431, pp. 129–154): Geological Society of America. https://doi.org/10.1130/2007.2431(06)
- O'Driscoll, L. J., & Miller, M. S. (2015). Lithospheric discontinuity structure in Alaska, thickness variations determined by *Sp* receiver functions. *Tectonics*, 34(4), 694–714. https://doi.org/10.1002/2014TC003669
- O'Neill, J. M., Ridgway, K. D., & Eastham, K. R. (2001). Mesozoic Sedimentation and deformation along the Talkeetna thrust fault, south-central Alaska—New insights and their regional tectonic Significance. 10. U.S. Geological Survey Professional Paper 1678.
- Otiniano, G. A., Porter, T. J., Benowitz, J. A., Bindeman, I. N., Froese, D. G., Jensen, B. J., et al. (2000). A late Miocene to late Pleistocene reconstruction of precipitation isotopes and climate from hydrated volcanic glass shards and biomarkers in central Alaska and Yukon. *Paleoceanography and Paleoclimatology*, e2019PA003791.
- Parrish, R. R., Carr, S. D., & Parkinson, D. L. (1988). Eocene extensional tectonics and geochronology of the southern Omineca Belt, British Columbia and Washington. *Tectonics*, 7(2), 181–212. https://doi.org/10.1029/tc007i002p00181
- Pavlis, T. L., Amato, J. M., Trop, J. M., Ridgway, K. D., Roeske, S. M., & Gehrels, G. E. (2019). Subduction polarity in ancient arcs: A call to integrate geology and geophysics to decipher the Mesozoic tectonic history of the Northern Cordillera of North America. Geological Society of America Today, 29(11). https://doi.org/10.1130/gsatg402a.1
- Pavlis, T. L., Chapman, J. B., Bruhn, R. L., Ridgway, K., Worthington, L. L., Gulick, S. P., & Spotila, J. (2012). Structure of the actively deforming fold-thrust belt of the St. Elias orogen with implications for glacial exhumation and three-dimensional tectonic processes. *Geosphere*, 8(5), 991–1019. https://doi.org/10.1130/ges00753.1
- Pecha, M. E., Gehrels, G. E., McClelland, W. C., Giesler, D., White, C., & Yokelson, I. (2016). Detrital zircon U-Pb geochronology and Hf isotope geochemistry of the Yukon-Tanana terrane, Coast Mountains, southeast Alaska. *Geosphere*, 12(5), 1556–1574. https://doi.org/10.1130/ges01303.1
- Piercey, S. J., & Colpron, M. (2009). Composition and provenance of the Snowcap assemblage, basement to the Yukon-Tanana terrane, northern Cordillera: Implications for Cordilleran crustal growth. *Geosphere*, 5(5), 439–464. https://doi.org/10.1130/ges00505.s3
- Preece, S. J., & Hart, W. K. (2004). Geochemical variations in the <5 Ma Wrangell Volcanic Field, Alaska: Implications for the magmatic and tectonic development of a complex continental arc system. *Tectonophysics*, 392(1–4), 165–191. https://doi.org/10.1016/j.tecto.2004.04.011
- Rasendra, N., Bonnin, M., Mazzotti, S., & Tiberi, C. (2014). Crustal and upper-mantle anisotropy related to fossilized transpression fabric along the Denali Fault, Northern Canadian Cordillera. *Bulletin of the Seismological Society of America*, 104(4), 1964–1975. https://doi.org/10.1785/0120130233
- Ratchkovski, N. A., Wiemer, S., & Hansen, R. A. (2004). Seismotectonics of the central Denali fault, Alaska, and the 2002 Denali fault earthquake sequence. *Bulletin of the Seismological Society of America*, 94(6B), S156–S174. https://doi.org/10.1785/0120040621
- Regan, S., Benowitz, J. B., Waldien, T. S., Holland, M., Roeske, S. M., O'Sullivan, P. B., & Layer, P. (2021). Long distance plutonic relationships demonstrate 33 million years of strain partitioning along the Denali fault. *Terra Nova*. In press. https://doi.org/10.1111/ter.12555
- Regan, S. P., Benowitz, J. A., & Holland, M. E. (2020). A plutonic brother from another magma mother: Disproving the Eocene Foraker-McGonagall pluton piercing point and implications for long-term slip on the Denali Fault. *Terra Nova*, 32(1), 66–74. https://doi.org/10.1111/ter.12437
- Renne, P. R., Deino, A. L., Walter, R. C., Turrin, B. D., Swisher, C. C., III, Becker, T. A., et al. (1994). Intercalibration of astronomical and radioisotopic time. *Geology*, 22(9), 783–786. https://doi.org/10.1130/0091-7613(1994)022<0783:ioaart>2.3.co;2
- Renne, P. R., Mundil, R., Balco, G., Min, K., & Ludwig, K. R. (2010). Joint determination of <sup>40</sup>K decay constants and <sup>40</sup>Ar\*/<sup>40</sup>K for the Fish Canyon sanidine standard, and improved accuracy for <sup>40</sup>Ar/<sup>39</sup>Ar geochronology. *Geochimica et Cosmochimica Acta*, 74(18), 5349–5367. https://doi.org/10.1016/j.gca.2010.06.017
- Riccio, S. J., Fitzgerald, P. G., Benowitz, J. A., & Roeske, S. M. (2014). The role of thrust faulting in the formation of the eastern Alaska Range: Thermochronological constraints from the Susitna Glacier Thrust Fault region of the intracontinental strike-slip Denali Fault system: Susitna Glacier thrust fault. *Tectonics*, 33(11), 2195–2217. https://doi.org/10.1002/2014TC003646
- Richter, D. H., & Dutro, J. T., Jr (1975). Revision of the type Mankommen Formation (Pennsylvanian and Permian), Eagle Creek area, eastern Alaska Range, Alaska. U.S. Geological Survey Bulletin 1395–B. B1–B25.
- Ridgway, K. D., Thoms, E. E., Layer, P. W., Lesh, M. E., White, J. M., & Smith, S. V. (2007). Neogene transpressional foreland basin development on the north side of the central Alaska Range, Usibelli Group and Nenana Gravel, Tanana basin. In K. D. Ridgway, J. M. Trop, J. M. G. Glen, & J. M. O'Neill (Eds.), Special Paper 431: Tectonic growth of a collisional continental margin: Crustal evolution of Southern Alaska (Vol. 431, pp. 507–547). Boulder, CO: Geological Society of America. https://doi.org/10.1130/2007.2431(20)
- Ridgway, K. D., Trop, J. M., Nokleberg, W. J., Davidson, C. M., & Eastham, K. R. (2002). Mesozoic and Cenozoic tectonics of the eastern and central Alaska Range: Progressive basin development and deformation in a suture zone. *The Geological Society of America Bulletin*, 114(12), 1480–1504. https://doi.org/10.1130/0016-7606(2002)114<1480:mactot>2.0.co;2
- Rioux, M., Hacker, B., Mattinson, J., Kelemen, P., Blusztajn, J., & Gehrels, G. (2007). Magmatic development of an intra-oceanic arc: High-precision U-Pb zircon and whole-rock isotopic analyses from the accreted Talkeetna arc, south-central Alaska. *The Geological Society of America Bulletin*, 119(9–10), 1168–1184. https://doi.org/10.1130/b25964.1
- Roeske, S. M., Mattinson, J. M., & Armstrong, R. L. (1989). Isotopic ages of glaucophane schists on the Kodiak Islands, southern Alaska, and their implications for the Mesozoic tectonic history of the Border Ranges fault system. *The Geological Society of America Bulletin*, 101(8), 1021–1037. https://doi.org/10.1130/0016-7606(1989)101<1021:iaogso>2.3.co;2
- Roeske, S. M., Snee, L. W., Pavlis, T. L., & Sisson, V. B. (2003). Dextral-slip reactivation of an arc-forearc boundary during Late Cretaceous-early Eocene oblique convergence in the northern Cordillera. In V. B. Sisson, S. M. Roeske, & T. L. Pavlis (Eds.), Special Paper 371: Geology of a transpressional orogen developed during Ridge-Trench interaction along the North Pacific margin (Vol. 371, pp. 141–169). Boulder, CO: Geological Society of America. https://doi.org/10.1130/0-8137-2371-x.141
- Romero, M. C., Ridgway, K. D., & Gehrels, G. E. (2020). Geology, U-Pb geochronology, and Hf isotope geochemistry across the mesozoic Alaska Range Suture Zone (South-Central Alaska): Implications for Cordilleran collisional processes and tectonic growth of North America. *Tectonics*, 39(3). https://doi.org/10.1029/2019TC005946
- Rusmore, M. E., Bogue, S. W., & Woodsworth, G. J. (2013). Paleogeography of the insular and intermontane terranes reconsidered: Evidence from the southern Coast Mountains Batholith, British Columbia. *Lithosphere*, 5(5), 521–536. https://doi.org/10.1130/l288.1
- Ryan, J. J., Hayward, N., & Jackson, L. E. (2017). Landscape antiquity and Cenozoic drainage development of southern Yukon, through restoration modeling of the Tintina Fault. Canadian Journal of Earth Sciences, 54(10), 1085–1100. https://doi.org/10.1139/cjes-2017-0053
- Sack, P. J., Colpron, M., Crowley, J. L., Ryan, J. J., Allan, M. M., Beranek, L. P., & Joyce, N. L. (2020). Allas of late Triassic to Jurassic plutons in the Intermontane terranes of Yukon (p. 378).

WALDIEN ET AL. 33 of 35



- $Saltus, R. W., \& \ Hudson, T. \ L. (2007). \ Regional \ magnetic \ anomalies, \ crustal \ strength, \ and \ the \ location \ of \ the \ northern \ Cordilleran \ fold-and-thrust \ belt. \ \textit{Geology}, 35(6), 567-570. \ https://doi.org/10.1130/g23470a.1$
- Samson, S. D., & Alexander, E. C., Jr (1987). Calibration of the interlaboratory <sup>40</sup>Ar/<sup>39</sup>Ar dating standard, MMhb-1. *Chemical Geology: Isotope Geoscience Section*, 66(1–2), 27–34. https://doi.org/10.1016/0168-9622(87)90025-x
- Sauer, K. B., Gordon, S. M., Miller, R. B., Jacobson, C. E., Grove, M., Vervoort, J. D., & Fisher, C. M. (2019). Deep-crustal metasedimentary rocks support Late Cretaceous "Mojave-BC" translation. *Geology*, 47(2), 99–102. https://doi.org/10.1130/g45554.1
- Saylor, J. E., Jordan, J. C., Sundell, K. E., Wang, X., Wang, S., & Deng, T. (2018). Topographic growth of the Jishi Shan and its impact on basin and hydrology evolution, NE Tibetan Plateau. *Basin Research*, 30(3), 544–563. https://doi.org/10.1111/bre.12264
- Saylor, J. E., & Sundell, K. E. (2016). Quantifying comparison of large detrital geochronology data sets. *Geosphere*, 12(1), 203–220. https://doi.org/10.1130/ges01237.1
- Sigloch, K., & Mihalynuk, M. G. (2017). Mantle and geological evidence for a Late Jurassic-Cretaceous suture spanning North America. GSA Bulletin, 129(11–12), 1489–1520.
- Smith, T. E. (1981). Geology of the Clearwater Mountains, south-central Alaska. Alaska Division of Geological & Geophysical Surveys Geologic Report 60, 72 p., 3 sheets, scale 1:63,360. https://doi.org/10.14509/406
- St. Amand, P. (1957). Geological and geophysical synthesis of the tectonics of portions of British Columbia, the Yukon Territory, and Alaska. *The Geological Society of America Bulletin*, 68(10), 1343–1370. https://doi.org/10.1130/0016-7606(1957)68[1343:gagsot]2.0.co;2
- Stamatakos, J. A., Trop, J. M., & Ridgway, K. D. (2001). Late Cretaceous paleogeography of Wrangellia: Paleomagnetism of the MacColl Ridge Formation, southern Alaska, revisited. *Geology*, 29(10), 947–950. https://doi.org/10.1130/0091-7613(2001)029<0947:lcpowp>2.0.co;2
- Stanley, B. (2012). Structural geology and geochronology of the Kluane schist, southwestern Yukon Territory (Unpublished master's thesis). Waterloo. ON: University of Waterloo.
- Stout, J. H. (1965). Bedrock geology between Rainy Creek and the Denali fault, Eastern Alaska Range, Alaska. (Unpublished master's thesis). Fairbanks, AK: University of Alaska.
- Sturrock, D. L., Armstrong, R. L., & Maxwell, R. B. (1980). Age and Sr isotopic composition of the Pyroxenite Creek ultramafic complex, southwestern Yukon Territory: An Alaskan-type ultramafic complex, in Current Research, Part B. Geological Survey of Canada Paper 80-1B, pp. 185–188.
- Tempelman-Kluit, D. J., & Wanless, R. K. (1975). Potassium–argon age determinations of metamorphic and plutonic rocks in the Yukon Crystalline Terrane. Canadian Journal of Earth Sciences, 12(11), 1895–1909. https://doi.org/10.1139/e75-167
- Terhune, P. J., Benowitz, J. A., Waldien, T. S., Allen, W. K., Davis, K. N., Ridgway, K. D., et al. (2015). Geochronological framework for the Cenozoic history of the southern Alaska Range fold and thrust belt. *Geological Society of America Abstracts with Programs*. 47(4), p. 60.
- Till, A. B., Roeske, S. M., Bradley, D. C., Friedman, R., & Layer, P. W. (2007). Early Tertiary transtension-related deformation and magmatism along the Tintina fault system, Alaska. In A. B. Till, S. M. Roeske, J. C. Sample, & D. A. Foster (Eds.), Special Paper 434: Exhumation associated with continental strike-slip fault systems (Vol. 434, pp. 233–264). Geological Society of America. https://doi.org/10.1130/2007.2434(11)
- Trop, J. M., Benowitz, J., Cole, R. B., & O'Sullivan, P. (2019). Cretaceous to Miocene magmatism, sedimentation, and exhumation within the Alaska Range suture zone: A polyphase reactivated terrane boundary. *Geosphere*, 15(4), 1066–1101. https://doi.org/10.1130/GES02014.1
- Trop, J. M., Benowitz, J. A., Koepp, D. Q., Sunderlin, D., Brueseke, M. E., Layer, P. W., & Fitzgerald, P. G. (2020). Stitch in the ditch: Nutzotin Mountains (Alaska) fluvial strata and a dike record ca. 117–114 Ma accretion of Wrangellia with western North America and initiation of the Totschunda fault. *Geosphere*. 16(1), 82–110. https://doi.org/10.1130/GES02127.1
- Trop, J. M., & Ridgway, K. D. (2007). Mesozoic and Cenozoic tectonic growth of southern Alaska: A sedimentary basin perspective. In K. D. Ridgway, J. M. Trop, J. M. G. Glen, & J. M. O'Neill (Eds.), Special Paper 431: Tectonic growth of a collisional continental margin: Crustal evolution of Southern Alaska (Vol. 431, pp. 55–94). Geological Society of America. https://doi.org/10.1130/2007.2431(04)
- Turner, D. L., & Smith, T. E. (1974). Geochronology and generalized geology of the central Alaska Range, Clearwater Mountains, and northern Talkeetna Mountains. Alaska Division of Geological & Geophysical Surveys Alaska Open-File Report 72, 13 p., 1 sheet, scale, 1:250,000. https://doi.org/10.14509/167
- Twelker, E., Waldien, T. S., Newberry, R. J., Freeman, L. K., Sicard, K. R., Lande, L. L., et al. (2020). Bedrock geologic map of the eastern Denali Highway area, Mount 1955 Hayes, Healy, and Talkeetna Mountains quadrangles, Alaska. Alaska Division of Geological & Geophysical Surveys Report of Investigation 2020-7: 1 sheet, 1:100,000 scale. https://doi.org/10.14509/30469
- Vallage, A., Devès, M. H., Klinger, Y., King, G. C. P., & Ruppert, N. A. (2014). Localized slip and distributed deformation in oblique settings: The example of the Denali fault system, Alaska. *Geophysical Journal International*, 197(3), 1284–1298. https://doi.org/10.1093/gii/ggu100
- Vermeesch, P. (2004). How many grains are needed for a provenance study? Earth and Planetary Science Letters, 224(3-4), 441-451. https://doi.org/10.1016/j.epsl.2004.05.037
- Vermeesch, P. (2012). On the visualisation of detrital age distributions. Chemical Geology, 312, 190–194. https://doi.org/10.1016/j.chemgeo.2012.04.021
- Vice, L. (2017). Late Cretaceous to Paleocene evolution of the Blanchard River assemblage, southwest Yukon; implications for Mesozoic accretionary processes in the northwestern Cordillera. (Unpublished master's thesis). Simon Fraser University.
- Vice, L., Gibson, H. D., Israel, S., & Abu-Alam, T. S. (2020). Late Cretaceous to Paleocene tectonometamorphic evolution of the Blanchard River Assemblage, Southwest Yukon: New insight into the terminal accretion of insular terranes in the Northern Cordillera. *Lithosphere*. (1) https://doi.org/10.2113/2020/2298288
- Wahrhaftig, C., Turner, D. L., Weber, F. R., & Smith, T. E. (1975). Nature and timing of movement on Hines Creek strand of Denali fault system, Alaska. *Geology*, 3(8), 463–466. https://doi.org/10.1130/0091-7613(1975)3<463:natomo>2.0.co;2
- Waldien, T. S., Roeske, S. M., Benowitz, J. A., Allen, W. K., Ridgway, K. D., & O'Sullivan, P. B. (2018). Late Miocene to Quaternary evolution of the McCallum Creek thrust system, Alaska: Insights for range-boundary thrusts in transpressional orogens. *Geosphere*, 14(6), 2379–2406. https://doi.org/10.1130/GES01676.1
- Waldien, T. S., Roeske, S. M., Benowitz, J. A., Twelker, E., & Miller, M. S. (2021). Oligocene-Neogene reactivation of Mesozoic lithospheric-scale terrane accretionary structures in the Alaska Range suture zone, southern Alaska. *Geological Society of America Bulletin*. 133(3-4), 691–716. https://doi.org/10.1130/b35665.1
- Wallace, W. K., Hanks, C. L., & Rogers, J. F. (1989). The southern Kahiltna terrane: Implications for the tectonic evolution of southwestern Alaska. *The Geological Society of America Bulletin*, 101(11), 1389–1407. https://doi.org/10.1130/0016-7606(1989)101<1389:tsktif>2.3.co;2 Wilson, F. H., Dover, J. H., Bradley, D. C., Weber, F. R., Bundtzen, T. K., & Haeussler, P. J. (1998). *Geologic map of Central (interior) Alaska*.

WALDIEN ET AL. 34 of 35

U.S. Geological Survey Open-File Report 98-133-A, 62 p., 3 sheets. https://doi.org/10.3133/ofr98133a



- Wilson, F. H., Hults, C. P., Mull, C. G., & Karl, S. M. (2015). Geologic map of Alaska. U.S. Geological Survey Scientific Investigations Map 3340, 196 p., 2 sheets, scale 1:1,584,000. Retrieved from https://alaska.usgs.gov/science/geology/state\_map/interactive\_map/AKgeologic map.html
- Wyld, S. J., Umhoefer, P. J., & Wright, J. E. (2006). Reconstructing northern Cordilleran terranes along known Cretaceous and Cenozoic strike-slip faults: Implications for the Baja British Columbia hypothesis and other models. In J. W. Haggart, R. J. Enkin, & J. W. H. Monger (Eds.), Paleogeography of the north American Cordillera: Evidence for and against large-scale displacements. Geological Association of Canada Special Paper 46, pp.277–298. Geological Association of Canada.
- Yokelson, I., Gehrels, G. E., Pecha, M., Giesler, D., White, C., & McClelland, W. C. (2015). U-Pb and Hf isotope analysis of detrital zircons from Mesozoic strata of the Gravina belt, southeast Alaska. *Tectonics*, 34(10), 2052–2066. https://doi.org/10.1002/2015TC003955
- York, D., Hall, C. M., Yanase, Y., Hanes, J. A., & Kenyon, W. J. (1981). 40Ar/39Ar dating of terrestrial minerals with a continuous laser. *Geophysical Research Letters*, 8(11), 1136–1138. https://doi.org/10.1029/gl008i011p01136
- Yukon Geological Survey. (2020). Yukon Geochronology A database of Yukon isotopic age determinations. Retrieved from http://data.geology.gov.yk.ca/Compilation/22

## **References From the Supporting Information**

- Amelin, Y., & Davis, W. J. (2005). Geochemical test for branching decay of 176Lu. Geochimica et Cosmochimica Acta, 69, 465–473.
- Bahlburg, H., Vervoort, J. D., & DuFrane, S. A. (2010). Plate tectonic significance of Middle Cambrian and Ordovician siliciclastic rocks of the Bavarian facies, Armorican terrane assemblage, Germany U-Pb and Hf isotope evidence from detrital zircons. *Gondwana Research*. 17(2-3), 223-235.
- Herriott, T. M., Crowley, J. L., Schmitz, M. D., Wartes, M. A., & Gillis, R. J. (2019). Exploring the law of detrital zircon: LA-ICP-MS and CA-TIMS geochronology of Jurassic forearc strata, Cook Inlet, Alaska, USA. *Geology*. 47 (11), 1044–1048.
- Horstwood, M. S., Košler, J., Gehrels, G., Jackson, S. E., McLean, N.M., Paton, C., et al. (2016). Community-derived standards for LA-ICP-MS U-(Th-) Pb geochronology—LUncertainty propagation, age interpretation and data reporting. *Geostandards and Geoanalytical Research*, 40(3), 311–332. https://doi.org/10.1111/j.1751-908X.2016.00379.x
- Hoskin, P. W., & Schaltegger, U. (2003). The composition of zircon and igneous and metamorphic petrogenesis. *Reviews in Mineralogy and Geochemistry: Zircon*, 53(1), 27–62.
- Matthews, W. A., & Guest, B. (2017). A practical approach for collecting large-n detrital zircon U-Pb data sets by quadrupole LA-ICP-MS. Geostandards and Geoanalytical Research, 41(2), 161–180. https://doi.org/10.1111/ggr.12146., v.
- Paces, J. B., & Miller, J. D., Jr (1993). Precise U-Pb ages of Duluth complex and related mafic intrusions, northeastern Minnesota: Geochronological insights to physical, petrogenetic, paleomagnetic, and tectonomagnatic processes associated with the 1.1 Ga midcontinent rift system. *Journal of Geophysical Research: Solid Earth*, 98(B8), 13997–14013. https://doi.org/10.1029/93JB01159
- Patchett, P. J. (1983). Importance of the Lu-Hf isotopic system in studies of planetary chronology and chemical evolution. *Geochimica et Cosmochimica Acta*. 47. 81–91.
- Patchett, P. J., & Tatsumoto, M. (1980). A routine high-precision method for Lu-Hf isotope geochemistry and chronology. *Contributions to Mineralogy and Petrology*, 75, 263–267.
- Paton, C., Woodhead, J. D., Hellstrom, J. C., Hergt, J. M., Greig, A., & Maas, R. (2010). Improved laser ablation U-Pb zircon geochronology through robust downhole fractionation correction. *Geochemistry, Geophysics, Geosystems*, 11(3). https://doi.org/10.1029/2009GC002618 Petrus, J. A., & Kamber, B. S. (2012). VizualAge: A novel approach to laser ablation ICP-MS U-Pb geochronology data reduction. *Geostand*-
- retrus, J. A., & Kamber, B. S. (2012). VizualAge: A novel approach to laser ablation ICP-MS U-Pb geochronology data reduction ards and Geoanalytical Research, 36(3), 247–270. https://doi.org/10.1111/j.1751-908X.2012.00158.x
- Piercey, S. J., Mortensen, J. K., & Creaser, R. A. (2003). Neodymium isotope geochemistry of felsic volcanic and intrusive rocks from the Yukon–Tanana Terrane in the Finlayson Lake Region, Yukon, Canada. *Canadian Journal of Earth Sciences*, 40(1), 77–97. https://doi.org/10.1139/e02-094
- Saltus, R. W., Hudson, T. L., & Wilson, F. H. (2007). The geophysical character of southern Alaska—Implications for crustal evolution. In K. D. Ridgway, J. M. Trop, J. M. G. Glen, & J. M. O'Neill (Eds.), Special Paper 431: Tectonic growth of a collisional continental margin: Crustal evolution of Southern Alaska (Vol. 431, pp. 1–20). Boulder, CO: Geological Society of America. https://doi.org/10.1130/2007.2431(01)
- Scherer, E., Münker, C., & Mezger, K. (2001). Calibration of the lutetium-hafnium clock. Science, 293(5530), 683-687.
- Schmitz, M. D., Bowring, S. A., & Ireland, T. R. (2003). Evaluation of Duluth Complex anorthositic series (AS3) zircon as a U-Pb geochron-ological standard: New high-precision isotope dilution thermal ionization mass spectrometry results. *Geochimica et Cosmochimica Acta*, 67(19), 3665–3672. https://doi.org/10.1016/S0016-7037(03)00200-X
- Söderlund, U., Patchett, P. J., Vervoort, J. D., & Isachsen, C. E. (2004). The <sup>176</sup>Lu decay constant determined by Lu-Hf and U-Pb isotope systematics of Precambrian mafic intrusions. *Earth and Planetary Science Letters*, 219, 311–324.
- Vervoort, J. D. (2010). Hf analysis in zircon by LA-MC-ICPMS: Promise and pitfalls. Geological Society of America Abstracts with Programs. 42(5), 667.
- Vervoort, J. D., Patchett, P. J., Söderlund, U., & Baker, M. (2004). Isotopic composition of Yb and the determination of Lu concentrations and Lu/Hf ratios by isotope dilution using MC-ICPMS. *Geochemistry, Geophysics, Geosystems*, 5(11).2004GC000721RR.
- Wieser, M. E. (2006). Atomic weights of the elements 2005 (IUPAC Technical Report). Pure and Applied Chemistry, 78(11), 2051–2066. https://doi.org/10.1351/pac200678112051
- Woodhead, J., Hergt, J., Shelley, M., Eggins, S., & Kemp, R. (2004). Zircon Hf-isotope analysis with an excimer laser, depth profiling, ablation of complex geometries, and concomitant age estimation. *Chemical Geology*, 209, 121–135.

WALDIEN ET AL. 35 of 35